Electrospun Polyaniline-Reduced Graphene Oxide Composite Nanofibers Based High Sensitive Ammonia Gas Sensor

Supervisors:

Prof.ª Dr.ª Cristina Delerue Matos

Dr. Viswanathan Subramanian

This page has been deliberately left blank.

Acknowledgements

I was honored to have the opportunity to work with Dr. S. Viswanathan and would like to acknowledge his guidance, direction, advice, support and humor through this entire project. Special thanks also go to Dra. Cristina Delerue Matos for hosting me in its lab, for its support, humor and focus along the work.

My thanks also go to my colleagues and friends in the GRAQ group, who came to my rescue when I needed and helped me to keep me grounded and sane.

My parents have always been my staunchest supporters. Finally, I would like to thank my girlfriend, for always being there.

This page has been deliberately left blank.

Index

Chapter 10

Index of figures

This page has been deliberately left blank.

Index of tables

This page has been deliberately left blank.

Abstract

Ammonia is an important gas in many power plants and industrial processes so its detection is of extreme importance in environmental monitoring and process control due to its high toxicity. Ammonia's threshold limit is 25 ppm and the exposure time limit is 8 h, however exposure to 35 ppm is only secure for 10 min.

In this work a brief introduction to ammonia aspects are presented, like its physical and chemical properties, the dangers in its manipulation, its ways of production and its sources. The application areas in which ammonia gas detection is important and needed are also referred: environmental gas analysis (e.g. intense farming), automotive-, chemical- and medical industries. In order to monitor ammonia gas in these different areas there are some requirements that must be attended. These requirements determine the choice of sensor and, therefore, several types of sensors with different characteristics were developed, like metal oxides, surface acoustic wave-, catalytic-, and optical sensors, indirect gas analyzers, and conducting polymers. All the sensors types are described, but more attention will be given to polyaniline (PANI), particularly to its characteristics, syntheses, chemical doping processes, deposition methods, transduction modes, and its adhesion to inorganic materials. Besides this, short descriptions of PANI nanostructures, the use of electrospinning in the formation of nanofibers/microfibers, and graphene and its characteristics are included.

The created sensor is an instrument that tries to achieve a goal of the medical community in the control of the breath's ammonia levels being an easy and non-invasive method for diagnostic of kidney malfunction and/or gastric ulcers. For that the device should be capable to detect different levels of ammonia gas concentrations. So, in the present work an ammonia gas sensor was developed using a conductive polymer composite which was immobilized on a carbon transducer surface. The experiments were targeted to ammonia measurements at ppb level. Ammonia gas measurements were carried out in the concentration range from 1 ppb to 500 ppb. A commercial substrate was used; screen-printed carbon electrodes. After adequate surface pre-treatment of the substrate, its electrodes were covered by a nanofibrous polymeric composite. The conducting polyaniline doped with sulfuric acid (H_2SO_4) was blended with reduced graphene oxide (RGO) obtained by wet chemical synthesis. This composite formed the basis for the formation of nanofibers by electrospinning. Nanofibers will increase the sensitivity of the sensing material. The electrospun PANI-RGO fibers were placed on the substrate and then dried at ambient temperature.

Amperometric measurements were performed at different ammonia gas concentrations (1 to 500 ppb). The *I-V* characteristics were registered and some interfering gases were studied

(NO$_2$, ethanol, and acetone). The gas samples were prepared in a custom setup and were diluted with dry nitrogen gas.

Electrospun nanofibers of PANI-RGO composite demonstrated an enhancement in NH$_3$ gas detection when comparing with only electrospun PANI nanofibers. Was visible higher range of resistance at concentrations from 1 to 500 ppb. It was also observed that the sensor had stable, reproducible and recoverable properties. Moreover, it had better response and recovery times. The new sensing material of the developed sensor demonstrated to be a good candidate for ammonia gas determination.

Resumo

O amoníaco é um elemento importante em muitas centrais elétricas e processos industriais, tornando-se extremamente importante a sua deteção na monitorização ambiental e para o controlo dos processos devido à sua alta toxicidade. O limite máximo de exposição é de 25 ppm para um limite de tempo de 8 h sendo que para 35 ppm o limite de exposição é drasticamente reduzido para apenas 10 min.

Neste trabalho é apresentada uma breve introdução às características do amoníaco tais como suas propriedades físicas e químicas, os perigos na sua manipulação, as suas formas de produção e as suas fontes. Também serão indicadas as áreas de aplicação onde é importante e necessário a deteção do gás amoníaco sendo elas a monitorização dos gases ambientais (por exemplo, agricultura intensiva), as indústrias automóveis, as indústrias químicas e as indústrias médicas. Com a finalidade de monitorar as diversas áreas tem de se cumprir alguns requisitos, os quais irão condicionar a escolha do sensor a utilizar. Devido a esse fator vários tipos de sensores foram desenvolvidos com diferentes características, tais como, os óxidos metálicos, os de onda acústica de superfície, os catalíticos, os óticos, os detetores de gás que o fazem de forma indireta e os polímeros condutores. Todos os tipos de sensores serão descritos mas será dada maior atenção aos sensores modificados que utilizam a polianilina (PANI). Assim, serão descritas as suas características, formas de síntese, processos de *doping*, formas de a depositar, modos de transdução e a formas de adesão aos materiais inorgânicos. Será ainda incluída uma descrição das suas nanoestruturas, da técnica *electrospinning* usada na criação de nanofibras e microfibras e ainda também do grafeno tal como as suas características.

O sensor criado procura ser um instrumento que vá de encontro com um objetivo da comunidade médica no controlo dos níveis de amoníaco presentes na respiração, sendo um método fácil e não-invasivo para o diagnóstico do mau funcionamento dos rins e/ou úlceras gástricas. Para isso, o dispositivo teria de ser capaz de detetar diferentes níveis de concentrações de gás amoníaco. Portanto, para este trabalho foi desenvolvido um sensor para a deteção de gás amoníaco utilizando um polímero condutor composto o qual foi imobilizado num transdutor de superfície em carbono (substrato comercial). O trabalho experimental realizado foi direcionado para a deteção de várias concentrações de gás amoníaco na escala ppb. As medições de gás amoníaco foram realizadas num intervalo de concentrações que vai de 1 ppb até 500 ppb. Após um pré-tratamento adequado do substrato, a área de trabalho dos elétrodos foi coberta por nanofibras de um polímero composto. O polímero composto, obtido através de síntese química, foi PANI dopada (H_2SO_4) com óxido de grafeno reduzido (RGO). Este composto foi a base para a formação de nanofibras através da técnica de *electrospinning*. As nanofibras vão potenciar a

sensibilidade do material sensitivo. As fibras de PANI-RGO foram posteriormente depositadas no substrato comercial e, em seguida, procedeu-se à sua secagem à temperatura ambiente.

Foram efetuadas medições amperométricas para diferentes concentrações de gás amoníaco (1 a 500 ppb). Foram também obtidas as características *I-V* dos sensores e foi realizado um estudo de interferência de alguns gases (NO_2, etanol e acetona) na análise. As amostras de gás foram preparadas num sistema de configuração personalizada e as diluições realizaram-se com azoto gasoso seco.

As nanofibras criadas a partir do composto PANI-RGO por meio da técnica de *electrospinning*, demonstraram uma melhoria na deteção de gás amoníaco quando comparado com as nanofibras preparadas só de PANI. Foi visível um maior intervalo de valores de resistência para concentrações de 1 a 500 ppb. Também foi observado que o sensor possui boas propriedades tais como a estabilidade, reprodutibilidade e capacidade de recuperação. Além disso, apresentou melhores tempos de resposta e de recuperação. O novo material sensitivo do sensor desenvolvido demonstrou ser um bom candidato para a determinação de gás amoníaco.

Palavras-chave: Gás amoníaco; Sensor de gás; Polímero condutor; *Electrospinning*; Nanofibras; Polianilina; Óxido de grafeno reduzido.

Chapter 1

Introduction

This page has been deliberately left blank.

Introduction

The atmosphere is composed of gases, vapor and particles. It completely surrounds the earth and remains in its place due to the earth's gravitational force. The atmosphere has an important role in life preservation on earth, by blocking the passage of most of the ultraviolet rays, by preserving the heat on its surface (greenhouse effect) and by preventing extreme temperature variation in the day/night cycle [1]. It is mainly composed of nitrogen (78%) and oxygen (21%), representing 99% of the total gaseous composition. The last percentage point is represented by several minor gases which are indicated in Table 1 [2].

Table 1. Gaseous constituents of the atmosphere [2].

Chemical species	Molecular weight (g mol^{-1})	Proportion by volume	Chemical species	Molecular weight (g mol^{-1})	Proportion by volume
N_2	28.01	78%	O_3	48.00	~500 ppb
O_2	32.00	21%	N_2O	44.01	310 ppb
Ar	39.95	0.93%	CO	28.01	120 ppb
H_2O (vapor)	18.02	~0.5%	NH_3	17.03	~100 ppb
CO_2	44.01	380 ppm	NO_2	46.00	~1 ppb
Ne	20.18	19 ppm	CCl_2F_2 (CFC-12)	120.91	480 ppt
He	4.00	5.2 ppm	CCl_3F (CFC-11)	120.91	480 ppt
CH_4	16.04	1.7 ppm	SO_2	64.06	~200 ppt
Kr	83.8	1.1 ppm	H_2S	34.08	~200 ppt
H_2	2.02	~500 ppb	air	28.97	

To ensure the best personal protection, safety and process control, it is necessary to perform analysis of biochemical and chemical substances that can be present in the environment. Therefore it is important to have qualitative and quantitative monitoring devices to control ambient air [3].

An interest arose to perform this type of monitoring and control. Therefore several organic and inorganic sensing materials have been the aim of study [3].

In the early stages, semiconductor sensors were those that were more widely available. They were mostly based on SnO_2, which is an inorganic material [3-5]. In order to obtain a good response both in sensibility and selectivity those sensors needed to operate at high temperatures

[3, 4]. For that reason new sensor materials have been developed. Organic layers like conducting polymers started to get global interest since the awarding of the Noble prize in chemistry in 2000[1] [4]. Polypyrrole was the first polymer presented for gas detection. But it was not good enough due to its low sensitivity and imperfect reversibility for the detection of gas molecules [3, 4]. To improve these negative factors polyaniline appeared as a new sensitive organic layer [3, 4, 6].

[1] The Nobel Prize in Chemistry was awarded in 2000 jointly to Alan J. Heeger, Alan G. MacDiarmid and Hideki Shirakawa *"for the discovery and development of conductive polymers"*.

Chapter 2

Ammonia

This page has been deliberately left blank.

2.1. Introduction

The word ammonia comes from the *Latin* word *sal ammoniacum*, *sal* is salt. The adjective of the salt, *ammoniacum*, has its origin in the fact that it was found around Siwa Oasis [7], previously called Ammon Oasis. Ammon was one of the most powerful ancient Egyptian Gods. The old Egyptian civilization called him the "King of the Gods", so this God became very important in Egyptian history [8].

The preparation of free ammonia was first performed by J. B. Priestley in 1774. After ten years (1784) C. L. Berthollet realized that ammonia is composed of nitrogen and hydrogen. The volumetric ratio of 1:3 was determined by W. Henry, in 1809, corresponding to the chemical compound NH_3 [7].

The first commercial synthesis of ammonia was performed in 1913 when the Haber-Bosh process was implemented by a plant. As a result of the success of this process other plants also implemented it. The success is due to the fact that ammonia had been hard to produce before that, quickly replacing the Chile saltpeter (source of sodium nitrate) [7].

2.2. Physical Properties

Ammonia is a chemical compound and its molecule is constituted by an atom of nitrogen and three atoms of hydrogen (NH_3), which are covalently bonded. Its structure shows a trigonal pyramidal form with a bond angle of 107.8° (Figure 1), this type of geometry occurs due to the formation of hybrid orbital, sp^3 [7].
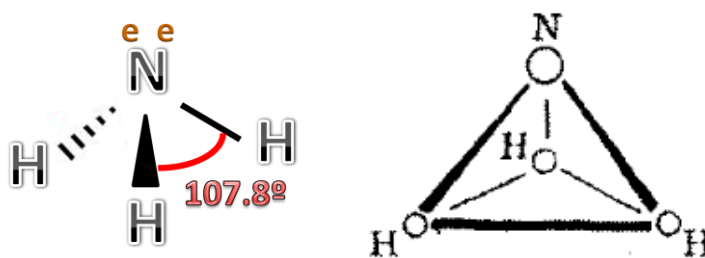
Figure 1. Ammonia trigonal pyramidal structure [7].

The nitrogen atom in the center of ammonia's structure has five outer electrons and three electrons from each of the three hydrogen atoms, totalizing eight electrons or, in other words, four electron pairs (Figure 2). Three electron pairs are bonded leaving one free pair. This lone pair is the one that has the strongest repealing force which results in the already referred trigonal pyramidal structure (Figure 1). Besides this, the lone pair turns ammonia into a proton acceptor (base) that can combine with a proton and result in a ammonium ion NH_4^+. The excess of charge (positive) of the four hydrogen atoms is distributed equally by all five atoms [7].
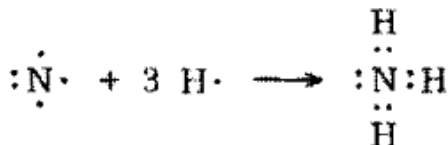
Figure 2. Ammonia molecule with the four electron pairs [7].

The trigonal pyramidal form and the polarization of the bonds of ammonia molecule give it a dipole moment of 1.5D [7].

The ammonia molecule has similarities with the water molecule, like the same electron configuration (isosterism), bond angles and in the way that it reacts in many reactions. Liquid ammonia has high solubility with many substances [7].

2.3. Chemical Properties

Several chemical properties of ammonia are presented in Table 2.

Table 2. Some relevant ammonia (NH_3) properties [7].

Some relevant ammonia (NH_3) properties	
Relative molar mass (M_r)	17.0312
Molecular volume (0º C, 101.3 kPa)	22.08 L/mol
Liquid density (0º C, 101.3 kPa)	0.6386 g/cm^3
Gas density (0º C, 101.3 kPa)	0.7714 g/L
Boiling point	-33.43º C
Liquid density (-33.43º C, 101.3 kPa)	0.682 g/cm^3
Gas density (-33.43º C, 101.3 kPa)	0.888 g/L
Critical pressure	11.28 MPa
Critical temperature	132.4º C
Critical density	0.235 g/cm^3
Critical volume	4.225 cm^3/g
Critical compressibility	0.242
Critical thermal conductivity	0.522 $KJ\ k^{-1}\ h^{-1}\ m^{-1}$
Critical viscosity	23.90×10^{-3} mPa·s
Melting point (triple point)	-77-71º C
Heat of fusion (101.3 kPa)	1370 kJ/kg
Ignition temperature acc. (DIN 51794)	651º C
Electrical conductivity:	
- **Very pure**	$1 \times 10^{-11}\ \Omega^{-1}·cm^{-1}$
- **Commercial**	$3 \times 10^{-5}\ \Omega^{-1}·cm^{-1}$
Explosive limits:	
NH_3-O_2 mixture	
- **20º C, 101.3 kPa**	15-79 vol% NH_3
NH_3-air mixture	
- **0º C, 101.3 kPa**	16-27 vol% NH_3
- **100º C, 101.3 kPa**	15.5-28 vol% NH_3

2.4. Dangers in handling ammonia

Table 3 gives an easy view of the hazard pictogram, its description and some cares to take when handling ammonia. Section 2.4.1 includes the current European legislation according to CLP Regulation (EC) nº 1272/2008 on classification, labeling and packaging for chemicals.

Table 3. Ammonia (NH_3) hazard pictograms [9].

Pictogram	Description	Cares
	GHS06 Toxic - Preparation, by inhalation, ingestion or skin penetration may involve serious risks, acute or chronic, and even death.	All contact with human body should be avoided.
	GHS09 Environmental hazards - The release of this substance in the environment can cause damage to the ecosystem in the short or long term.	Because of its potential risk, should not be released in pipes, soil or the environment.
	GHS05 Corrosive - These chemicals causes destruction of living tissue and inert materials.	Do not inhale and avoid contact with skin, eyes and clothing.
	GHS04 Gas under pressure - Contains gas under pressure, may explode if heated.	Do not heat, keep away from ignition sources.

2.4.1. Classification according to Regulation (EC) No 1272/2008 [CLP/GHS]

According to European regulation Nº 1272/2008, ammonia dangers are classified as follows: flammable gas (H221), gas under pressure (H280), causes severe skin burns and eye damage (H331) and is very toxic to aquatic life (H400). Still following the European regulation nº 1272/2008, the precautions are: keep away from heat/open flames/hot surfaces/no smoke (P210), avoid breathing dust/fume/gas (P261), avoid environment release (P273), wear protective clothes (P280), in case of eye contact wash them with plenty water, remove contact

lenses if present (P305+P351) and if in direct contact to the chemical call immediately poison center/doctor (P310) [9].

2.5. Ammonia production

The production of ammonia appeared with the needs of none expensive nitrogen for nitric acid production for the creation of explosives. Nowadays the ammonia production aims to create chemical products, refrigerating systems, and fertilizers which contain the ammonium salts that are used in farming [10].

Almost all industrial ammonia is obtained, using a catalytic process, from hydrogen and nitrogen gases that are enriched with an iron catalyst. In addition, ammonia is one of the most inorganic chemicals manufactured. This process was developed by Fritz Haber[2] and Carl Bosh[3], it was only possible thanks to the discovery of iron catalyst by Alwin Mittasch. The process previously indicated is called the Haber-Bosh process. In the literature it is referred that this process [7, 10], which was implemented in 1913 on an industrial scale in Germany by the BASF Oppau plant [11], did not suffer many changes in its original concept and is still being used nowadays with almost the same basic arrangement as firstly implement in primary ammonia production plants. One of the changes was due to the introduction of a ruthenium-based catalyst which replaced the iron catalyst, allowing the reduction of the pressure that was needed in the synthesis phase [7].

The process starts with a reaction of hydrogen and nitrogen gases over an iron catalyst at a pressure of above 100 bar at a very high temperature (400 to 500 °C) [7]. Figure 3 illustrates the Haber-Bosch process.

---

[2] Fritz Haber was awarded in 1918 the Nobel Prize in Chemistry *"for the synthesis of ammonia from its elements"*.

[3] Carl Bosch was awarded jointly to Friedrich Bergius in 1931 the Nobel Prize in Chemistry *"in recognition of their contributions to the invention and development of chemical high pressure methods"*.
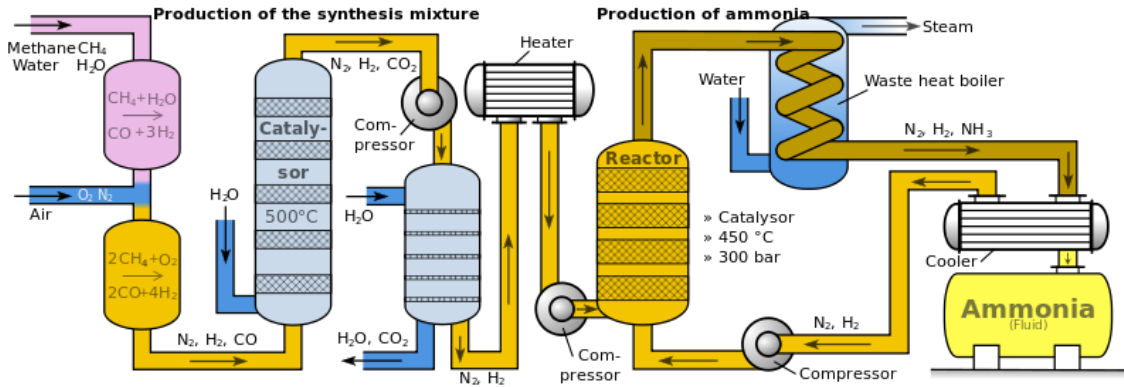
Figure 3. Haber-Bosh process in the production of ammonia [12].

2.6. Sources of ammonia

Ammonia (NH_3) is a gas that can be found all over the atmosphere at low concentrations [2]. It is present mainly in the form of ammonium salts and its natural formation is primarily by the nitrogen cycle (Figure 4) or by volcanic activity [7].

Most of the existing ammonia in the earth's atmosphere is due to human activities either by direct or indirect emissions [2].

When ammonia combines with its oxidative elements, ammonium nitrate and nitrite will be formed [7].
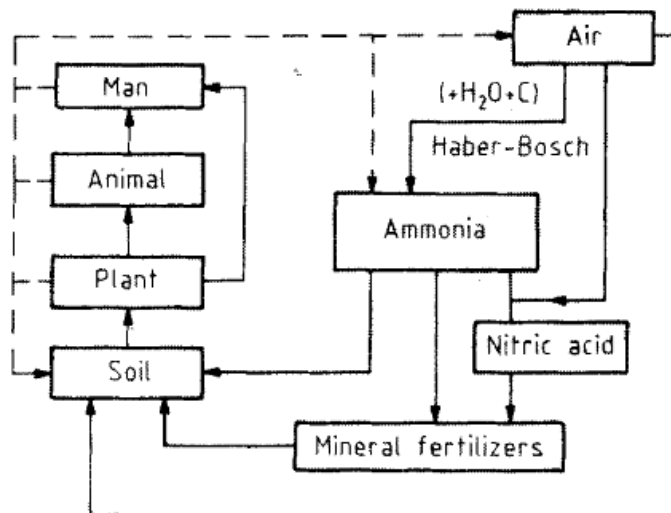
Figure 4. Nitrogen cycle [7].

According to EEA-32, it is noticeable that there was a 24% reduction in NH_3 emissions from 1990 to 2008. Agriculture activity is the most responsible, accounting for 94% of total emissions in 2008. It is also mentionable that since 1990 agriculture emissions suffered a

reduction which was due to a decrease in livestock farming, new methods of handling and management of manures, and the lower use of nitrogenous fertilizers. But the reductions had little effect because the transport sector, energy industry and others sectors increased their emissions [13].

Generally, the EEA-32 country members reduced their emissions below their emission ceilings for 2010 that were set in the National Emission Ceilings Directive (NECD) [13].

There are three major classes of ammonia sources. The first one is related to the entrance of nitrogen in the ecosystem (Figure 4) through a process called nitrification in two natural ways. One way is through atmospheric deposition which is the deposition of ammonium and nitrate salts mixed with water into the ground. This is exacerbated in agricultural activities by the application of large quantities of fertilizers (that contain ammonium) to the soils, originating in an excess of ammonium, which leads to an increase of the ammonia concentration in the atmosphere [14]. Other way of nitrification is by nitrogen fixation provided by some species of bacteria that can bind nitrogen which can be found in soils and on roots of certain plants [10]. The same type of fixation can also be found in blue green algae. The referred bacteria and algae contain an enzyme called *Nitrogenase* that allows them to convert nitrogen to ammonia (25 ºC, 1 bar) that is released into the environment [15].

The second ammonia source is called ammonification and consists of a sequence of metabolic activities in the decomposition of organic nitrogen (e.g. animal manure) which is performed by bacteria and fungi. In this process ammonium ions and ammonia vapors are converted by *Nitrosomonas* to nitrites (NO_2^-) and then *Nitrobacter* converts the nitrites to nitrates (NO_3^-). Denitrification is the final step and is achieved by *Pseudomonas*, resulting in the release of nitrogen from the nitrates. Therefore nitrogen is released back into the atmosphere [16, 17].

The third and last source of ammonia is combustion, which is originated by chemical plants in the production of fertilizers and refrigeration systems. Another source comes from fossil combustion present in all fuel vehicles [18].

This page has been deliberately left blank.

Chapter 3

Areas of application

This page has been deliberately left blank.

3.1. Introduction

Due to the fact that ammonia gas at high concentrations is easily detectable by the human nose, there is no need to develop sensors for qualitative analysis at these concentrations, which is only necessary when quantification is required. On the other hand, low concentrations are not detectable and in this case sensor development for detection and quantification is needed [10].

In the following sub-chapters four relevant areas are mentioned where ammonia concentration measurements are needed and how that need is important in each area.

3.2. Analysis of the environmental gas

The inhalation of high concentrations of ammonia could be a very serious threat against a good health condition. So, an interest exists in knowing what the concentration levels near farms are in order to prevent sickness of farmers and the animals because in intensive farming the exposure limit can be exceeded [10].

The concentration levels in the pretended application determine the required time resolution of the sensor equipment. The literature gives some examples that demonstrate the large variety of detection limits and response times in environmental gas analysis. For example, in The Netherlands the average concentration of ammonia in the air is around 1.9 ppb, so in order to be able to detect this concentration ammonia detectors with a 1-ppb detection limit are needed. Regarding intense farming the ammonia concentration is much higher; it can be above 10 ppm, so the detection limit needed in this case is about 5 ppm. So it is understandable that the type of sensor depends on what application is pretended, relatively to the response time the detection interval is very large so there is no need for fast detections. Contrasting with the two previous examples, when an environmental analysis of controlled venting systems is performed a sensor response time of one minute is advisable [10].

3.3. Automobile industries

3.3.1. Exhaust gases

Exhaust gases are a significant concern in urban site pollution, so gas measurement plays an important role [19]. The emissions of ammonia by exhaust gases are up to about 8 ppm [20].

3.3.2. Air quality control in vehicles cockpit

Beyond exhaust gases the automotive industry is also concerned with the presence of ammonia in the vehicles' cockpits since these are equipped with air conditioning systems [19]. These systems can control the outside air that could contain smoke and/or high ammonia concentrations from manure in fertilized camps and near farms, presenting a strong odor. For inside air quality the limit should be detected by sensors with fast response times (in the order of seconds) in order to prevent smell detection, which is around 50 ppm [10].

3.3.3. NO$_X$ reduction in diesel engines

Another application for ammonia sensing devices in this area is the NO$_X$ reduction in diesel engines, due to its high air to fuel ratios that originates great concentrations of NO and NO$_2$. To reduce the toxicity of NO$_X$ ammonia is injected in the exhaust system. The reduction is exemplified by equation (1) [10].

$$4NO + 4NH_3 + O_2 \rightarrow 4N_2 + 6H_2O \qquad (1)$$
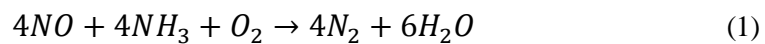
So it is important to optimize the injection to prevent high ammonia release. For that the sensor must have a fast response time (about 1 min.) and the ability to detect low ammonia concentrations, and must be able to resist to high temperatures [10].

3.4. Chemical industries

As already described in section 2.5, the main pure ammonia production of today goes to fertilizers, chemical production and refrigerating systems. So it is important to control possible leaks of ammonia in the systems in order to prevent health threatening situations. To achieve this, chemical industries should have detection systems to guaranty the workspace safety concentration level, which is about 20 ppm. For this type of detection a low response time sensor (minutes order) is sufficient. High temperature resistance is needed for the sensors used in ammonia production processes due to the high temperature necessary for its synthesis from nitrogen and hydrogen gases (Haber-Bosch process) [10].

3.5. Medical industries

3.5.1. Human health hazards

The human nose's detection limit for ammonia stands at 50 ppm (40 $\mu g/m^3$), lower limits, near the indicated 50 ppm, can still damage the respiratory system, skin and eyes. Therefore, the occupational exposure for workers is situated at 20 ppm [10, 21].

Besides the health implications due to exposure to high ammonia concentrations indicated in Table 4, lower concentrations are believed not to cause any health pathology because of the fact that ammonia is natural to the human body, that has the ability to excrete ammonia in the form of urea and ammonium salts through the urine and some by the sudoriparous glands [10]. Actually, the human body produces ammonia by itself and its amount varies with a variety of parameters [10, 22].

Table 4. Human health hazards at high ammonia concentrations [21, 23].

NH$_3$ concentration	Health implications
500 ppm	Causes serious injuries to the throat and upper mucous.
1000 ppm	Pulmonary edema can occur, the symptoms can take 24 h to develop, causes chest squeeze and breathing difficulties. At some time of exposure, lung failure and permanent respiratory complications may occur.
5000 - 10000 ppm	It should be lethal but an accident proved that the lethal exposition should be higher.

3.5.2. Medical interest in ammonia sensing

The medical community got quite interested in measuring the breath's ammonia levels with the intention of creating diagnostic methods for patients with kidney malfunction which causes disorder in urea balance or gastric ulcers caused by *Helicobacter pylori* bacteria (Figure 5) [22, 24] .
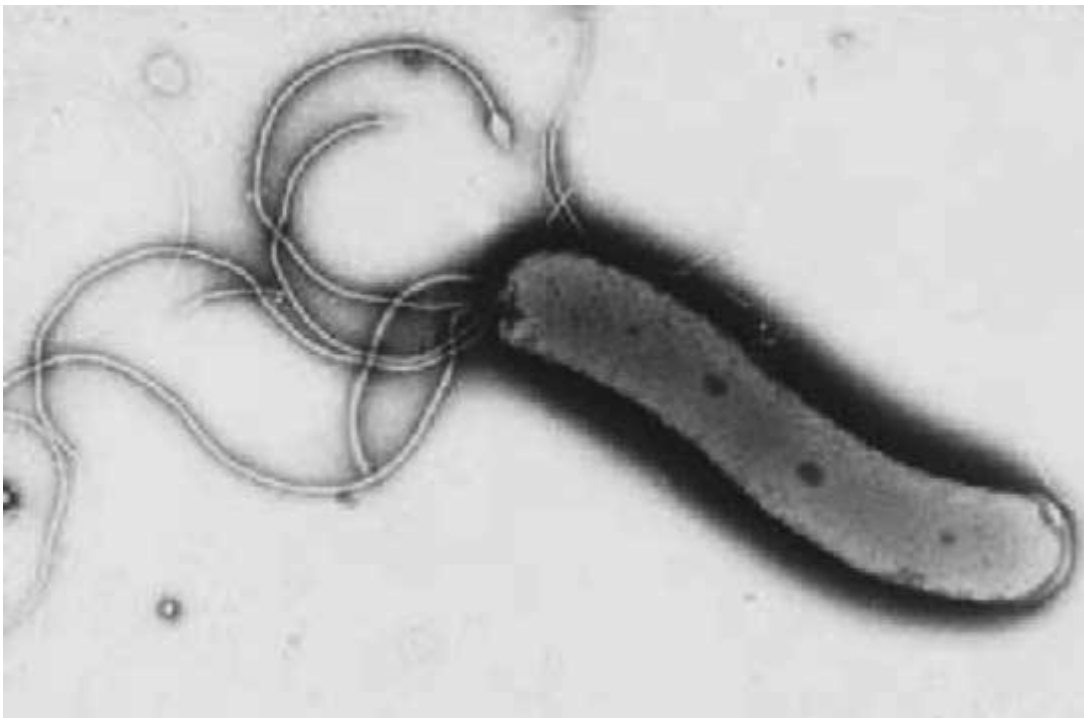
Figure 5. *Helicobacter pylori* in a micrograph made by an electron microscope [10].

The sensor for this kind of application has to determine the concentration with only a few millimeters of the patient's breath. However, the response time does not need to be very fast, but at least it should be in the order of a few minutes [10].

3.5.2.1. Stomach infection by *H. pylori*

3.5.2.1.1. Introduction

The bacteria *Helicobacter pylori* are usually present in the human's stomach. The infection level in the worldwide population is nearly 50%. Most of the population that is infected with *H. pylori* does not reach to experience symptoms and the infection does not take progress. Even so, the bacteria can cause digestive problems like ulcers and in rare cases stomach cancers. Nowadays it is still not quite understandable why some people get infected and others do not [25, 26].

3.5.2.1.2. *H. pylori* action in stomach/duodenum

An infection by *H. pylori* (Figure 6) is most likely due to the consumption of contaminated food or water, normally containing fecal matter. This bacterium can penetrate both the stomach and duodenum by invading the protective mucous barrier in the way to be protected from stomach acid gastric [10, 25, 26]. The bacteria have the ability to produce an enzyme called urease. This enzyme catalyzes the hydrolysis of urea into bicarbonate and ammonia, building up a safe house for the bacteria allowing it to survive near the gastric acid [10].

At some point the immunitary system will detect the intruder and as it usually does it will attack the invader element. As the bacterium is protected in its shell the antibodies will firstly attack the outer bacteria shell, which is not more than the outer lining cells of the stomach, that attack will lead to damages allowing the formation of peptic ulcers or in rare cases cancer [27], like referred in the previous section.
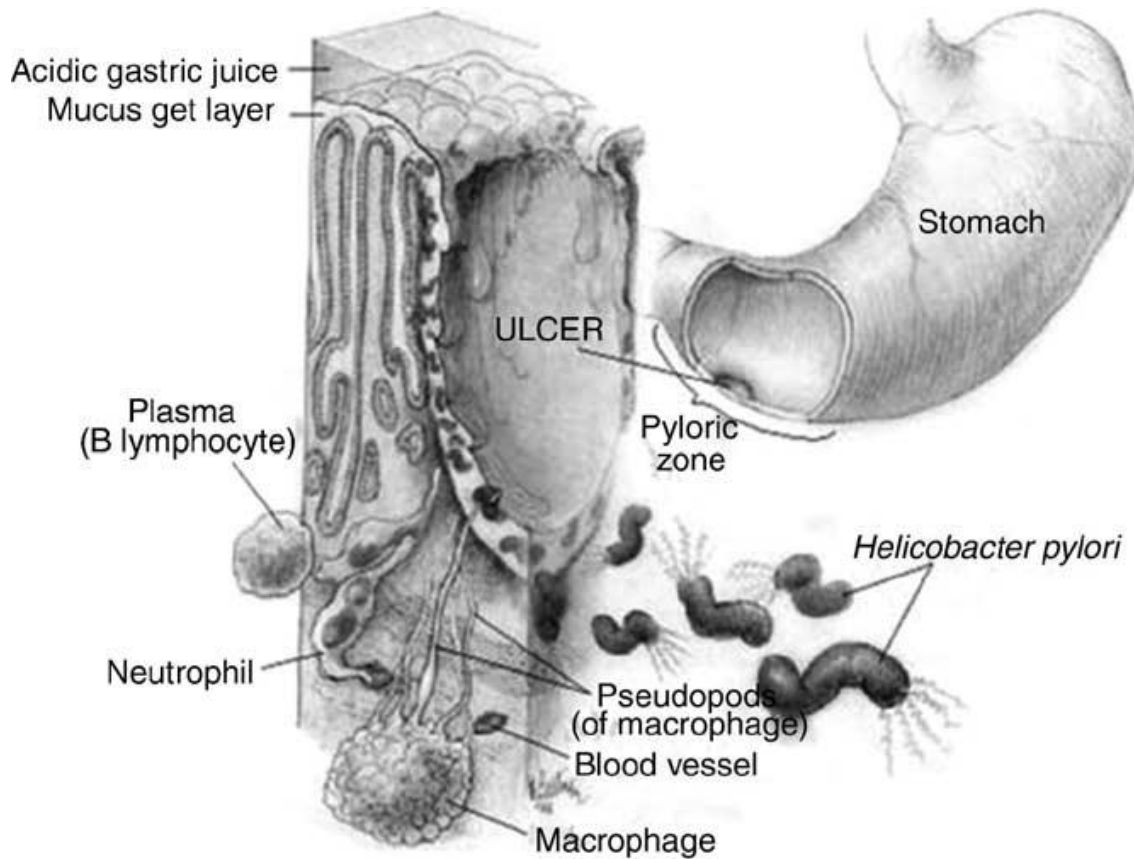
Figure 6. An illustration of a stomach ulcer provoked by *Helicobacter pylori* [10].

3.5.2.1.3. Detection methods of *H. pylori* infection

The *H. pylori*, as already referred, have the ability to convert urea to ammonia and bicarbonate thanks to its urease enzyme and that capability of conversion is used to determine whether a person is infected or not [10].

One of the methods is based on an endoscopy in order to measure the amount of CO_2 present in the stomach which is linked to the concentration level of bicarbonate. This methodology is classified as an invasive test due to the fact that the measuring equipment needs to get into the patient. Another methodology, which is classified as non-invasive, uses the exhaled air to get a value of CO_2 and NH_3 concentrations. As the exhaled air has a high CO_2 concentration the measurement process is made by isotopic labeling of urea, so the measurement is obtained by labeled CO_2. The literature indicates that the resulting measurements of this method are excellent but it has a drawback due to the use of a radionuclide, making this methodology expensive and avoidable to use. For that reason, using a proper ammonia breath analyzer offers the best cost benefit. The ammonia sensor should be able

to measure low levels (50 ppb) in the presence of up to 3% of CO_2 as an interfering gas, the response time can be a few minutes and the sensor should be capable to perform measurements with small amount of exhaled air [10].

3.5.2.2. Ammonia measurement in sport activities

Another medical interest is to know the ammonia levels in blood when people perform a sports activity because during this activity the body will produce an exponential increase of ammonia. According to Timmer *et al.*[10], ammonia can diffuse from the blood into the lungs when the ammonia concentration inside the body exceeds its concentration in the air. The range that a sensor must cover for expired ammonia is from 0.1 to 10 ppm.

3.5.2.3. Other potential future applications

Because ammonia can diffuse out of the blood into the lungs when in higher concentrations than in the air, the possibility is created for clinical blood ammonia measurements in a non-invasive way. In clinical terms there are some conditions associated to changes in nitrogen level and consequently ammonia in blood, such as:

- **Hepatic Encephalopathy**

The liver and kidneys are the organs involved in nitrogen metabolism and consequently in the ammonia removal from the body. A problem involving any of the indicated organs will cause a rise in the ammonia blood levels to dangerous values. The analyses methodology involves drawing blood in order to measure ammonia levels. The potentialities of breath ammonia measures could turn to be an alternative to the invasive methodology [28].

- **Hemodialysis**

When the kidney fails some dangerous conditions appear like uraemia (e.g. blood urea increase), edema (e.g. elevated water retention) and acidosis (e.g. high levels of H^+). Other problems that derive from kidney failure are hormonal imbalances, reduced amount of red blood cells, blood pressure increases, and bone strength losses. The first method used to compensate renal failure is hemodialysis which will act as a kidney filtering the toxins of the blood [28]. During the hemodialysis process it is necessary to know if urea is successfully being removed.

Therefore, a measure based on the calculation of the urea reduction ratio (URR) (equation 2), that should be at least 65%, is performed [24].

The measurements of ammonia in breath have the potential to substitute this calculation due to the discovery of a correlation between creatinine levels and breath ammonia (0.83) and between BUN (blood urea nitrogen) and breath ammonia (0.95) [24].

$$URR = \left[\frac{(BUN\ before\ treatment - BUN\ after\ treatment)}{BUN\ before\ treatment}\right] \times 100 \qquad (2)$$

With these correlation factors it is possible to warranty an efficient hemodialysis with breath ammonia method.

- **Halitosis**

In the oral cavity there are some bacteria that can generate ammonia. Halitosis is originated by volatile sulphur compounds (VSC), causing malodor and tissue damages in the oral region. Methyl mercaptan is one of the VSCs and is correlated with ammonia with a value of 0.39. Normally ammonia presence in the oral cavity is too low to be able to measure but if the methyl mercaptan amount rises, the ammonia level also rises. Moreover, if there is an increase of bacteria in the oral region the ammonia concentration also increases. So, the ammonia level from the bacteria and the methyl mercaptan levels associated with VSC measurements can evaluate halitosis [28].

- **Pulmonary dysfunction**

It was reported that asthmatics have lower levels of ammonia than healthy people. One detection method is based on the capture of exhaled breath, which is condensed in a lamellar condenser and analyzed with a solid state ion-selective electrode. However, using the analysis of gaseous breath ammonia will simplify the whole process [28].

3.6. Final considerations

The Table 5 summarizes the application areas referred previously and presents aspects like detection limit, response time and temperature that are required.

Table 5. Sensor equipments required parameters in some applications.

Aplication	Detection limit	Response time required	Temperature required
Enviromental			
Ambient monitoring [10]	0.1 ppb – >200 ppm	minutes	0 – 40ºC
Stable monitoring [10]	1 – >25 ppm	~1 min	10 – 40ºC
Automotive Industries			
Exhaust system [29]	10 ppm	<1s	Up to 600ºC
Cockpit air system [10]	50 ppm	~1s	0 – 40ºC
Chemical Industries			
Leak alarm [10]	20 – >1000 ppm	minutes	Up to 600ºC
Medical Industry			
Breath analysis [28]	50 – 2389 ppb	~1min	20 – 40ºC

This page has been deliberately left blank.

Chapter 4

Ammonia gas measurement principles

This page has been deliberately left blank.

4.1. Introduction

There are many methods for measuring ammonia gas, which vary depending on the intended application. A sensor that is implemented to monitor environmental gases differs from one that is applied as exhaled gas analyzer. Some of the current measuring methods use metal oxide gas sensors, catalytic ammonia gas sensors, conducting polymer gas analyzers and optical gas detectors.

4.2. Metal oxide ammonia gas sensors

Metal oxide sensors are the most widely manufactured and studied sensors for the detection of ammonia gas, some of the most commonly oxide materials studied are SnO_2, ZnO, TiO_2 and WO_3 [3, 30, 31]. This is due to the fact that these sensors are robust and inexpensive, which makes them very appealing for research and development [10]. One drawback of metal oxide sensors is their need to operate at high temperatures [3]. They are usually used in combustion gas detectors and gas alarm systems like the ones to detect ammonia leaks in refrigeration systems [10].

The conductance modification as a result of chemisorption of gas molecules on the sensing layer is the base operating principle of the gas sensors and is already known for a long time. The metal oxide sensors have a similar mode of operation and consist of a set of grains which are all in contact with each other. When applying a charge the gas molecules will be trapped in the grains' limits, originating the formation of a double Schottky potential barrier. Its height will influence the conductance value. When a gas, like ammonia, which is a chemically reductive gas, passes through the metal oxide film it will create an interaction with oxygen resulting in gas oxidation at the sensor's surface. As the oxygen is being removed by the gas the grains' surface will suffer the reduction effect, decreasing the barrier height [10]. Figure 7 shows the grains and the barrier height variation.
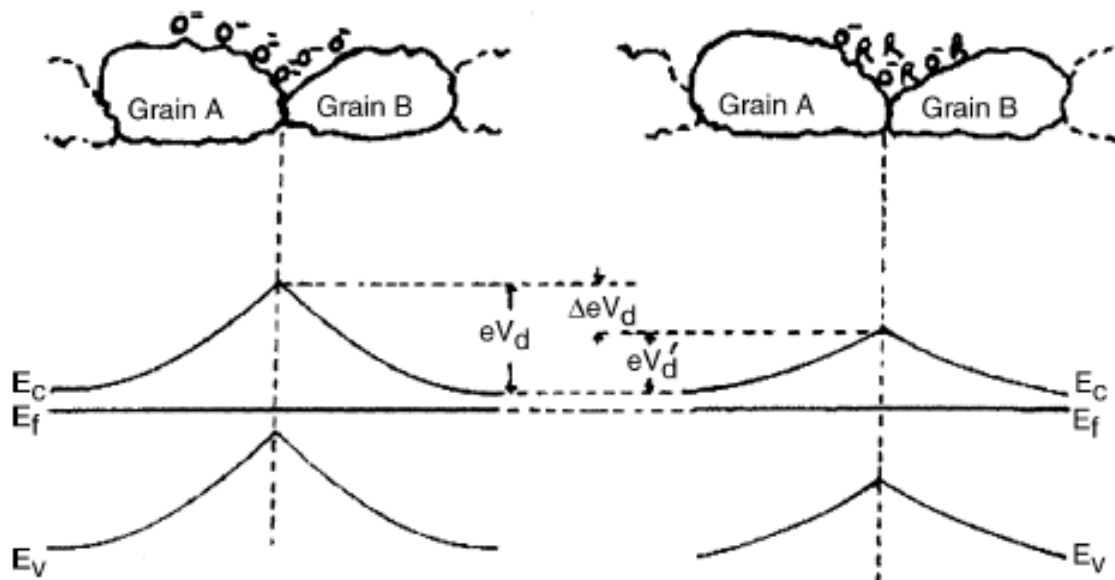
Figure 7. Energy band diagram that shows the grains connected and the height variation of the Schottky barrier when there isn´t (at left) and when there is (at right) a gas chemical reduction process [10].

The major problem of metal oxide sensors is that they are not selective to one particular gas. In order to change that many research has been carried out to create selectivity in these sensors. One path taken was to add metals or additives to enhance selectivity. Studies demonstrated that WO_3-based sensing material responds to NH_3 and NO [10]. To increase the sensitivity and selectivity towards these gases many materials were studied, like for example WO_3-nanostructured films [32]. Another base sensing material for ammonia detection is SnO_2 and the additives to enhance its sensitivity are Pb, Bi and $AlSiO_3$ or Pt and SiO_2 [10].

Aiming to solve another of the major problems of metal oxide sensors, namely the operating temperature, many studies have been performed [30]. It is known that ZnO has a natural ability to detect NH_3. Sensors based on ZnO have been studied for the detection of NH_3 at room temperature [30, 33, 34]. Other ways to deal with the operating temperature issue are referred in sections 4.7 and 4.8.

4.3. Surface acoustic wave ammonia gas sensors

The surface acoustic wave (SAW) ammonia gas sensors are highly sensitive to surface perturbations, providing the detection of ppb levels. Their greatest advantages are: low cost, accuracy, speed, real time measurements, reliability, and wireless sensing at inaccessible places. The SAW devices are composed of a piezoelectric substrate which forms interdigital transducers to excite surface acoustic waves. A specific chemical interface for NH_3 gas detection is deposited on the SAW propagation path enabling it to be more selective. The modifications (adsorption and desorption) of the chemical interface induced by the measured gas will change characteristics like phase, velocity, and attenuation, which is used to quantify the gas concentration [35].

Raj *et al.* [35] reported a ZnO one-port surface acoustic wave (SAW) resonator for ammonia gas sensing. This study used commercial one-port SAW resonators of ST-X Quartz (stable temperature-cut in x propagation) that were coated with different ZnO thin films (20, 40, 80 and 100 nm). By the use of an optimized growth of ZnO thin films they got a strong adherence and uniform distribution on the SAW surface. Furthermore the ZnO thin film presented reproducibility, reversibility, and reliability for ammonia gas sensing. The ZnO-SAW oscillators showed lower frequency by some MHz than uncoated SAW. When exposed to ammonia gas a positive frequency shift occurred. The sensor showed a sensing ability in a wide concentration range, even in humid environments. Studies concerning the oscillators' sensing mechanisms have been undertaken and it was observed that the elastic effect is the main aspect for ammonia gas sensing.

4.4. Catalytic ammonia gas sensors

There are some catalytic metals that react specifically with a certain type of gas, like for example ammonia. The type of catalytic metal, the metal layer morphology, and the operating temperature are important to define the selectivity of this kind of sensors [10].

The catalytic reaction of the metal layer with ammonia gas can be combined with solid-state conducting materials to form a gas sensing system called chemical cells. The catalytic reaction will change the potential of the sensing electrode, so to obtain the gas concentration the potential difference between the sensing and the counter electrode is used. These sensors have a detection limit in the lower ppm range and a limited accuracy. For ammonia detection the

developed chemical cell was based on an Ag/AgCl counter electrode and a Cu electrode connected to an anion exchange membrane [10].

Zeng *et al.* [36] reported the synthesis of flowerlike ZnO nanostructures created by a hydrothermal process followed by a wet chemical process. This material was added to Pd, forming Pd-sensitized ZnO nanostructures, and its response to ammonia gas was investigated and compared to pure ZnO. The results showed that pure ZnO had a low response in operation temperatures of 190 to 390 ºC, having a maximum response for 5.8 ppm at 350 ºC. On the other hand, Pd-sensitized ZnO showed a maximum for 45.7 ppm at 210 ºC. The lower operating temperature is explained by the weak-bonded complex of Pd atoms with oxygen molecules at lower temperatures, the catalyst atoms activate the reactions of NH_3 to adsorb oxygen originating more electrons in the ZnO band thus better NH_3 gas response at lower temperature. The saturation point was 1000 ppm and a linear response was obtained between 20 and 150 ppm for Pd-sensitized ZnO. This sensor had response times of 12.6 and 6.4 s at 210 and 250 ºC, respectively. Moreover, at 50 ppm it performed at 100 ºC with response- and recovery times of 20 and 60 s. The sensor also works at room temperature, but has a limitation regarding the recovery time (>40 min).

4.5. Optical ammonia gas analyzers

There are two major optical techniques of ammonia gas detection, one is by color change of a reagent when in contact with ammonia and the other method is based on the optical absorption principle [10, 6].

4.5.1. Spectrophotometric ammonia gas detection

This technique is based on reactions that cause a coloration of an analyte and the gas measurements are always performed in aqueous solution [10].

There are two reaction methods for dissolved ammonia, the Nessler reaction and the Berthelot reaction. The former uses a very toxic reagent and one of the reaction products is insoluble in water, making it hard to implement in miniaturized detection systems. The reagent used in the Nessler reaction is dipotassium tetraiodomercurate(II) in dilute alkaline solution (e.g. sodium hydroxide). The second one employs less toxic chemicals and the reaction products are soluble in water, making it appropriate for miniaturized analysis. The detection is performed by mixing the sample with phenol and hypochlorite and if there's ammonia present a blue color will appear indicating a positive result [10].

4.5.2. Ammonia determination by optical absorption

This system uses a spectrometer and a laser. The use of a laser implies that the sensor obtains results at light speed, which is very quick (299,792,458 m/s), what can delay the result output is the processing unit, but in general these sensors have very fast response times. For example, the final result of a full measurement in systems with a 1-ppb detection limit is obtained in just 1 second. The light spectrum that reaches the sensitive detector will be affected by the gas composition that is aim of study. Figure 8 presents the absorption spectrum and clearly demonstrates the variation of the results, so it is perceptible that ammonia gas is distinguishable from gases like carbon dioxide and water vapor with this method [10].
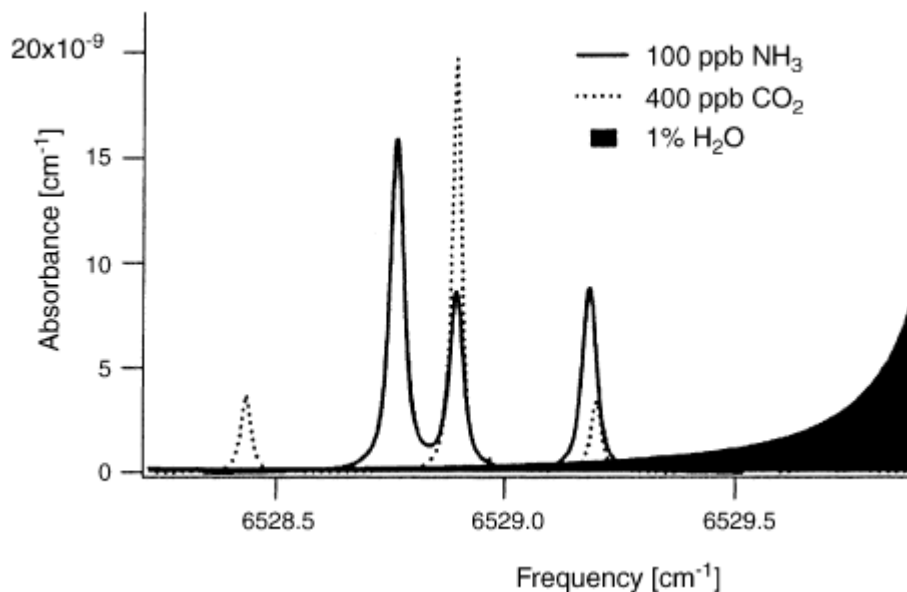
Figure 8. Spectrogram that demonstrate the ease in the distinguishing of the three gases under consideration, ammonia, carbon dioxide and water vapor [10].

In general the biggest problem of optical sensor systems is that they are quite expensive, complex, and not suitable for measurements in small volumes. In the first case the problem is due to the price of the equipment needed and for the last case the increase in the detection limit when this type of sensors are miniaturized poses a problem [10, 37].

In order to change that some studies have been performed and reported optical systems based on reflectance spectroscopy from porous Si chips. An optical gas sensing miniaturization presents several advantages such as high specific surface area, compactness, and larger adsorption capacity of the sensing element. The porous Si by itself is not selective to any determinate gas so its surface modification is required. The surface will be sensitive and selective for the detection of NH_3 gas if the porous film is modified with a dye of a pH indicator like bromothylmolblue (BTB). As most dye molecules are not strongly adsorbed on the porous Si surface, they will be vulnerable to degradation as long as the gas passes through the sensor film leading to a lower sensor lifetime. Coating the surface with a chitosan hydrogel film crosslinked by glycidoxypropyltrimethoxysilane (chitosan-GPTMS) will bring high dye adsorption capability and as it is a transparent polymer it will not interfere in optical measurements. The novel prepared sensor presents high stability, sensitivity and selectivity. The light intensity reflection variation due to different ammonia gas concentrations can be obtained by real-time measurements and this optical system has the potential to be miniaturized for ammonia gas detection. Is also referred that this type of setup is suitable for others gases being only necessary to coat the porous Si substrate with a different dye that is sensitive to a pretended gas and then use a dye supported polymer [37].

4.6. Indirect ammonia gas measurement with nonselective detectors

The biggest problem that exists in most ammonia gas sensing principles has to do with the selectivity of the method. Despite this, measurements can be performed using non-selective methods. For this it is necessary to isolate the pretended gas in the vicinity of the detector. The gas isolation can be achieved utilizing gas diffusion separation with the help of permeable membranes. For gas measurement gas samplers are necessary (denuders/diffusion scrubbers) to place ammonia into a liquid [10].

The biggest advantage of this technique lies in the fact that the ammonia is pre-concentrated by passing a large amount of the sample through a small volume of liquid, where the ammonium ions are formed. There are studies that describe selective ways to measure low ammonium concentrations [38].

4.7. Conducting polymers for ammonia gas detection

4.7.1. Introduction

For conducting polymer-based sensors several materials have been reported like polypyrrole and polyaniline [4, 6]. Polypyrrole was one of the first conducting polymers studied for measuring ammonia gas [3, 6]. The detection mechanism of polypyrrole films can occur in two ways, one is by irreversible reaction of ammonia with the polymer and the second way is based on the fact that the oxidized form of this polymer can be reversibly reduced by ammonia gas [4].

The working principle of the polymeric films is based on their reduction process which changes the film's conductance, turning them perfect for measuring methods like resistometry and amperometry for the quantification of ammonia. The reduction characteristic of the polymers leads to a decrease in sensitivity when they are being exposed to ammonia gas. To overcome this problem some regenerating techniques have been presented [4].

However, polyaniline (PANI) is a more stable conducting polymer and additionally has a high environmental stability and a unique conduction mechanism. Its detection mechanism is based on deprotonation by the action of ammonia gas resulting in a change in its conductivity [4]. These advantages combined with its ease of synthesis and selectivity to ammonia gas turns polyaniline in the most promising conducting polymer to sense ammonia [31].

4.7.2. Polyaniline as organic material

When comparing organic materials like polymers to inorganic materials like the largely used SnO_2, it is noticeable that organic materials have better sensitivity at room temperature. But not everything is good in polymers, like with inorganic materials PANI (Figure 9) is also sensitive to humidity due to the formation of hydrogen bonds and swelling in itself. Despite this disadvantage the effects of humidity are completely reversible by heating, which breaks the hydrogen bonds between water and polymer [4].

Another limitation is the life time of the polymer-based sensors when exposed for long times to ammonia gas which can cause an irreversible process (the process is completely reversible for exposures of less than 10 minutes). Besides gas exposure also the natural aging of the organic layer is observed leading to a sensitivity decline along its life time, which may be

due to dedoping reaction within the film $(PANi - H^+ + A^- \rightarrow PANi + HA)$, ammonium residues or too long exposition to ammonia gas (> 1h) [4].
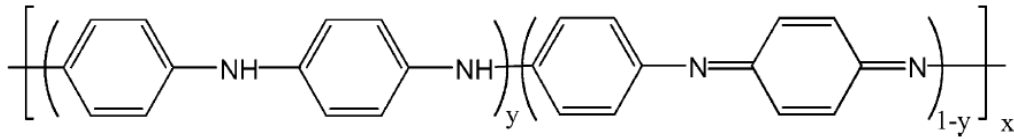
Figure 9. Polyaniline structure [4].

4.7.3. Polyaniline as sensing layer

The polyaniline form that has the best conducting behavior is called protonated polyemeraldine or polyemeraldine salt, and has a green color and a conductive value of 15 S cm^{-1}. On the other hand, the less conductive form is named polyemeraldine base which has a conductivity of about 10^{-5} S cm^{-1} (Table 6). As reference, an isolator has a conductivity of around 10^{-8} S cm^{-1} and a metal near 10^{3} S cm^{-1} [4] (Figure 10).

Table 6. Different polyaniline states [4].

y-value	Name	Color	Conductivity (S cm^{-1})
1 (reduced form)	Polyleucoemeraldine base Polyprotoemeraldine base	Transparent	$<10^{-5}$
0.5	Polyemeraldine base Polynigraniline base	Blue	$<10^{-5}$
0 (oxidized form)	Polypernigraniline base Polyemeraldine salt	Purple Green	$<10^{-5}$ ~15
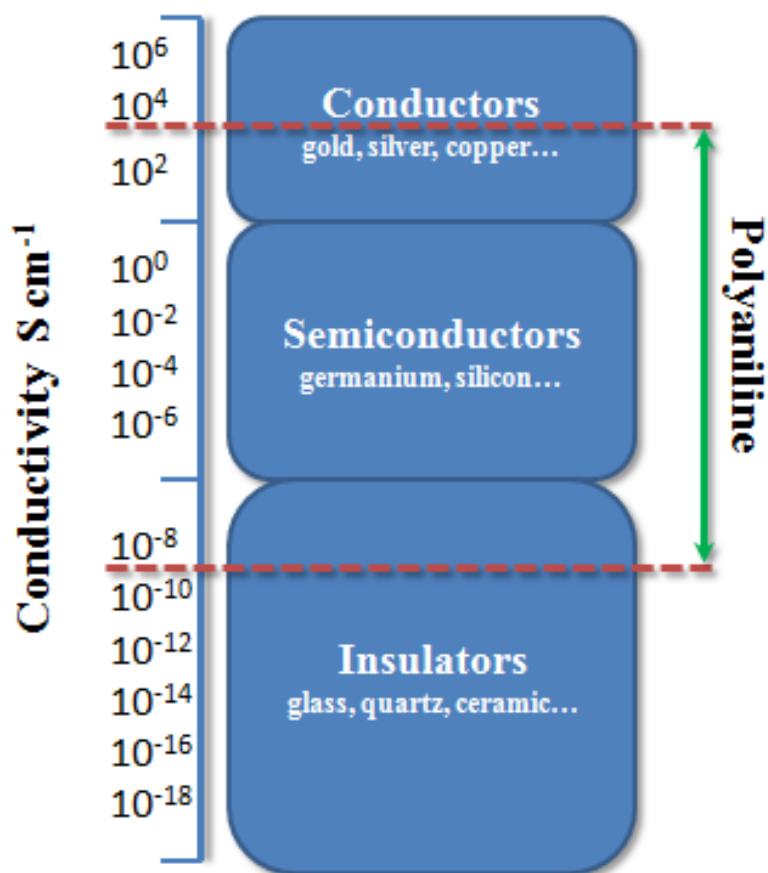
Figure 10. Electrical conductivity scale of several materials at room temperature and where polyaniline conductivity fits in its different states.

4.7.4. Ways of synthesizing polyaniline

Polyaniline is usually synthesized by oxidation of aniline through two methods: using a chemical oxidant or electrochemistry. Beside these main methods, others have been suggested, like autocatalytic polymerization [39], inverse emulsion polymerization [40], emulsion polymerization [41] and plasma polymerization [42].

4.7.4.1. Chemical synthesis

For this method three reagents are required: aniline, an oxidant, and an acid in aqueous or organic medium [4]. The chemical oxidation is performed by joining the monomer (aniline) with an oxidant in a solution; then an acid is needed to produce a polymer with linear structure. The typical acids used are sulfuric acid (H_2SO_4) and hydrochloric acid (HCl). The most

common oxidants used are for example ammonium persulfate ($(NH_4)_2S_2O_8$), potassium dichromate ($K_2Cr_2O_7$), potassium iodate (KIO_3), hydrogen peroxide (H_2O_2) and cerium sulfate ($Ce(SO_4)_2$) [4, 43].

4.7.4.2. Electrochemical synthesis

In this method there are three types of procedures that can be used for the synthesis of polyaniline. When a constant current is applied the technique is called galvanostatic, when a constant potential is applied it is called potentiostatic and if the current and the potential vary with time it is called potentiodynamic. In all three procedures the system is composed of a set of three electrodes where one of them is the working electrode where the polymer will be deposited, the counter/auxiliary electrode (platinum) and the reference electrode which mostly is a saturated calomel electrode (SCE) [4, 43].

When a comparison of the two methods of synthesis is made, electrochemical syntheses has several advantages, like being a cleaner method, because in this case there's no monomer-solvent-oxidant extraction; the doping and thickness is controlled by the electrode potential and the polymer thin layer is synthesized and deposited at the same time [4].

4.7.5. Polyaniline doping

If it is intended to obtain an electrical conducting polymer film, polyaniline has to be doped. The doping of a conducting polymer consists in the insertion of electron donor molecules (reduction) or electron acceptor molecules (oxidation). The obtained polymer is then an n-type or a p-type one, respectively [4].

The oxidative doping is realized through chemical or electrochemical processes from the totally reduced form of PANi: polyleucoemeraldine base. This doping method is very efficient and simple but as a negative aspect the doping level is hard to control, to solve that easily the electrochemical doping controls it only by adjusting the applied voltage between the counter electrode and the polymer. The other form is acidic doping, which is less employed. In this doping process the number of electrons associated to the polymer doesn't suffer any change. This method applies a strong acid (H_2SO_4 or HCl) to the emeraldine base that will induce protonation, originating the polyemeraldine salt, but the hydrochloride polyemeraldine salt is not soluble in the widely used solvents and has an unstable conductivity when exposed to moisture. To improve this issue some research has been performed [4].

4.7.6. Deposition methods of PANI layers

Several methods are available to deposit PANI films on a substrate. The ones that are most widely implemented are drop-coating, dip-coating, spin-coating, electrochemical deposition, Langmuir-Bloggett (LB), thermal evaporation, self-assembly techniques and inkjet-print. A brief description of these methods is made below:

- **Drop-coating**

The polymer solution is dried dropwise. This method can also be done directly on the substrate by in-situ reaction of some drops of monomer with an oxidant solution. So this technique is presented as simple but generally non-uniform [43, 44].

- **Dip-coating**

A substrate is dipped in a chemical polymerization solution and then removed, some amount of the polymer will come over the substrate surface [45]. This procedure can be also done by multiple immersions of the substrate in the monomer with an oxidant solution; the solution that stays on the surface will be polymerized on it. The technique controls the film thickness by the time that the substrate is dipped [44].

- **Spin-coating**

The substrate is placed in a rotating device after that, with an already prepared polymerized solution, a dispersion is performed on top of the substrate [3, 46]. This method is reported as simple for soluble conducting polymers based films, the layer is ready after proper solvent drying. The solution concentration and the spin rate of the rotating device affect the film thickness so the manipulation of these parameters will change the film thickness to an intended one. Beyond what has already been described, this method also gives the possibility to deposit conducting polymers on insulating substrates instead of only on conducting ones [43].

- **Electrochemical deposition**

Literature defines this technique as the most convenient one for conducting polymers deposition, the thickness is controlled by the applied voltage at electrodes along the polymerization process [4, 47]. This kind of deposition is only possible to be performed in conducting substrates, but it was already reported that if in between substrate electrodes the gap is in the order of some tens of microns then there is a possibility that during the film growth it could cover up the gap and short-circuit the electrodes [48].

- **Langmuir-Bloggett (LB)**

There are two different ways in the application of LB technique, one is by direct polymer deposition and the second way is by monomer deposition and then on substrate polymerization [49, 50]. The LB procedure is famous for its ultrathin films, a monomolecular layer, knowing that if a thicker film is pretended it is only necessary to perform more LB film depositions [43].

- **Thermal evaporation**

This technique is made under vacuum and the conducting polymer is heated to evaporate, then it will deposit on a predefined target in the substrate. The film thickness is controlled by the time duration of the evaporation process [49, 51].

- **Self assembly (Layer-by-Layer)**

The substrate is immersed several times first in a polymeric acid solution (dopant agent) and secondly in polyemeraldine base solution. If a thicker film is pretended it is only needed to repeat the process. In the literature polystyrenesulfonic and isopolymolybdic acids are referred as utilized dopants [50, 52].

- **Inkjet-print**

This is an interesting and versatile technique to control the deposition of functional elements. Vacuum and specific temperatures are not a requirement and moreover it doesn't need anything between the substrate and the deposition equipment. The main drawbacks of this method is the solution's viscosity that needs to be below 20 cP and the surface tension has to be in the range 28 to 350 mN·m^{-1}. It was already reported that it is possible to print polymers as long as they are in a diluted solution. As referred, this technique is implementable only for soluble conducting polymers, but is a suitable methodology for thin film manufacturing and its mass production [53].

4.7.7. Polyaniline and inorganic substrates

An important step to mass producing good organic (polymer-based) gas sensing devices was joining an organic element, like polyaniline, as sensing layer to an inorganic element like silicon as substrate. This is due to the fact that silicon is widely implemented and a well-know industrial technology. The implementation was at first very difficult, there were some technical issues with the adherence to the substrates and the conductivity of the PANI films. In the path of discovering new ways to achieve better results, several studies have been made concerning the improvement of the deposition process [4].

In recent years new studies have reached good results for the issue referred before, Sutar *et al.* [54] have developed highly crystalline nanofibrous PANI films which were prepared on amino self assembled monolayers (SAM)-modified silicon substrates. The method is referred as simple, with highly adherent films and with proper conditions for mass production. The results obtained were very satisfactory since the prepared sensors showed fast response/recovery times and good sensitivity at low concentrations (0.5 ppm) of ammonia gas.

4.7.7.1. Self assembled monolayers (SAM)

Self-assembled monolayers are composed of amphiphilic molecules, which means that it has an hydrophilic head and an hydrophobic tail just like the ones that are present in the phospholipid bilayer of human cell membranes. The SAM structure is formed by an organized automatic process that can take minutes to hours. The head groups will attach to the metallic substrate by chemisortion forming crystalline structures. The tail groups will be standing up far from the substrate (Figure 11). This process will end once the SAM molecules finish or when the substrate surface is completely filled. For conducting polymer films the better SAM are the ones with functional silane molecules [54-56].

Sutar *et al.* [54] reported the preparation of nanofibrous polyaniline films on silicon (Si) substrates pre-treated with piranha solution for 1 h (H_2SO_4:H_2O_2 in a 2:1 proportion) to generate a hydroxyl (-OH) rich surface. The SAM layer was then deposited using an amino-silane solution (in anhydrous ethanol) at an mM concentration. The polymerization of aniline was performed by chemical oxidation. In Figure 11 the process described previously is illustrated and shows how the SAM layer attaches on one side to the inorganic layer and on the other side to the organic layer.
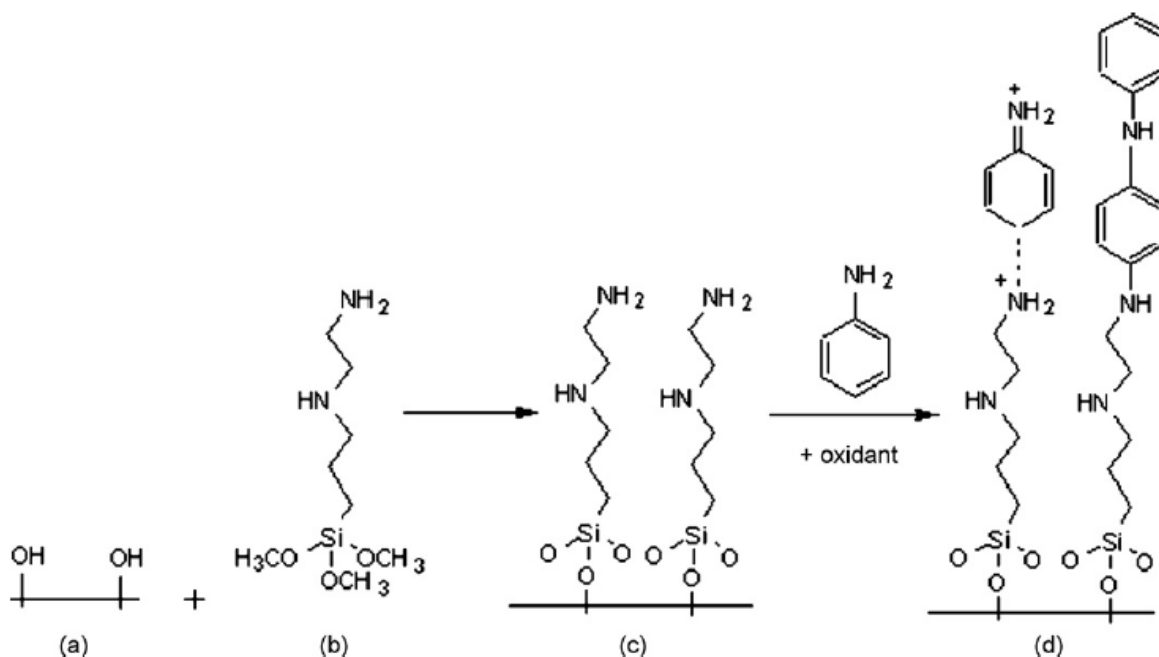
Figure 11. Amino-silane SAM layer attached with the head group to silicon and tail group to PANI. (a) Silicon substrate riched with hydroxyl, (b) amino saline molecule, (c) silicon+SAM and (d) silicon+SAM+PANI [54].

4.8. Metal oxide with conducting polymers sensors

The combination of nanocomposites of metal-oxides with conducting polymers is taking a relevant role in materials for nanotechnology. The combination of these organic-inorganic elements has raised large attention of researchers due to its physical properties and wide possibility of application areas. The improvement of physical properties is easy to understand since the objective is to combine the major properties of the materials with each other. One important factor is the fact that now metal-oxides operate at room temperature [31].

Khan *et al.* [31] have reported the first cation exchange hybrid material for ammonia gas sensor application, in particular polyaniline-titanium(IV)phosphate (TiP) cation exchange nanomaterial synthesized by a sol–gel method. This organic-inorganic composite presented excellent cation exchange behavior, reproducibility, electrical conductivity, stability, and selectivity. The response time increases with the increase of ammonia concentration, the recovery time increases when exposed to air for a few minutes (10s for 3-6% and <10s for 12%). The sensing mechanism is based on the polymer behavior towards ammonia, when exposed the film will expand, reducing the pathways for charged particles (reducing electrical conductivity). It was also reported that the PANI-TiP nanocomposite doped with *p*-toluene sulphonic acid (*p*-TSA) responds more quickly than the ones doped with HCl.

Li *et al.* [57] presented a film of polyaniline nanotubes with Mn_2O_3 nanofibers and claim that they are the first to produce polyaniline nanotubes utilizing Mn_2O_3 as reactive template to form the PANI nanotubes. The Mn_2O_3 nanofibers were prepared by an electrospinning technique with polyvinylpyrrolidone (PVP)/manganese acetate as precursor. The average nanofibers diameter was 72 nm. The PANI nanotubes had an outside and an inside diameter of 80 nm and 38 nm, respectively. The sensor substrate were prepared in the lab; in a glass recipient two Au electrodes were added, with a gap of ~60 μm, then this device was used as cathode to collect the Mn_2O_3 nanofibers and after that it was immersed into a aniline solution, which converted Mn_2O_3 nanofibers in PANI nanotubes. The prepared sensor presented good reversibility and high sensitivity, detecting 25 ppb of ammonia gas.

Tai *et al.* [58] presented an exhaustive study on PANI/inorganic oxides. They studied the morphology, chemical structure, optical properties and NH_3 gas sensing properties of the composites, which, besides PANI thin film, included polyaniline/indium oxide (PANI/In_2O_3), polyaniline/tin oxide (PANI/SnO_2), and polyaniline/titanium dioxide (PANI/TiO_2) thin films. The results obtained from the composites were better in terms of selectivity, reproducibility, longer stability, and faster response/recovery times, but only one presented a higher sensitivity for NH_3 gas measurements. All thin films were prepared by an in-situ self-assembly method. Results of X-ray diffraction (XRD) showed that PANI doesn't affect the crystallization of nanoparticles. Moreover, FTIR and UV-vis results confirmed the interaction of PANI with all the studied metal oxide nanoparticles. SEM images showed that all thin films have a porous structure, and TEM pictures revealed that the PANI nanocomposites had a core-shell structure.

Gong *et al.* [59] claim that they are the first ones reporting an ultrasensitive NH_3 gas sensor. The sensor is composed by TiO_2 nanofibers (n-type) surrounded by polyaniline nanograins (p-type) forming a p-n junction in between them. This construction allows the sensor to detect ammonia in air down to 50 ppt. The sensor has excellent reversibility to the gas. It quickly recovers from gas exposure by flowing air through the sensor chamber.

4.9. Final considerations

After the description of the several types of sensors for ammonia gas detection, Table 7 presents some reported sensors based on different measuring principles.

Table 7. Ammonia gas sensor parameters of the different principles.

Principle	Lower detection limit	Response time	Recovery time	Temperature range
Metal-Oxide				
-WO$_3$ nanostructured [32]	10 – 100 ppm	~1s	~5 s	500 ºC
-ZnO nanostructured [33]	50 – 500 ppm	<10s	<10 s	25 – 200 ºC
Catalytic metal				
-Pd-sensitized ZnO [36]	45.7 – 50 ppm	~3 s	~9 s	210 ºC
-Pt doped WO$_3$ [60]	15 – 4000 ppm	30 s	5 min	350 – 450 ºC
Surface acoustic wave (SAW)				
-ZnOSAW [35]	25 – 7500 ppm	n.a.	n.a.	room
Optical analyzers				
-Porous Si BTB coated chitosan-GPTMS [37]	0 – 100 ppm	<15 s	~50 s	room
-ZnO nanostructure [61]	50 – 5000 ppm	20 – 30 s	20 – 30 min	room
Conducting polymers				
-PPy thin film [62]	4 – 80 ppm	~20 s	~20 min	room
-PANI nanofibers [63]	5 – 200 ppm	~10 s	~100 s	room
-PANI nanoparticles [58]	1 ppm	23 – 50 s	50 – 70 s	room
Metal-Oxide w/Polymers				
-PANI nanotubes+Mn$_2$O$_3$ nanofibers [57]	25 – 300 ppb	~50 s	~100 s	room
-PANI/TiO$_2$ nanocomposite [58]	1 ppm	2 – 3 s	30 – 60 s	room
-PANI/In$_2$O$_3$ nanocomposite [58]	1 ppm	<10 s	20 – 45 s	room
-PANI/SnO$_2$ nanocomposite [58]	1ppm	2 – 3 s	15 – 30 s	room
-PANI nanograins/TiO2 nanofibers [59]	50 ppt – 50 ppm	n.a.	n.a.	room

Chapter 5

Transduction modes on PANI layers

This page has been deliberately left blank.

5.1. Introduction

Several gas sensors based on PANI layers measure conductivity changes [49, 52, 64]. As already referred in section 4.7.2, the advantage of polymers over inorganic materials is their sensitivity in conductivity variation measurements at room temperature, but, like inorganic materials, PANI is moisture sensitive which can be reversed by heating the sensitive layer. The heating process is also commonly used as a technique to counteract the aging effect [4].

5.2. Electrical conductivity variations

To improve the sensitivity and selectivity of PANI films some factors have been the aim of study, for example dopant nature, the type of aniline ring substituent, film deposition method, PANI post-treatment, and composites added to PANI. Additional physical parameters like electrode geometry and temperature can change the measurement results so it is important to improve or to take precautions with them [4].

5.2.1. Dopant nature

The nature of the dopant is one factor that influence parameters like the ones mentioned before.

5.2.1.1. Mineral Acid dopant exposed to NH_3

Mineral acids HA (A=Cl (HCl), HSO_4 (H_2SO_4), etc) are often utilized as dopant. When a sensor with this type of dopant is exposed to ammonia gas the resistance of the sensing layer increases [6, 52, 65]. PANI layers possess high affinity to NH_3, this is justified by the almost equal behavior of nitrogen atoms of both compounds when binding with protons [4].

The way that an acid doped layer reacts to NH_3 is through a mechanism called deprotonation-reprotonation [4], which is represented in Figure 12.

polyemeraldine salt
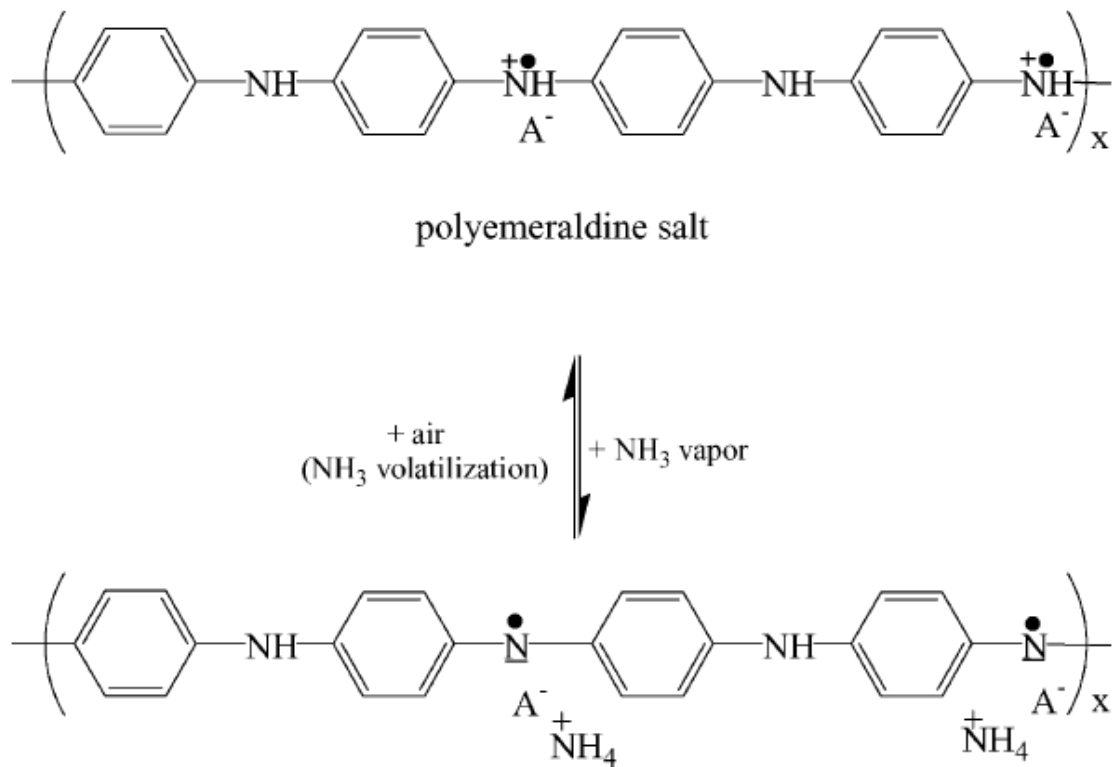
Figure 12. Deprotonation-reprotonation mechanism on acid doped layers (PANI-HA). Legend: A= Cl (HCl),HSO$_4$ (H$_2$SO$_4$). [4].

In the ammonia molecule the free nitrogen can bind with the free atomic orbital of the dopant proton. The described process leads to the deprotonation of PANI nitrogen atoms, which subsequently leads to the loss of charge carriers and consequently to an electrical resistance increase [66]. Kukla *et al.* presented an equation that describes the resistance variation with ammonia gas concentration [6]:

$$R = R_0{}^{[(\alpha N)^{1}/_2]} \tag{3}$$

R_0, is the resistance in air of the PANI layer;

N, is the concentration of NH$_3$ (*ppm*);

α, is the dimensional coefficient ($5.65 \times 10^{-3} ppm^{-1}$)

5.2.1.2. Mineral Acid dopant exposed to NH₃

In some studies other types of acids than the organic ones, like acrylic acid, have also been utilized as dopant. In these cases a decrease of the sensing layer's resistance is observed, which is contrary to what happens with mineral acids. This phenomenon is due to the NH$_3$ adsorption of $\overset{+\cdot}{N}H$ sites in the PANI-AA layer that originates a resistance increase but the NH$_3$ adsorption also occurs on acrylic acid molecules, allowing a way of conduction that causes a resistance decrease. The second event will prevail and it defines the resistance variation mode. The resistance decrease was proved by FTIR analysis [65], the phenomena is illustrated in Figure 13.
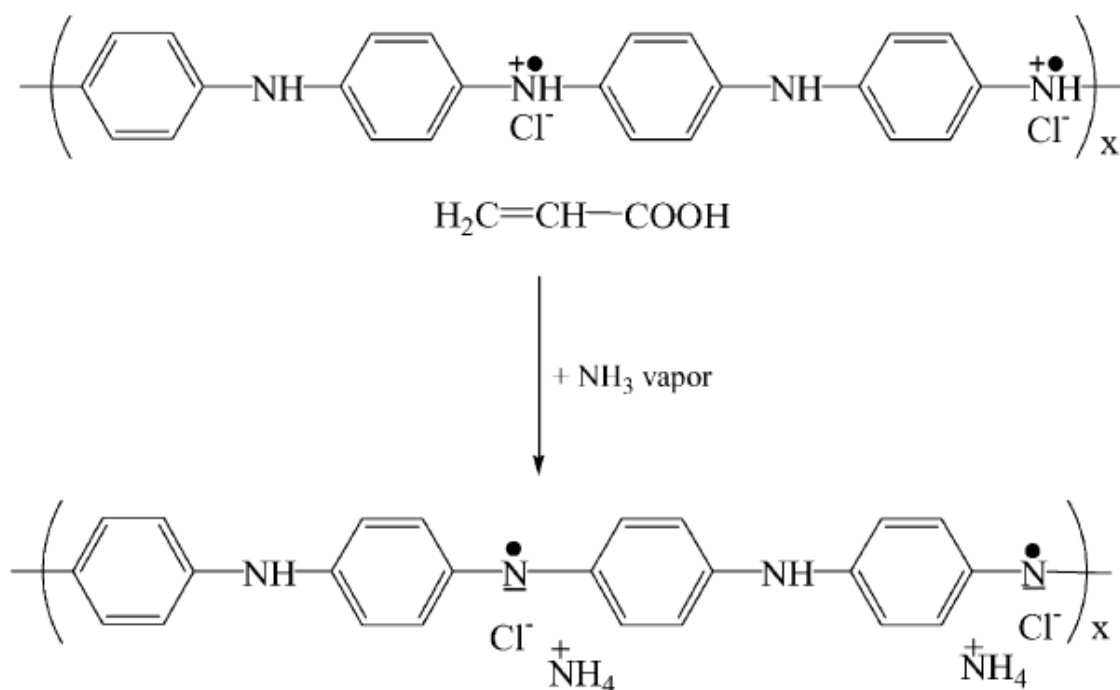
Figure 13. Mechanism of resistance decrease of PANI-AA based sensor [4].

5.2.2. Substituents on aniline ring

A study of Athawale *et al.* [67] refers the comparison of a set of sensors regarding their response while exposed to alcohol gases. The sensors were based on PANI derivatives like poly(*o*-toluidine), poly(*o*-anisidine), poly(*N*-methylaniline), poly(*N*-ethylaniline), poly(2,3-

dimethylaniline), poly(2,5-dimethylaniline), and poly(diphenylamine). It was observed that methanol, ethanol and propanol (small chain alcohols) originated a decrease in the resistance. On the other hand, an increase was obtained for butanol and heptanol. All sensors presented fast response times and the resistance difference is due to the alcohols' chain lengths and to their dielectric constant values.

5.2.3. Sensing layer deposition method

Agbor *et al.* reported the deposition by spin-coating, thermal evaporation and LB technique of non-doped PANI layers. The sensor's conductivity increased when exposed to H_2S, except for one obtained by thermal evaporation [49]. It is referred that the sensitivity and the response time to NO_2 of Langmuir-Blodgett PANI layers increase with increasing number of layers. Furthermore, the conductivity is also high thanks to protonation from the use of acetic acid in the deposition phase. The conductivity of the PANI films obtained by the thermal evaporation method is higher than spin-coating layers due to its homogeneous structure [50].

5.3. Electrical conductivity characteristics on field effect transistor

Field effect transistors (FET) have also been used for gas measurement (GasFET). In some studies these sensors were developed using PANI as the sensing layer. When comparing them with resistive sensors they demonstrate improvements relatively to electrical signal and consequently in signal to noise ratio. Another advance is the prevention of drift that is commonly present in resistive sensors [4].
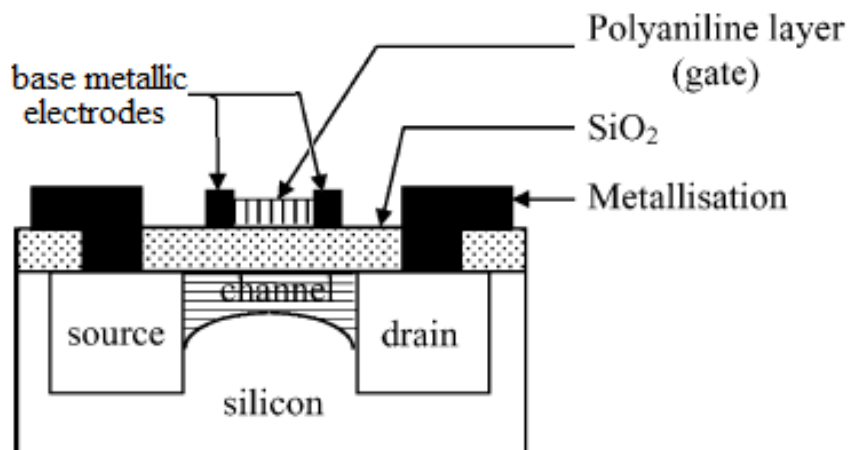
Figure 14. Diagram of a GasFET based sensor with a PANI layer [4].

Also reported was a polyemeraldine base layer deposited by spin-coating between two metallic electrodes (gate) of a GasFET for gas measurements (Figure 14). When applying a gate bias higher than the MOSFET threshold voltage, the gate's metallic electrodes become loaded but the PANI layer doesn't so quickly due to its elevated resistance, originating a delay. So a delay is necessary in order to properly charge the organic layer and consequently for the drain current to reach the saturation point. The delay depends on the temperature and the gas nature [4].

5.4. Electrical conductivity characteristics of optical parameter

Ultraviolet-visible and near infrared radiation is able to reflect electron arrangements of conducting polymers. The doping process of conducting polymers causes a change in its spectral absorbance due to the creation of polarons and bipolarons. This process is completely reversible. For example, ammonia gas when making its passage near the conducting polymer film is detectable by UV-vis or NIR spectral modifications. For this kind of application technique it is important that the sensing film is as thin as possible in order to permit the light passage. The gas sensing measurements are obtained by comparison of the transmittance or absorbance of the film before and after gas passage [4].

Figure 15 presents two common setups for optical equipments. Figure 15A shows a configuration in which the sensitive layer is placed transversely in the fiber optic [68], and Figure 15B presents a setup in which the sensing film is placed in small fractions along the

optical fiber cladding [69]. The working mechanism of the first setup is the direct measuring technique [68], on the other hand in the second mechanism the light will propagate through a multi-mode optical fiber, the light will reflect on the fiber surface where the conducting polymer is present, like referred before, giving an absorption value change in the output [69].

Conducting polymer spectra measurement analysis is a technique that allows the direct study of their electron configuration [43].
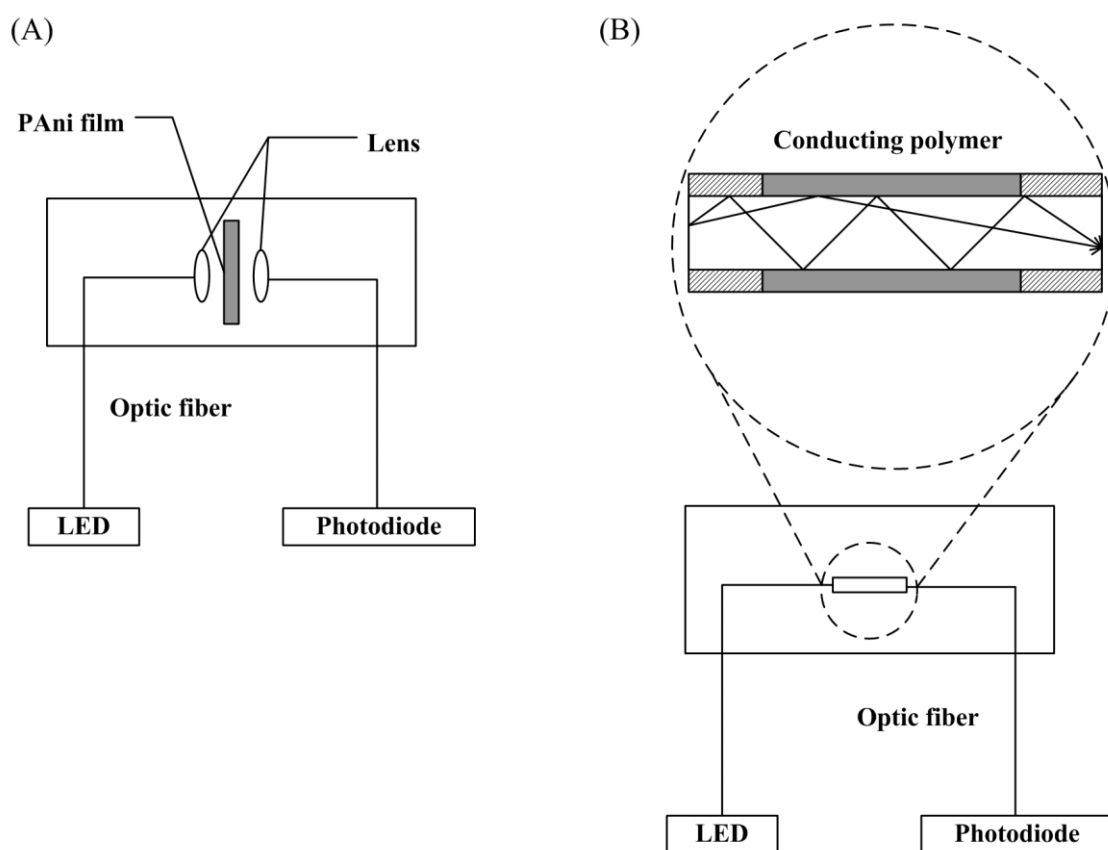
Figure 15. Diagrams of two common optical sensor configurations with conducting polymers as sensitive layer [43].

Chapter 6

PANI nanostructures

This page has been deliberately left blank.

6.1. Introduction

PANI nanostructures started attracting much attention a couple years ago for sensing proposes. Some of the materials used for this kind of applications are carbon nanotubes, semiconducting nanowires, and conducting polymer nanofibers. The chemiresistor gas sensors based on nanostructured conducting polymers can be easily modified either chemically or structurally in order to demonstrate high sensing capability to several gases. As they are polymer-based sensors they operate at room temperature. A polymer that has been widely studied is polyaniline due to its good characteristics like simplified synthesis, easy handling, excellent acid/base properties, wide range of applicability, and stable electrical conductivity [6, 49, 54]. The nanostructures applied to PANI (nanofibers, nanorods, nanowires) are created by techniques like templates, surfactants, interfacial polymerization and electrospinning. Polyaniline nanostructures increase the sensing surface area, which improves performance in many applications providing fast gas diffusion into the structure when comparing with non-nanostructured PANI [54].

This chapter will only focus on polyaniline nanofibers.

6.2. Elaboration of polyaniline nanofibers

6.2.1. Physical techniques

6.2.1.1. Electrospinning

Electrospinning is an efficient technique to generate submicrofibers, nanofibers (NFs), and PANI-NFs. On the contrary to conventional fiberspinning methods (e.g. melt spinning, wet spinning, dry spinning), this kind of methods are able to create fibers with spinnable (e.g. polyethylene oxide) and non-spinnable polymer films (e.g. camphorsulfonate) but only with a micrometer range [70-74].

The electrospinning technique is an electrostatic process and uses a high voltage electric field between polymer solution and a metallic target (cathode) to create fibers from a stream of conducting polymer solution which passes through a needle with a millimeter-scale diameter. As the stream travels in the direction of the cathode, the solvent will evaporate and the fibers will be collected at the cathode. PANI-camphorsulfonate (PANI-CPH) and PANI-polyethylene oxide (PANI-PEO) nanofibers of 5 nm were reported [71] and pure PANI solutions doped with H_2SO_4 showed a fiber conductivity of ~0.1 S cm^{-1} with a minimum diameter of 96 nm [70].

6.2.1.2. Ultrasonication

A meta-cresol solution of solid PANI and abundant camphorsulfonic acid (CSA) formed PANI-NFs buried in CSA crystals. Those crystals were dissolved by ultrasonication in deionized water originating a grid of nanofibers with 30 to 50 nm. The resulting solution was then sonicated in aqueous medium, producing PANI-CSA nanofibers of 1 to 2 nm [75].

6.2.1.3. Spin-coating

Chaudhuri *et al.* [76] reported the preparation of thin films of undoped PANI-NFs by spin-coating deposition from N-methyl pyrrolidone solution of undoped PANI, performed by MacDiarmid's method, on a pyrolytic graphite substrate.

6.2.2. Polymerization of aniline by chemical oxidation

There are several ways, discovered by researchers along the years, for aniline polymerization by chemical oxidation. In the following sub-chapters the techniques found in the literature are indicated for general information.

6.2.2.1. Hard template techniques

- Nanoporous hard-template [77, 78];
- Nanostructured seed template [79, 80];
- Nanostructrured template [81, 82];

6.2.2.2. Soft template techniques

- Synthesis of oligomer-assisted and polymer-assisted [83, 84];
- Synthesis of surfactant assisted and amphiphilic acid-assisted [85, 86].

6.2.2.3. Template free techniques

- Not-shaked-Not-stirred [87];
- Aqueous/Organic interfacial polymerization [88, 89];
- Rapid mixing [90, 91];
- Dilute polymerization [92, 93];
- Synthesis of photo-assisted [94, 95];
- Radiolythic synthesis [96];
- Sonochemical synthesis [97, 98];

- Synthesis by solid-state mechanochemical [99, 100];

- Dopant free [101, 102];

- Hydrophobic surface [103, 104];

- Self-assembled [105, 106];

6.2.3. Polymerization of aniline by electrochemical oxidation

This way of polymerization is a simple and effective technique for the production of PANI nanofibers and other nanostructures. The created nanostructures, controlled by the applied voltage, are deposited on the electrode surface [107].

6.2.3.1. Electrochemical template techniques

- Electrochemical template [108, 109];

6.2.3.2. Electrochemical template-free techniques

- Voltammetric [110, 111];

- Potentiostatic [112, 113];

- Galvanostatic [114, 115];

6.3. Polyaniline nanofibers properties and structure

In the literature there are references that powders and films of PANI nanofibers and normal PANI have the same results in the FTIR and UV-vis techniques when in the emeraldine oxidation form [79, 116]. It was also found that both polymers have similar diffraction patterns and optical spectra. These factors were proven by X-ray diffraction and UV-vis absorption analysis, the PANI nanofibers were obtained by dilute polymerization [117]. The spectroscopic analysis helped to conclude that PANI nanofibers and non-fibrous PANI have quite similar chemical structures. But on the other hand it was observed that the PANI nanofibers show some little differences in the near-infrared region, demonstrating a higher absorbance. No important changes were visible in their aqueous electrochemistry; the cyclic voltammogram presented the same two redox peaks, but their capacitances were quite different, the PANI emeraldine hydrochloride nanofibers had 122 F g^{-1} and the non-nanofiber PANI emeraldine hydrochloride had 33 F g^{-1}, when the polymers were obtain by the seed template method. Generally the capacitance is elevated in polymers prepared by seed templates, the charge/discharge cycles were better in PANI nanofibers due to their larger working area [87].

PANI nanofibers prepared by interfacial polymerization have higher torsion angles of $C_{ring} - N - C_{ring}$ segments which were observed in the analysis of electron paramagnetic resonance (EPR) spectra, Fourier Transform Infrared Spectroscopy (FTIR) and resonance Raman measurement results. This occurred due to an increase in the number of bipolarons in the PANI nanofibers' backbones when compared with conventional PANI [118]. Measurements done with small angle neutron scattering (SANS), nuclear magnetic resonance (NMR) and wide- and small-angle X-ray scattering, also showed differences between polymers, particularly in the supramolecular packing, and better ordered molecular structure in PANI nanofibers. Besides this, sharper and better organized interfaces were also confirmed [119].

For the application in biological applications, it was found that the PANI-CSA nanofibers, prepared by interfacial polymerization technique, are easily dispersed in water [120].

It was also discovered that PANI nanofibers have higher antioxidant activity than the standard PANI due to the larger working area which increases with the diameter decrease of the nanofibers [95].

It was also found that PANI-NFs doped with perflurosebacic [121] and perfluorooctanesulfonic acid produce conductive 3D microstructures exhibiting superhydrophobic capabilities [122].

Chapter 7
Electrospinning technique in the formation of PANI nanofibers

This page has been deliberately left blank.

7.1. Introduction

This technology was first discovered, developed, and patented by Formhals in 1930. Nowadays the interest in this technique is higher than ever, thanks to its great cost-benefit and effectiveness. It is applied in many scientific areas like sensors for electronics and medicine, filtration, composites, and catalysis [123]. Moreover, due to the fact that the technique is capable of working continuously renders it perfect for the mass production of nanofibers [124].

Electrospinning is utilized to create 3D, long and ultrafine fibers in a range from 100 nm to 1 μm. The nanofibers produced have great advantages like high surface area, very high porosity, capability to retain electrostatic charges, excellent cost-benefit, high permeability, providing the ability to adjust pore size and surface properties, among others. This customizable ability gives this technique the capability to fulfill any application requirement, which is a big advantage over the other techniques [125, 126]. Ceramic- and carbon nanofibers were already prepared, which increases the applicability range of electrospinning [124].

7.2. Electrospinning principle

The electrospinning setup is quite simple but can produce high quality ultrathin fibers from several polymers like PANI, polypyrrole (PPy), polythiophene (PTh), polyphenylene vinylene (PPV) and others. This is an electrostatic-based technique which commonly uses a high-voltage field between two points. It uses a high voltage electric field between polymer solution and a grounded metallic target (cathode) to create fibers from a jet of charged conducting polymer fluid which passes through a needle with a millimeter scale diameter. The jet is stretched by the intense voltage on its way to the cathode. During the transport the solvent will evaporate and the charged fibers will be collected at the cathode (Figure 16) [127, 128].
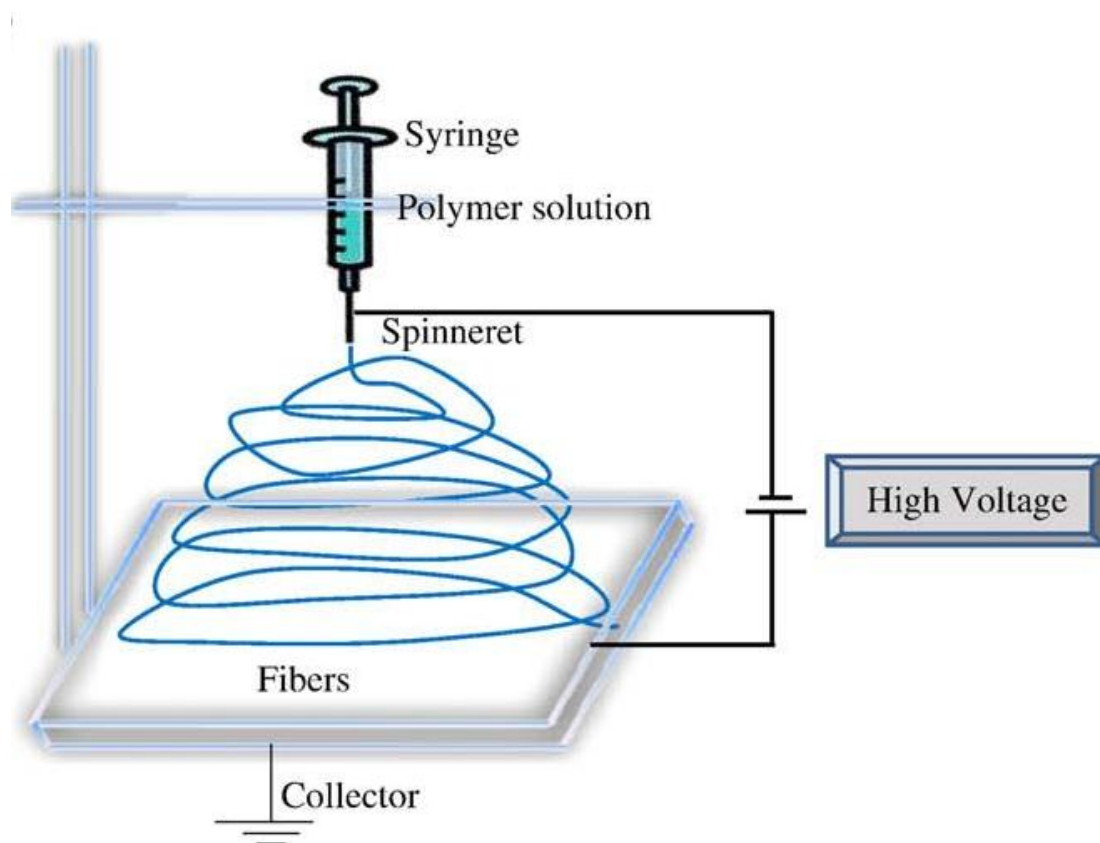
Figure 16. A typical vertical setup used in the electrospinning technique (missing the reference to the bomb that will push the polymer out of the syringe) [129].

Some great advantages of this technique is that the nanofiber structure creation is achieved in milliseconds, the huge length rate formed (1000 s^{-1}) and cross-sectional area reduction (10^5 to 10^6) [130].

The electrospinning setup has been changed several times with the objective of controlling it and adapting the microfibers/nanofibers' structure. A setup with dual syringe spinneret allows the creation of functional nanofibers like nanotubes, core-shell fibers and hollow nanofibers [130]. Another modification gives the possibility to control the fibers' orientation [131].

7.3. Electrospinning process parameters

To control the nanofibers' morphology it is needed to be aware of some parameters such as the solution properties, process and ambient conditions [126].

7.3.1. Solution properties

The solution properties include molecular weight and its distribution, chemical structure of the polymer and properties like viscosity, dielectric constant, conductivity and surface tension. The nanofibers' diameter is commonly associated to the concentration of the conducting polymer solution, so decreasing concentration will result in thinner fibers and if the decreasing continues it will reach a threshold value that changes the fiber shape into beads (Figure 17). The parameters that can originate beads are the surface tension, solution viscosity, and net charge density. High values of viscosity and net charge density prevent beads creation but if the surface tension is also high it will increase the number of beads. Besides this, the surface tension also controls the fibers' width and distribution. The addition of surfactants in the solution increases the net charge density and, as already mentioned, will prevent the formation of beads. The choice of the polymer solvent also has an important role in fiber morphology and affects the properties referred above [132].
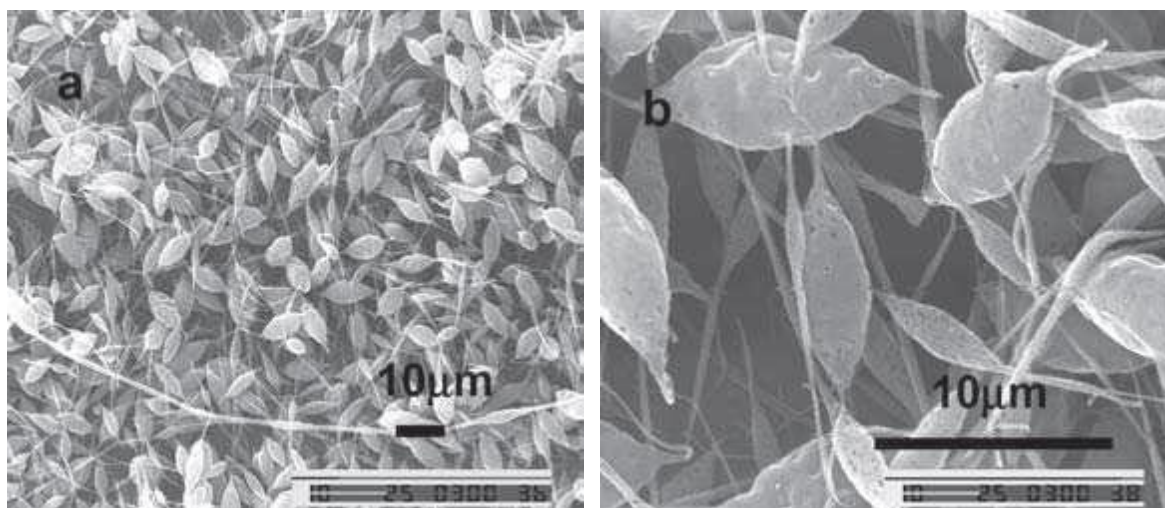
Figure 17. Two SEM images (a and b) that exemplify the bead shape. In this case are electrospun beads of polypropyl carbonate in dichloromethane [132].

7.3.2. Process conditions

The process conditions, also known as operational parameters, cover process parameters such as spinning voltage, solution feed rate, needle diameter, needle tip to target (cathode) distance and target motion. A too low voltage results in the formation of beads and a too high voltage will also create bead structures and also may cause fiber irregularities due to jet

instability and high rate of solvent evaporation, which can lead to solidification inside the tip needle. Distance changes can modify the nanofibers structure [129].

7.3.3. Ambient conditions

Ambient conditions comprise parameters like relative humidity, temperature, atmospheric pressure and spinning chamber air velocity. The humidity affects fiber pore formation, above a threshold value fiber pores are formed and if the humidity keeps raising the number of pores and their size also increases. The pores can be used positively to capture nanoparticles like enzymes or for surface increase in order to use in filtration applications. Temperature increase can be used for process acceleration, but can create abnormal structures (e.g. beads) [129].

7.4. Polyaniline nanostructures by electrospinning

7.4.1. Polyaniline nanofibers

Applying the electrospinning technique Diaz-de Leon *et al.* [133] prepared PANI nanofibers doped with sulfuric acid, PANI-polystyrene (PANI-PS) and PANI-polyethylene oxide (PANI-PEO) composites. They reported that PANI-PS has lower fiber diameters (<100 nm). The chain alignment was better in PANI-PS and PANI-PEO which leads to a higher conductivity of these nanofibers. Moreover, the obtained nanofibers appeared with cross junctions which could be used in nanoelectronics.

Most organic solvents aren't able to dissolve PANI, therefore electrospun PANI fibers are mainly found as blends. MacDiarmid *et al.*[70] reported PANI doped with camphor sulfonic acid (PANI-HCSA) ultrathin fibers blended with PEO. The fibers' structure presented uniform thickness along the fiber and the diameter range was between 950 nm and 2.1 μm. The conductivity was high for a blended film (~33 S cm^{-1}), suggesting great polymer chain alignment in the fibers.

Desai and Sung [134] studied the electrospinning method for the creation of PANI-PMMA (polyaniline and polymethylmethacrylate) fibers and their morphology. The nanofibers were obtained from PANI in the emeraldine base state which was doped with camphor sulfonic acid (CSA).

Pinto's research group [72] investigated PANI-PEO doped with CSA nanofibers. The conductivity obtained was between 0.3 and 1.0 S cm^{-1} with a fiber diameter of 100 to 200 nm. The conductivity was poor in comparison to pure PANI but they claimed that the studied nanofibers are highly adherent to SiO$_2$ and gold electrodes, which can be quite important for possible future devices.

Zhou *et al.* [71] described PANI-PEO nanofibers with average diameters smaller than 30 nm. Its electric behavior was evaluated by scanning conductance microscopy (SCM) and a single fiber transport experiment. Nanofibers lower than 15 nm behaved as electrical isolators. For *I-V* characteristic measurements electrical contacts were needed which were made by shadow mask evaporation. With the contacts, *I-V* characteristics were performed and the results showed agreement with the SCM output in the case of 15-nm fibers.

Hong *et al.* [135] developed conducting composites of PANI/nylon-6 with elevated conductivity (0.5 to 1.5 S cm^{-1}) and excellent lightness and flexibility. PANI was chemically polymerized on top of a nylon-6 electrospun nanofiber web.

Chao et al. [84] prepared oligoaniline derivative/polyvinylpyrrolidone (PVP) nanofibers with silver nanoparticles. PVP was used to immobilize Ag nanoparticles and as reducing agent oligoaniline derivative was used. The diameters obtained rounded 240 nm.

Conducting nanofibers of PANI-Al$_2$O$_3$ (polyaniline with aluminum oxide) composite were created by oxidative polymerization of aniline and by seeding with alumina nanofibers. The prepared nanofibers had diameters of around 37 to 52 nm and it was stated that the conductivity reduces when Al$_2$O$_3$ is increased [136].

7.4.1.1. PANI coaxial nanofibers and PANI nanotubes

Fibers of PANI-PMMA (polyaniline and polymethylmethacrylate) were formed by the electrospinning technique. SEM images and spectral studies prove the formation of PANI-PMMA coaxial fibers with 290 nm against the 30 nm of standard PANI fibers. The coaxial structure of the electrospun fiber mat is due to the solvent's dielectric constant, the presence of soluble organic salts, the molecular weight, and the solution's concentration. It was reported that PANI-PMMA coaxial fibers have higher conductivity than the electrospun PANI-PEO (polyaniline with polyethylene oxide) nanofibers and other PANI-based films [137].

The literature demonstrates that it is also possible to prepare PANI nanowires and PANI nanotubes by electrospinning. PANI nanotubes can be obtained by using sub-micrometer

polymer fibers as templates. The nanotubes are created by firstly electrospinning the core fibers followed by the *in-situ* deposition of conductive PANI on top of these fibers. After that the resulting PANI coaxial fibers are removed by pyrolysis forming the PANI tubular fibers [138].

7.4.1.2. PANI nanofibers with carbon nanotubes

Carbon nanotubes (CNTs), which have an excellent electrical conductivity, are a way to increase electrical capabilities of electrospun conducting fibers. Shin *et al.* presented a composite of PANI-PEO-MWNT. The multi walled carbon nanotubes (MWNT) are inserted in order to raise the PANI-PEO's electrical behavior. When exposing the conducting composite nanofibers it was verified that the CNTs that are inside the conducting polymer started to self-heat, causing a transition in the conductivity. This shift is due to the fact that the composite fibers suffered a change in their location (Figure 18). The thermal dissipation ability can be used to increase the electrical behavior of the conducting composites nanofibers by adding more CNTs [139].
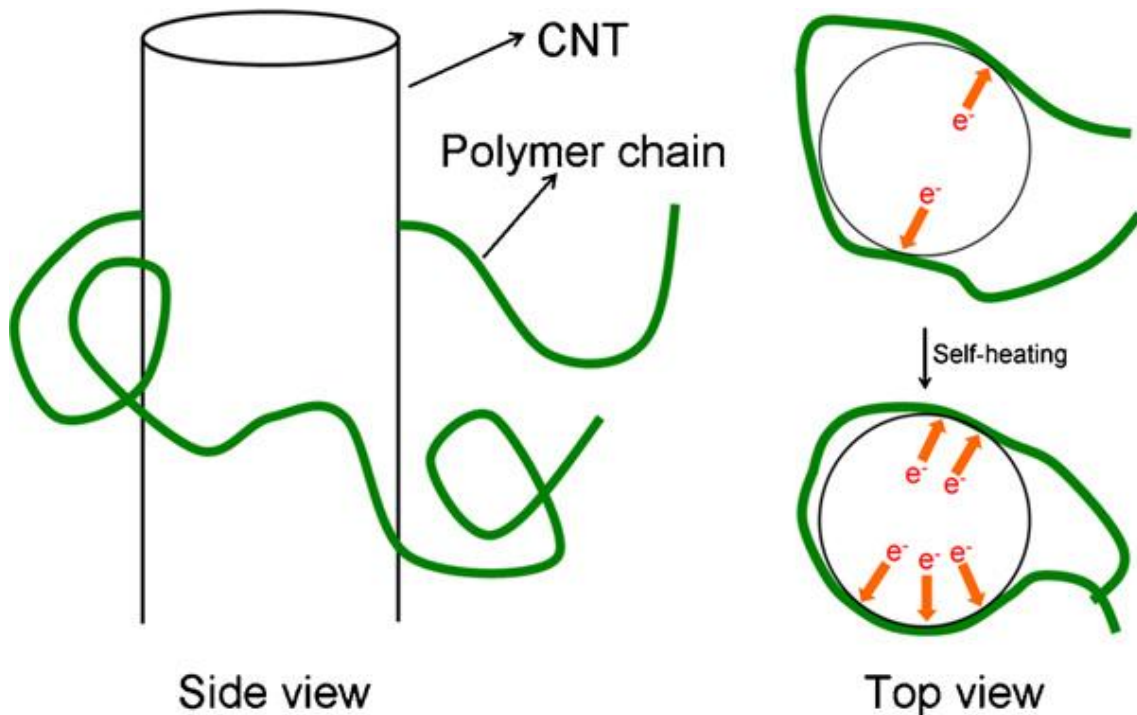
Figure 18. Location change due to the conductivity transition caused by CNT self-heat [139].

Chapter 8

Graphene

This page has been deliberately left blank.

8.1. Introduction

Graphene is a planar monolayer with strongly arranged carbon atoms in a two dimensional structure, like a honeycomb. The carbon-carbon bonds have a length of 0.142 nm. Moreover, it has great characteristics that are important for nanoelectronic applications such as the very fast electron mobility at room temperature ranging from 120 000 [140] to 250 000 [141] $cm^2 \cdot (Vs)^{-1}$, high theoretical surface area (2600 $m^2 \cdot g^{-1}$), great mechanical properties and excellent thermal conductivity (5000 $W \cdot (mK)^{-1}$) [140-142]. Their potentialities cover gas detection, devices for energy storage, transparent conducting electrodes and composites. Therefore, graphene is widely studied for use in new materials to be applied in electronics and composites. The work "for ground breaking experiments regarding, the two-dimensional material graphene" was awarded with the 2010 Nobel Prize in Physics to Andre Geim and Konstantin Novoselov [141].
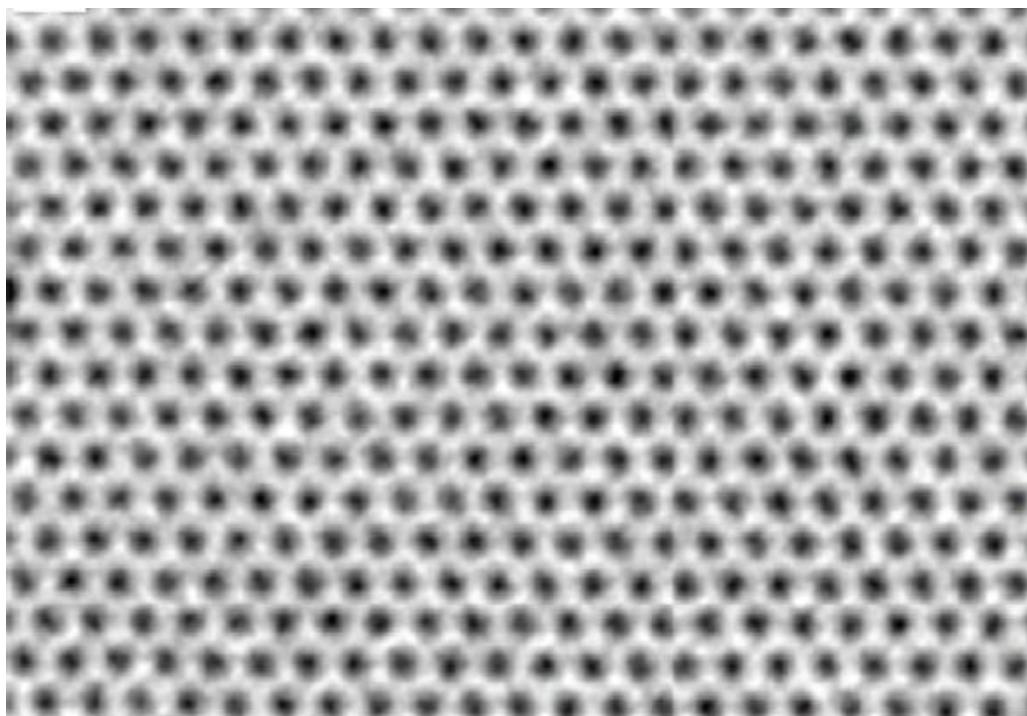
Figure 19. Transmission electron microscopy (TEM)+monochromator image of graphene membrane at 1 Å of resolution at an acceleration voltage of 80 kV [141].

8.2. Graphene oxide (GO)

Graphene oxide (GO), as its name suggests, is the oxidation state of graphene with oxygen functional groups like carbonyl, epoxide, carboxyl and hydroxyl. Its properties are extended thanks to the functional groups that provide good dispersion in water and organic solvents. The

hydrophilic capability allows an easy synthesis of polymer-GO composites by simple chemical routes. Some polymers have been reported for composites polymer-GO, such as polyaniline, poly(methyl methacrylate) and poly(acrylonitrile) for several applications, but PANI conducting polymer is the preferable choice thanks to its easy synthesis, room temperature stability, high conductivity and thermal stability [142].
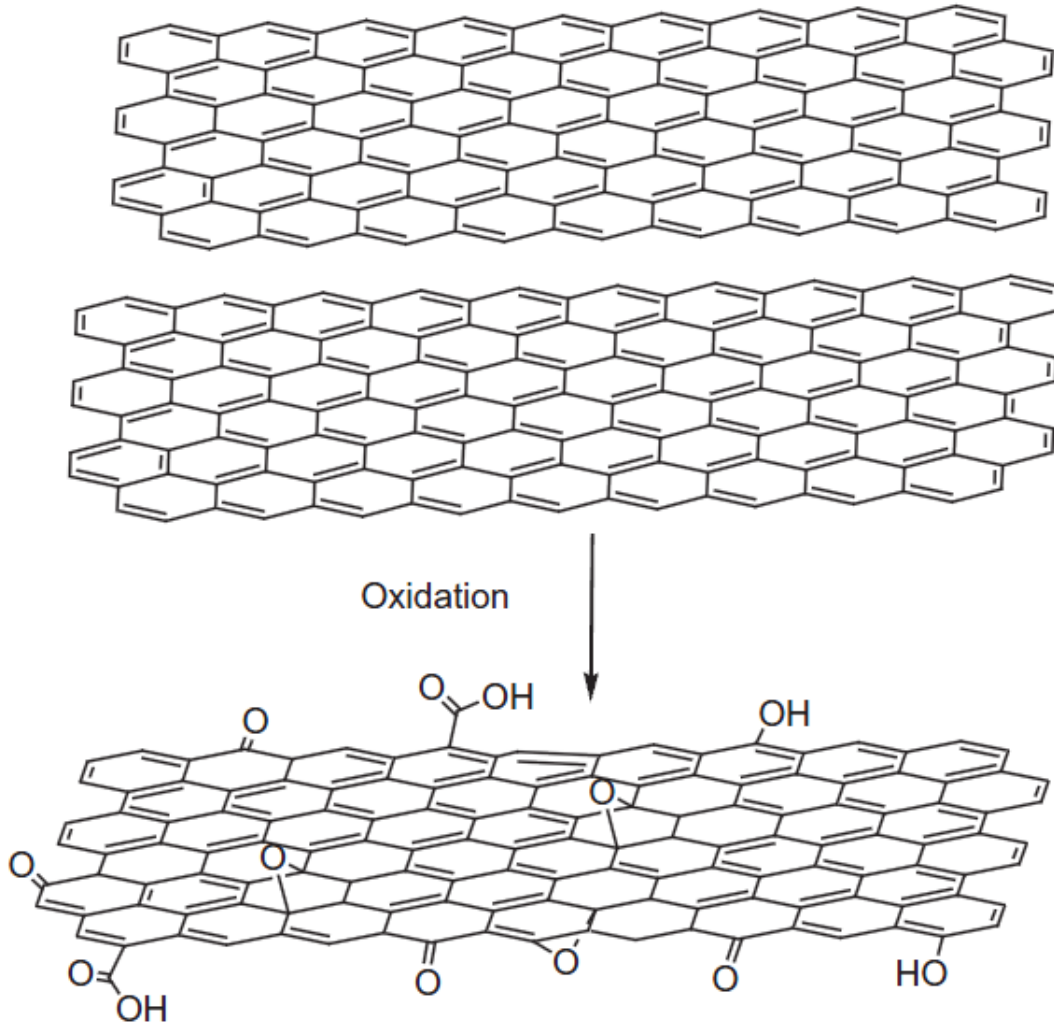
Figure 20. Oxidation process of graphite to graphene oxide [141].

8.3. Reduced graphene oxide (RGO)

GO naturally behaves as an electrical insulator material, so it is not a good material for conducting purposes, unless it is further processed as conductive nanomaterial. Moreover, the presence of functional oxygen groups turns GO thermally unstable; below 100 °C it starts losing mass and at ~200 °C the main mass loss is due to pyrolysis of the unstable oxygen functional

groups producing vapors, carbon oxide (CO) and carbon dioxide (CO_2). GO's electrical conductivity can be restored by chemical reduction. Several reducing agents were tested to chemically reduce graphene oxide sheets and hydrazine hydrate ($H_2NNH \cdot H_2O$) was found to be the best for thin graphene-like sheets production [143].

8.4. Polymer-graphene composites

The reinforcement of polymers provided by graphene brings excellent properties to the composites in industrial areas such as aerospace, automotive, electronics and green energy. Several researches have obtained successful composites similar to polymer-CNT composites but the 2D graphene has better mechanical, electrical and thermal capabilities plus a larger surface area [141].

The synthesis of graphene with polymers to form polymer-graphene composites are obtained by methods like melt mixing, solution blending, and *in situ* polymerization, which are the most common ones [141].

For graphene nanoparticle synthesis there are some problems to be aware of, such as the individual separation of pure graphene sheets, the non-uniform dispersion of NPs in graphene sheets, the NPs 2D structure connections, the role of functional groups in the new structures, NPs and graphene interactions and effects, and the presence of graphene defects. To solve many of the reported issues three main methods appeared which are the pre-graphenization, post-graphenization and syn-graphenization (one-pot strategy) [141].

This page has been deliberately left blank.

Chapter 9

Experiments

This page has been deliberately left blank.

9.1. Experimental steps

9.1.1. Materials

9.1.1.1. Reagents and solutions

The chemicals used were sodium chloride ($\geq$99.5 %, Sigma-Aldrich), potassium phosphate dibasic (Sigma-Aldrich), potassium phosphate monobasic ($\geq$99.0 %, Sigma-Aldrich), sulfuric acid (96 %, Panreac), methanol (Sigma-Aldrich), ethanol (Panreac), acetone (Merk), lead (II) nitrate (Riedel-de Haën), hydrochloric acid (Fluka), potassium chloride (Pronolab), aniline ($\geq$99.5 %, Sigma-Aldrich), sodium hydroxide (Pronolab), potassium peroxodisulfate (Riedel-de Haën), ammonium hydroxide (28–30wt % Acrôs Organics), phosphorus pentoxide (Sigma-Aldrich), potassium permanganate (Sigma-Aldrich), sodium nitrate (Sigma-Aldrich), hydrogen peroxide (Sigma-Aldrich), graphite (Merk), and hydrazine monohydrate (Sigma-Aldrich). All chemicals were used as received.

All the solutions were freshly prepared with high purity water (18.0 MΩ·cm) obtained from a Millipore (Elix 3 Advantage) water purification system. For addition of volumes Gilson Medical Electronics (pipetman®) micropipettes of 100 μL, 200 μL, 1000 μL, 5000 μL and 10 mL were used.

All pH measurements were made with the analyte in buffer medium using a pH meter (Crison, GLP 22).

9.1.1.2. Equipment

A personal computer equipped with Windows XP SP3, Intel Core2Duo (3GHz), integrated video card (Intel) and 3GB RAM was used.

An Autolab PGSTAT 12 Potentiostat/Galvanostat (EcoChemie, The Netherlands) was employed for most of the electrochemical studies. The GPES version 4.9 (EcoChemie, The Netherlands) software was used to perform a variety of electroanalytical techniques.

The majority of the electrochemical measurements were made using a custom setup (section 9.1.6.2.); the commercial sensor with a home-made film was placed in a chamber filled with an inert atmosphere of dried N_2 gas. The used techniques were cyclic voltammetry for PANI-nanofiber characterization and *I-V* characterization of PANI-RGO films, and amperometry (0.1 V) for ammonia gas measurements using PANI-RGO films. All methods and measurements were performed at room temperature (25ºC).

The polymer fibers were obtained by electrospinning. The electrospinning setup was lab made and was composed of a peristaltic pump (Gilson, Miniplus3), liquid paraffin, a polymer solution, a deposition plate, and a high voltage unit (Glassman high voltage, inc, series EH).

SEM images were obtained using a JEOL scanning electron microscope (Model FEI Quanta 400FEGESEM/EDAX PEGASUS X4M).

UV-Vis spectra were acquired using a Thermo Scientific Evolution 3000 UV-vis spectrophotometer.

9.1.2. Electrode pre-treatment

A cell stand with an undivided 25-mL glass cell was used. The glass cell was covered with a Teflon top which has three separate holes for the insertion of the electrodes viz. working electrode, counter electrode and reference electrode. The commercial screen-printed carbon electrodes (SPCEs) used in the present study (Figure 21) were supplied by DropSens (DRP-110). Ag/AgCl and platinum wire (Metrohm) were used as reference and counter electrodes respectively. Electrochemical cleaning was carried out in 0.5 M H_2SO_4 using cyclic voltammetry (25 cycles) and a potential range between –0.2 V and 1.4 V at a scan rate of 0.1 $V \cdot s^{-1}$.
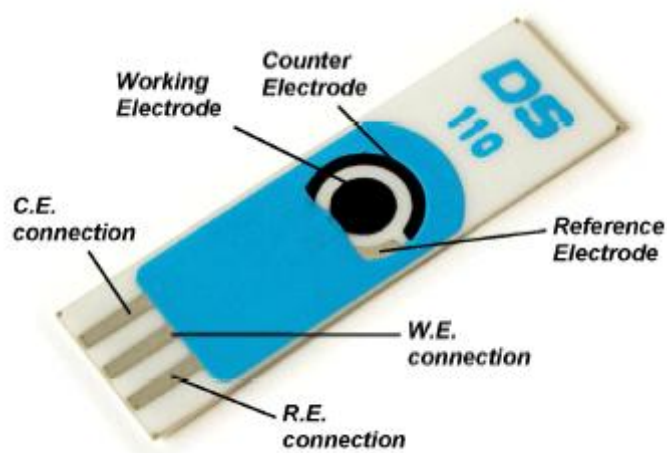

Figure 21. Screen-printed carbon electrodes used.

9.1.3. PANI synthesis

The polyaniline synthesis was based on a standard procedure [144]: oxidation of 0.5 M aniline, dissolved in 1 M aqueous hydrochloric acid, by dropwise addition of a 0.8 M potassium peroxodisulfate solution. The mixture was vigorously stirred at 5 °C for one day. To remove low molecular weight and monomeric residue, the precipitated emeraldine salt was filtered through a 0.2-nm nylon filter membrane and washed in 1 M of aqueous HCl until the filtrate was clear. To obtain the polyaniline emeraldine base state, the filtered solution was treated with 1 M of ammonium hydroxide for 10 h at room temperature. The polymer was subsequently washed with water and then with methanol. After the washing procedure the polymer was dried under vacuum conditions at room temperature for 24 h.

To 300 mg of PANI 2 mL of H_2SO_4 was added, the resulting solution was used in the electrospinning technique. The formed electrospun fibers were centrifuged at 10000 rpm for 10 min. After the deposition of the PANI nanofibers the clean liquid was discarded and pure water was added. The resulting mixture was then stirred and placed in the centrifuge again. This process was repeated 3 times. The dispersed PANI nanofibers were then dropped on the working area of the screen-printed carbon electrodes and characterized by cyclic voltammetry at different pHs using phosphate buffer saline (PBS) (section 10.1).

9.1.4. Reduced graphene oxide synthesis

Reduced graphene oxide (RGO) was prepared from ultra pure graphite powder according to Hummers and Offeman [145, 146]. The graphite powder (4 g) was oxidized at 80 °C in a solution of concentrated sulphuric acid (24 mL), potassium peroxodisulfate ($K_2S_2O_8$, 8 g) and phosphorus pentoxide (P_2O_5, 8 g). A dark blue mixture appeared which was thermally isolated and then slowly cooled to room temperature for 6 h. After that, the mixture was diluted to 300 mL and filtered through a 0.2-nm nylon filter membrane. The resulting product was dried for 12 h at 60 °C. The preoxidized graphite powder (2 g) was mixed with 92 mL of cold (0 °C) H_2SO_4 and 12 g of potassium permanganate ($KMnO_4$) was progressively added under stirring in an ice bath. After 15 min of stirring, 2 g of sodium nitrate ($NaNO_3$) was added to the mixture. The stirring was continued for 2 h at 35 °C with 200 mL of deionized water. The reaction stopped with the addition of deionized water (560 mL) and hydrogen peroxide (10 mL, 30%). In order to purify, the resulting mixture was washed with 1:10 HCl and then with deionized water. The GO product was replaced in pure water, forming a brown dispersion, which was subjected to dialysis to remove residual metal ions and acids. The purified dispersed GO was sonicated for

1.5 h to exfoliate GO, and the unexfoliated GO was removed by centrifugation at 3000 rpm for 5 min.

The GO was reduced according to a reported method [147]; 0.1 g of GO was dispersed in 50 mL of ultrapure water, 0.1 mL of hydrazine monohydrate was added, and the solution was heated at 95 ºC for ~1 h. When the reaction finished the RGO was filtered and a black powder was obtained. This powder was washed with ultrapure water for a few times in order to remove the hydrazine excess. The resulting mixture was dried under vacuum at 80 ºC to obtain the desired material. The prepared RGO samples were then characterized with UV-vis spectrophotometry (section 10.2).

9.1.5. PANI-RGO composite synthesis

The synthesis of the polyaniline reduced graphene oxide (PANI-RGO) composite was similar to the synthesis of polyaniline that is described in section 9.1.3.: oxidation of 0.5 M aniline, dissolved in 1 M aqueous hydrochloric acid, and 500 μL (for 50 mL aniline) of reduced graphene oxide, previously prepared (section 9.1.4.), by dropwise addition of a 0.8 M potassium peroxodisulfate solution. The mixture was then treated as referred in section 10.1.3, so it was vigorously stirred at 5 ºC for one day. To remove low molecular weight and monomeric residue, the precipitated emeraldine salt was filtered through a 0.2 nm nylon filter membrane and washed in 1 M of aqueous HCl until the filtrate was clear. To obtain the polyaniline emeraldine base state, the filtered solution was treated with 1 M of ammonium hydroxide for 10 h at room temperature. The polymer was subsequently washed with water and then with methanol. After the washing procedure the polymer composite was dried under vacuum at room temperature for 24 h [147].

9.1.6. Experimental setup

Three custom-made setups were used to study the properties of the synthesized PANI-RGO conducting composite. Setup 1, was used to perform the electrospinning technique, setup 2 was used to measure several ammonia gas concentrations, and finally setup 3 served to trap ammonia and to study the interfering gases.

9.1.6.1. Setup 1

Setup 1 was used to perform electrospinning. A peristaltic pump with a tube filled with liquid paraffin and 2 syringes were used to produce a hydraulic movement. To one of the previously referred syringes another syringe (glass), in which the polymer was placed, was attached. The needle of this syringe was connected to the high voltage unit. These elements were placed vertically at some distance from the base onto which the electrospun nanofibers were deposited. The used base was an inox plate, connected to ground, with 50 mL of 5% H_2SO_4. The layout of this setup is presented in Figure 22.
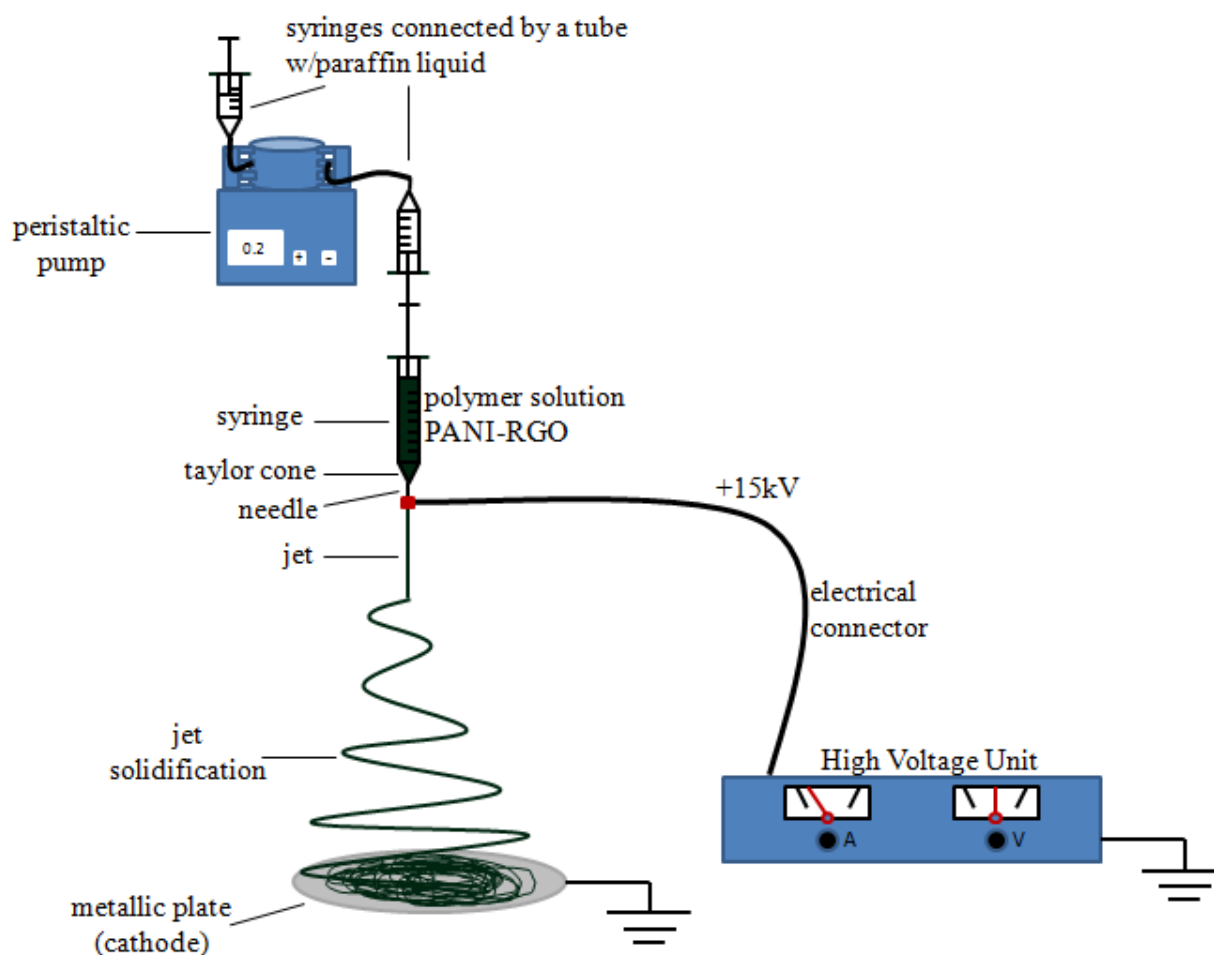
Figure 22. Diagram of the home-made setup for electrospinning, setup 1.

9.1.6.2. Setup 2

Setup 2 was used to measure several ammonia gas concentrations and was constituted by a 20-mL chamber in which the sensor was placed, an Autolab PGSTAT 12 (EcoChemie), a computer, and all necessary connectors. Connected to the chamber were: an inlet for ammonia

gas, an inlet for nitrogen gas, and an outlet for gas removal. A chamber filled with sodium hydroxide was placed in the middle of the nitrogen supplier tube to remove moisture from the gas. The layout of setup 2 is presented in Figure 23.
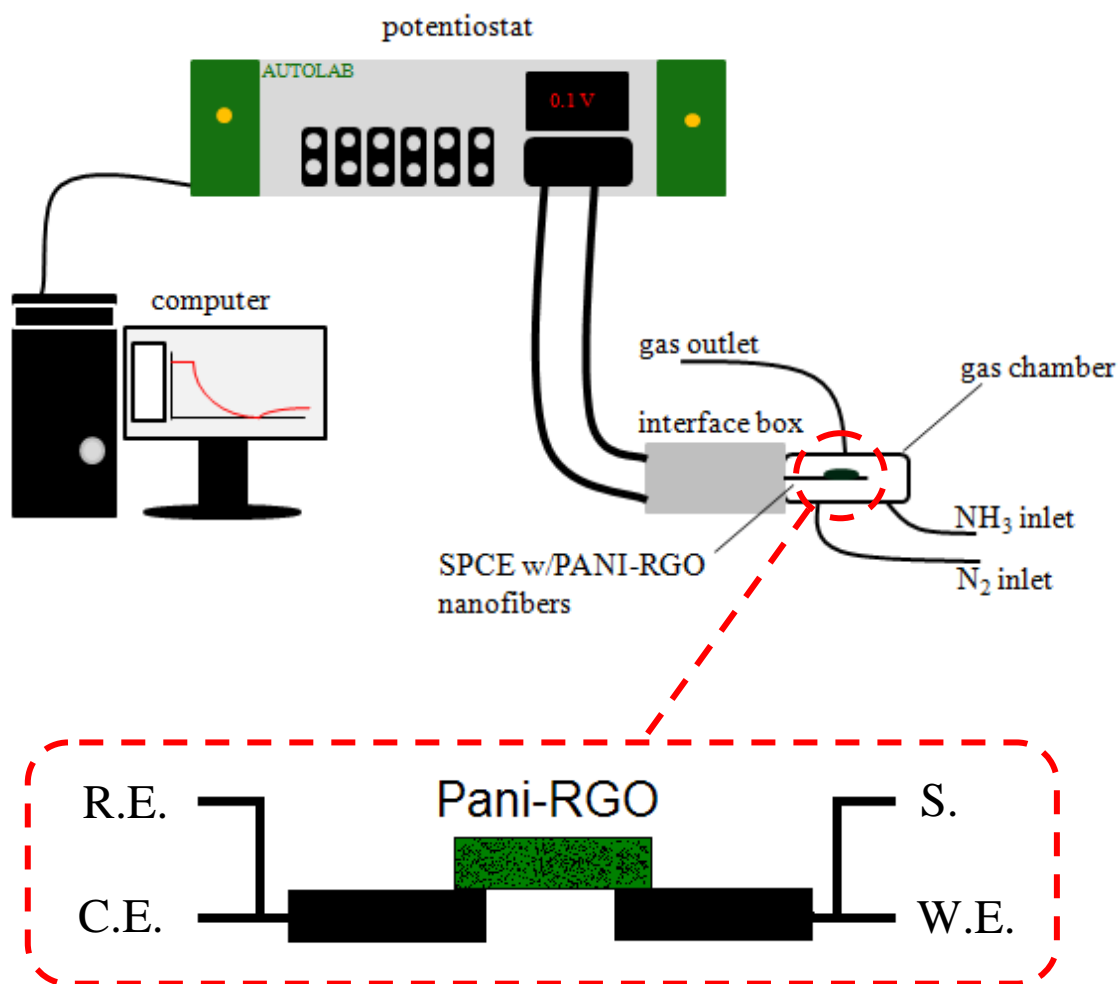
Figure 23. Representation of setup 2 which is the one where the ammonia gas was measured. The lower diagram shows in particular the sensor connection to the potentiostat, R.E.- Reference electrode; C.E.- Counter electrode; W.E.- working electrode; S. - sense electrode.

9.1.6.3. Setup 3

Setup 3 served to trap the ammonia and the interfering gases and was constituted of a 2 L glass container with 2 openings, one was used to insert ammonium hydroxide and the other contained a stopper connected to a tube. This tube (outside the glass container) was connected to

a sodium hydroxide moisture trap and a syringe that was used to collect 20 mL of dry ammonia gas that will be injected in setup 2 for measurement. The glass container is then placed in a heater. The layout of setup 3 is presented in Figure 24.
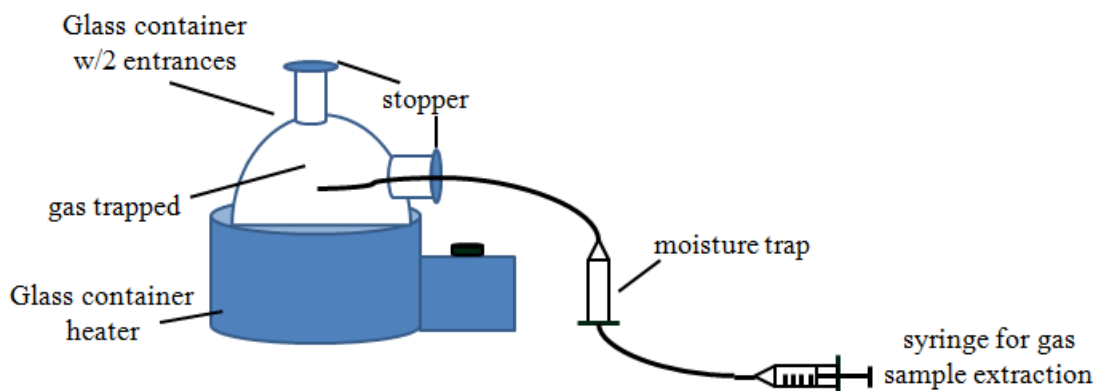
Figure 24. Diagram showing home-made setup 3 for trapping ammonia gas.

9.1.7. Ammonia sensing experiments

9.1.7.1. Electrospinning process

In order to create a sensitive layer for ammonia gas detection, a PANI-RGO composite was synthesized (section 9.1.5.). A 300 mg portion of the dried composite was mixed with 2 mL of H_2SO_4 and stirred vigorously, originating a new solution. Using setup 1, 0.5 mL of this polymer solution was placed in a glass syringe. The needle of the syringe, with a diameter of a few millimeters, was connected to the terminal of the high voltage unit which will provide a tension of 15 kV. The previous components were all placed vertically. The resulting electrospun nanofibers were collected on a grounded inox plate with 50 mL of 5 % H_2SO_4. The electrospun fibers were collected in a glass container and left for some hours to deposit. The liquid excess was then removed and the nanofibers were centrifuged at 10000 rpm for 10 min. The PANI-RGO nanofibers were deposited on the bottom and again the liquid excess was discarded and pure water was added then stirred and placed in the centrifuge. This process was repeated 3 times in order to remove contaminants. After this process the dispersed PANI-RGO nanofibers were stored and diluted in eppendorf tubes: 50 µL of PANI-RGO nanofiber solution was added to 950 µL of water. This final solution was stored in an eppendorf tube and was used to coat the working area of commercial screen-printed carbon electrodes for ammonia gas measurements by amperometry. After coating the sensor with polymer composite it was placed under vacuum and left to dry at room temperature.

9.1.7.2. Ammonia gas samples

In order to produce ammonia gas setup 3 was used. The glass container had 2 entrances, which were both covered with stoppers; one had a tube connected to it where the ammonia gas will travel when captured. At the end of the tube (outside the glass container) a sodium hydroxide-filled chamber for the removal of moisture from the ammonia gas was placed. This chamber was connected to a syringe for the collection of samples. The ammonia gas was formed by heating the glass container with a specific amount of ammonium hydroxide. Like this, the pretended ammonia gas and some water vapor were released according to equation (4).

$$NH_4^+ + OH^- \rightarrow NH_3 + H_2O \tag{4}$$
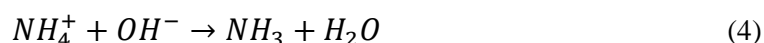
9.1.7.3. Ammonia gas measurements

The experimental setup for ammonia gas detection is shown in Figure 23. As described in setup 2, the commercial SPCE, which has a polymer-coated (PANI- or PANI-RGO nanofibers) working area, was housed in a gas chamber (20 mL capacity) at 25 ºC. One of the inlets of the gas chamber was linked to a 20 mL syringe that was previously filled with dry ammonia prepared in the setup 3. Gas injection was performed at a constant rate. The concentration of ammonia gas was fixed in setup 3, and in order to change the gas concentration dilutions were made with dry nitrogen gas. For example, if the syringe is completely filled (20 mL) there will be 500 ppb of ammonia gas, but if only 10 mL of ammonia gas is drawn and the remaining 10 mL are made-up with nitrogen gas, the final ammonia gas concentration will be 250 ppb. Before ammonia gas measurements the *I-V* characteristics of the coated SPCEs were checked by cyclic voltammetry between 0 V and 1 V at a scan rate of 0.1 V·s^{-1} for 2 cycles in a N_2 atmosphere. Then the SPCEs were protonated with HCl gas until the saturation point is reached (increase of current) being left for some minutes, then N_2 gas was injected at a constant rate to remove the HCl gas from the sensor chamber (current decrease), this removal ended when the current stabilized. Then the ammonia gas measurements were performed, several exposures were made for each concentration in order to obtain average values. The measurements were performed using an amperometric method at a fixed potential of 0.1 V and the variations in measurements were recorded.

Before the ammonia gas measurements the best film thickness for its detection (0.18, 0.35, 0.53, 0.70 and 0.88 mg /cm^2) was studied. The procedure was based on the one already referred

for measuring ammonia gas, only differing in the used ammonia concentration, which was fixed for all thicknesses. Studies of interfering gases were performed in the same way as in the thickness study. The interfering gases were added to the ammonia gas in setup 3 and then extracted by a 20 mL syringe and injected in the sensor gas chamber where measurement was performed. The selected potential (0.1 V) was based on the fact that applying a potential to a circuit as low as it admits, brings advantages, like better energy efficiency, which lead to lower losses by heat dissipation and therefore longer material lifetimes.

This page has been deliberately left blank.

Chapter 10

Results and Discussion

This page has been deliberately left blank.

10.1. Electrochemical characterization of PANI nanofibers

The electrochemical behavior of polyaniline nanofibers on the commercial SPCE was investigated by cyclic voltammetry in buffer electrolytes at different pH values. The electrochemical response that was observed was the well defined redox couple in the potential range between -0.2 and 0.8 V.

At pH=1 the cyclic voltammogram of polyaniline (Figure 25, curve **a.**) shows one well defined redox peak at 0.222 V with a current intensity of 28.34 µA. When the pH of the electrolyte was increased from 3 to 10 a shift in the peak potential towards more negative values was observed (Figure 25). At pH 3 a reduction peak is presented at a potential of 0.210 V (current intensity: 18.17 µA). In Figure 26 it is more clearly visible that at pH 4 and pH 5 a peak is still obtained, but the peak is attenuated, presenting a reduction of 92.61% and 98.77 %, respectively, in comparison to pH 1. For higher pH values the peaks disappear, which means that polyaniline lost its conductance and becomes almost electroinactive at a pH higher than 7 [148].
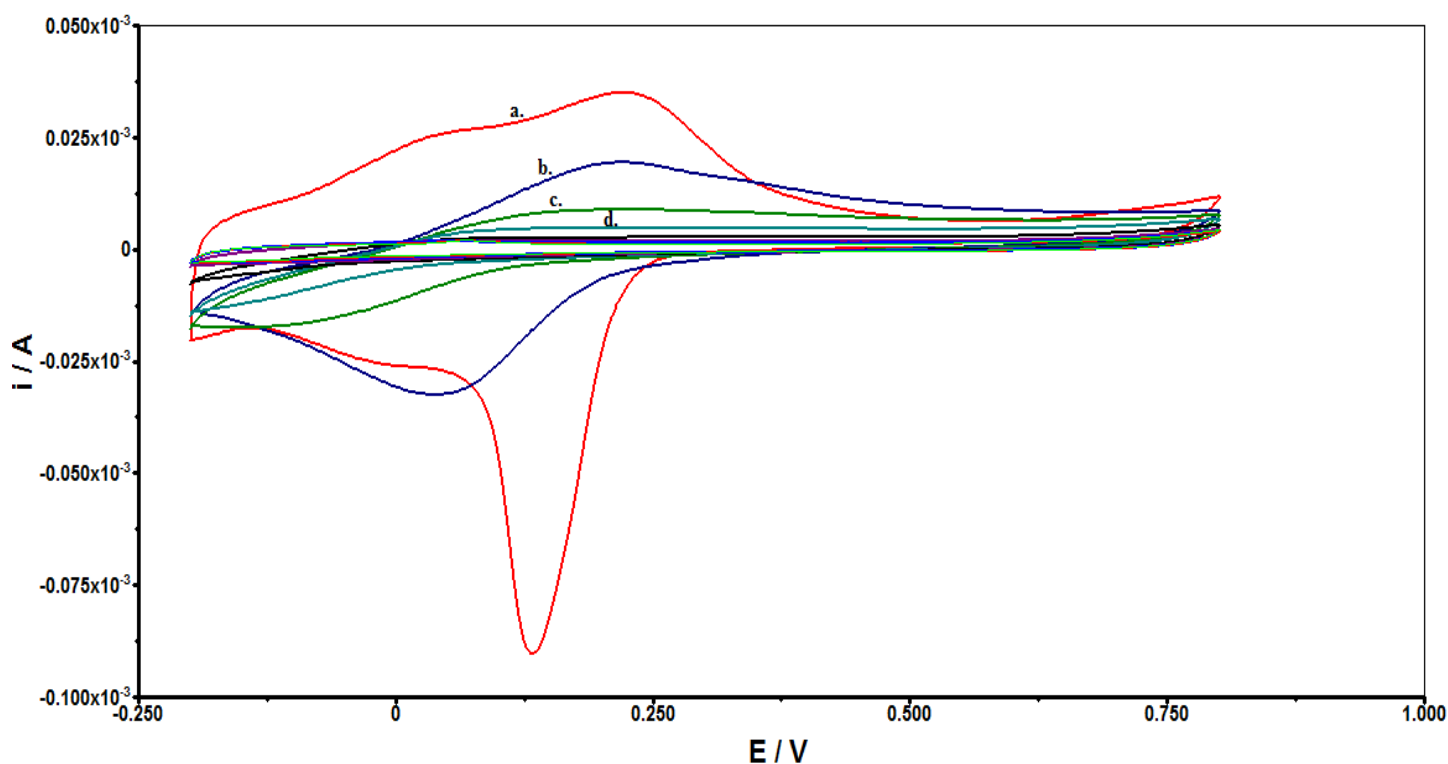
Figure 25. PANI nanofibers behavior when exposed to a drop of PBS pH variation: curve **a.** is pH=1, curve **b.** is pH=3, curve **c.** is pH=4, curve **d.** is pH=5, the other curves are from pH=6 to pH=10 at a scan rate of 0.1 V·s⁻¹.
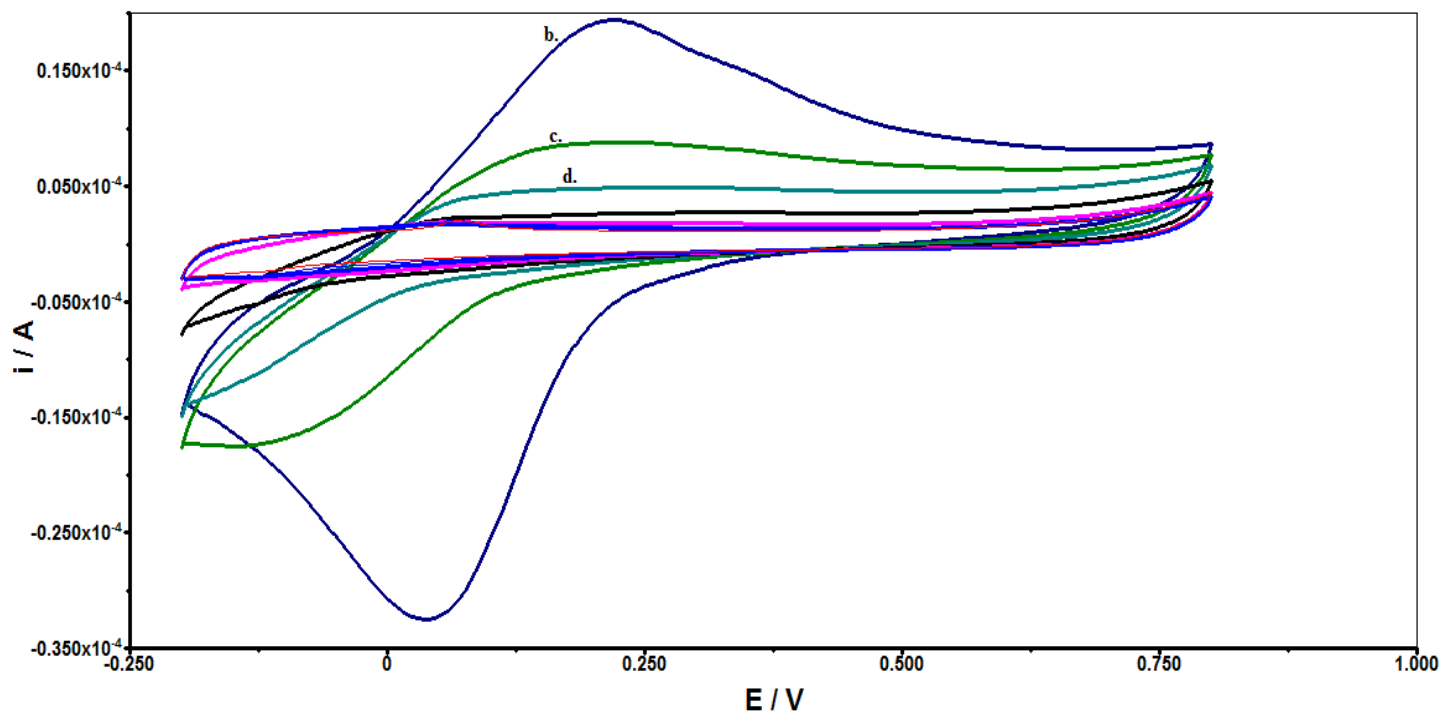
Figure 26. Similar to the Figure 25, the change is that pH=1 is not present so PANI nanofibers behavior when only exposed to a drop of PBS pH variation are more visible: curve **b.** is pH=3, curve **c.** is pH=4, curve **d.** is pH=5, the other curves are from pH=7 to pH=10 at a scan rate of 0.1 $V \cdot s^{-1}$.

That indicates that the oxidation-reduction in the polyaniline film presents changes in its electrical conductivity or resistance, which is the basis of electrical conductive change on NH_3 polymers based sensor.

10.2. UV-vis characteristics of RGO

One property of graphene is its photoluminescence (PL). RGO was observed to be a blue PL which is the most important for displays and lighting applications. As RGO has PL properties its absorbance was investigated using UV-vis spectrophotometry using RGO suspended in a solution of ultrapure water. The absorbance peak was found at ~270 nm (Figure 27), which is in agreement with previous reports [149]. This absorbance wavelength is an indication that significant electronic conjugation has been restored at least to some range, after chemical reduction, in the carbon framework of the graphene nanosheets.
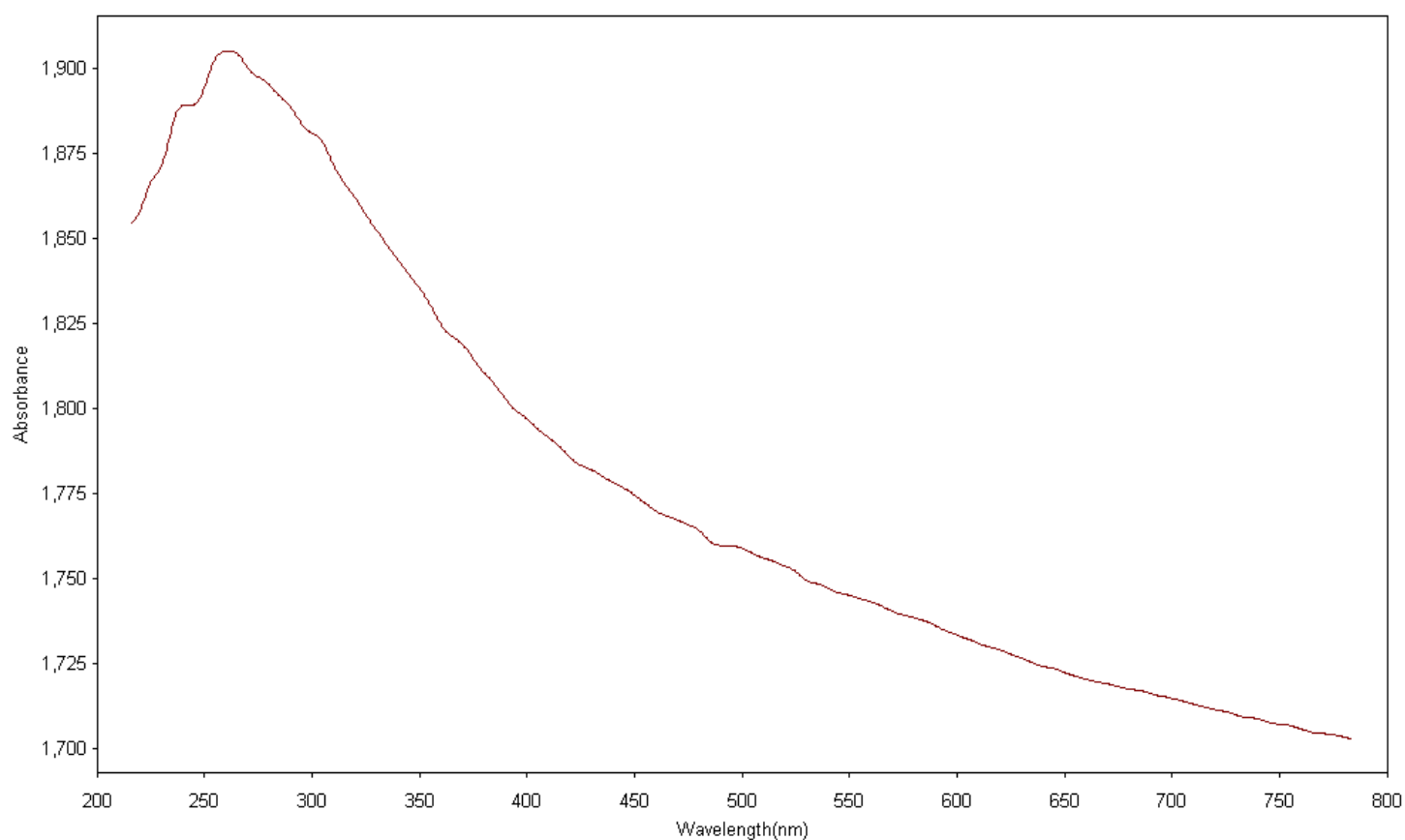
Figure 27. UV-vis spectrum of reduced graphene oxide (quartz cuvette).

10.3. SEM images of PANI-RGO nanofibers

The morphology and fiber diameter of the fabricated PANI-RGO electrospun fibers was checked using SEM (Figure 28). The individual electrospun PANI-RGO fibers appear to be indiscriminately dispersed in the mat, the thickness was generally uniform along the fiber and no bead presence was found. The average nanofiber diameter was about 500 nm.
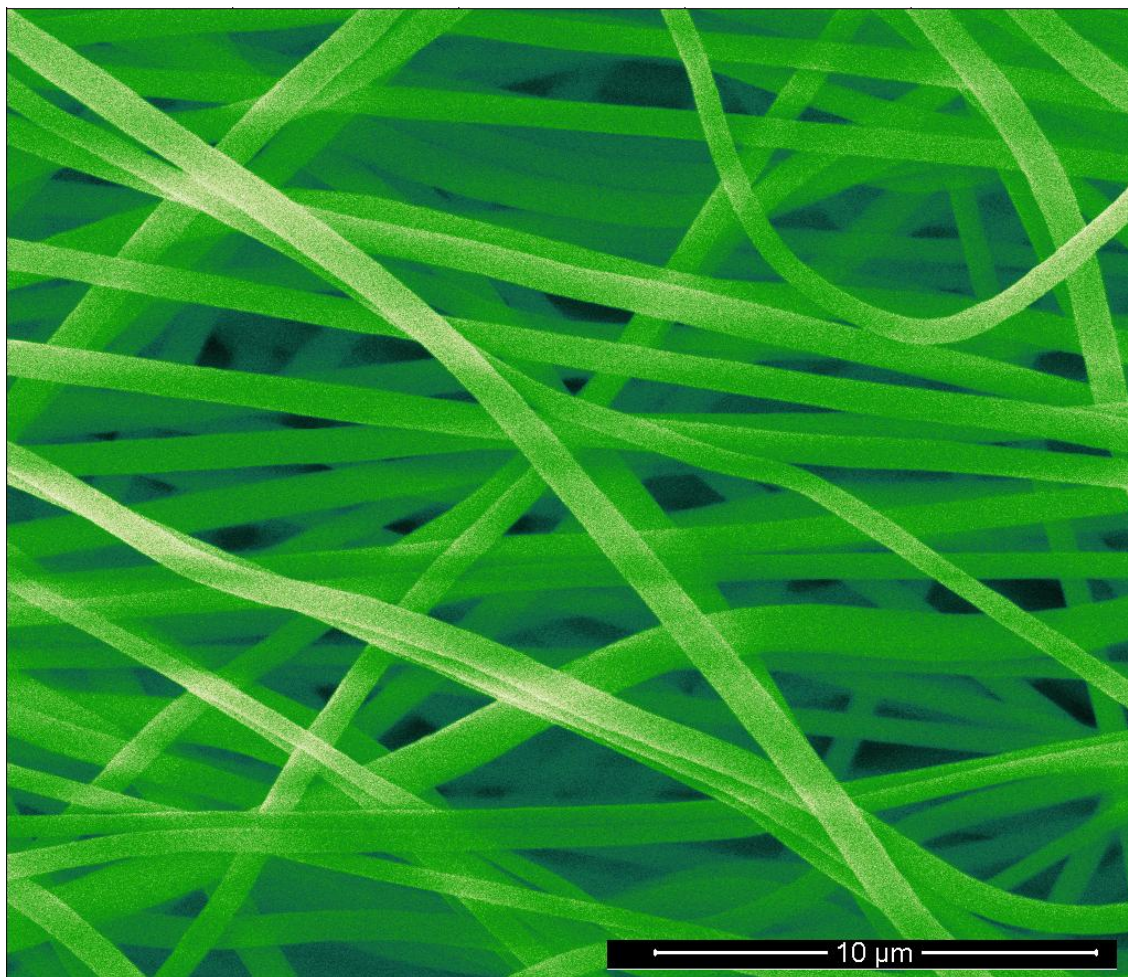
Figure 28. SEM image of electrospun PANI-RGO nanofibers.

10.4. Layer thickness study of PANI-RGO nanofibers

A key attention in the fabrication of the sensor was the effect that the thickness of PANI or PANI-RGO layers would have on the sensor's behavior. Thicker films would presumably result in better conductance and therefore, greater measured currents. However, this may have a negative impact on the response time of the sensor. In terms of production, thinner films mean less material and faster manufacture. However, care must be taken to ensure that viable and reproducible films are obtained. To this end, the relationship between layer thickness and electrode response to ammonia was investigated to determine the optimum amount of deposited PANI-RGO nanofibers composite. The PANI-RGO nanofibers were deposited as follows: for the 0.35 mg /cm^2 (20 μL) thickness, 20 μL of a 20-mg/ml PANI-RGO nanofiber dispersion was placed to cover the printed electrode and the electrode gap (1.13 cm^2) of the SPCE and then dried; for the 0.53 mg /cm^2 (30 μL) thickness, 15 μL of the 20-mg/ml dispersion was dropped on the SPCE, which was then dried and afterwards a second volume of 15 μL was added and the

sensor was left to dry again; for the 0.70 mg /cm^2 (40 µL) thickness, a 20-µL volume of the 20 mg/ml dispersion was added and once the coat dried a second volume of 20 µL was added and the senor was then dried again; finally for the 0.88 mg /cm^2 (50 µL) thickness a drop of 15 µL was added first and after drying another drop of 15 µL was added and after the film dried another 20 µL was added, and the sensor was left to dry. The method of dropping several layers was used due to the fact that if all the PANI-RGO was added at once, for example 40 µL, the polymer composite could run off the sensor's area of interest and some film amount would render worthless as sensitive film for gas measuring. The objective was the uniform coating of the sensing area.

The ammonia gas measurements were performed as soon as all the SPCE were prepared. The used ammonia gas concentration (~2 ppm) was obtained after dilution using experimental setup 3 (section 9.1.6.3.) and the measurements were performed with setup 2 (section 9.1.6.2.). In these experiments the relative resistance responsivity was defined as $S=(\Delta R/R_0)\times100\%$, where R_0 and R are the original resistance (before exposure of ammonia) and the maximum resistance (after exposure of ammonia) of the film upon exposure to the ammonia gas, respectively. The average responses of five independent measurements of 1.83 ppm ammonia for different PANI-RGO film thicknesses are shown in Figure 29.
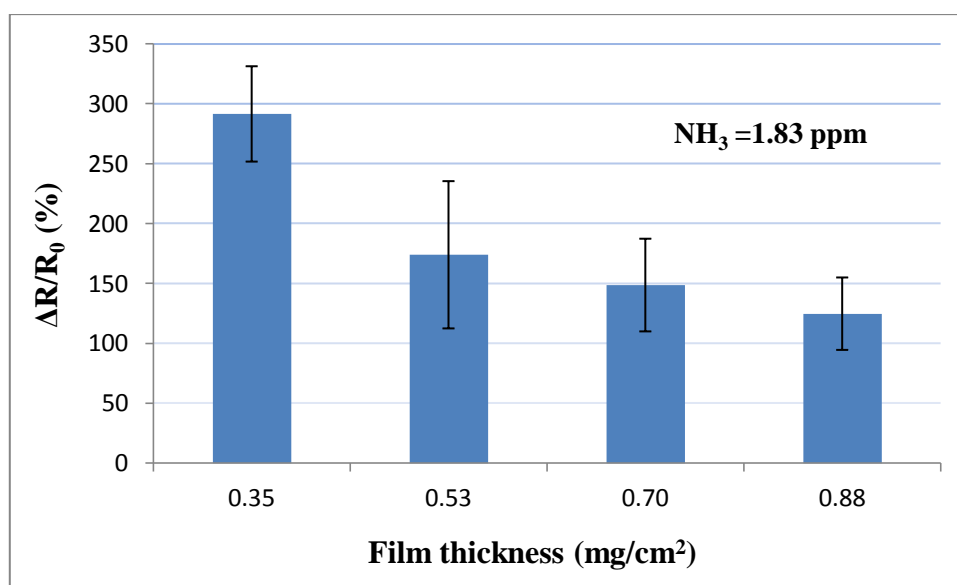
Figure 29. Responses ($\Delta R/R_0$) of SPCE with 4 different drop amounts of PANI-RGO composite, is important to refer that 0.18 mg/cm^2 (10 µL) film was also tested but didn´t give any response. All measures were performed at ~2 ppm.

The obtained results (Figure 29) revealed that the 20-µL film provided the highest response ($\Delta R/R_0$) of all sensors, therefore it was chosen for ammonia gas analysis. The response of the

PANI-RGO film decreased gradually with increasing PANI-RGO film thickness. However, film thicknesses of 0.35 mg /cm^2 (20 µL) and 0.70 mg /cm^2 (40 µL) were selected for further studies.

10.5. *I-V* characteristics of PANI and PANI-RGO nanofibers

The *I-V* characteristics of PANI- and PANI-RGO-nanofiber films of 0.35 mg /cm^2 (Figure 30) and 0.70 mg/cm^2 (Figure 31) were measured in nitrogen ambient. They appeared to be strictly linear in the 0 to + 1 V range and showed a total absence of contact or hysteresis phenomena. The only difference is that the PANI films have a lower current/resistance range than the PANI-RGO films. The latter are therefore better for wide range measurements. Nevertheless, all results point to an ohmic behavior and an increase in current range of both the PANI- and the PANI-RGO nanofibers.
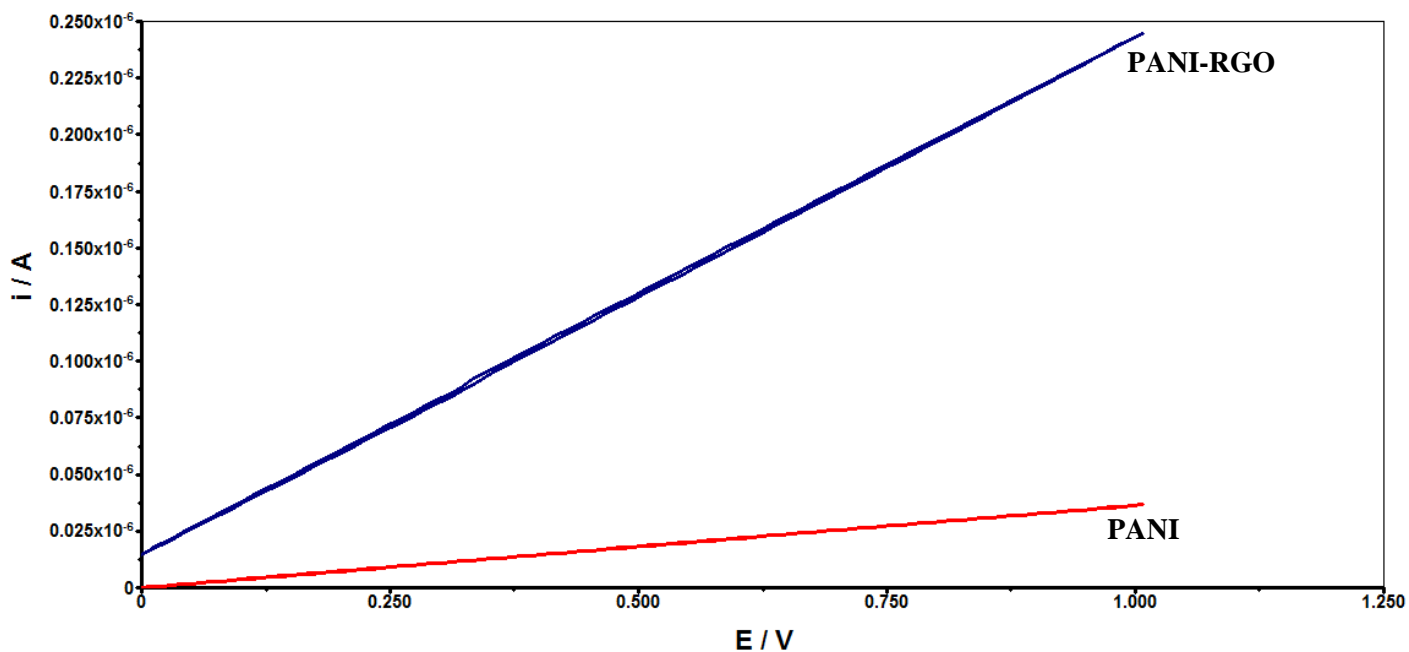
Figure 30. *I-V* characteristics of 0.35 mg /cm^2 of PANI-RGO and PANI nanofibers films in a range of 0 to +1 V.
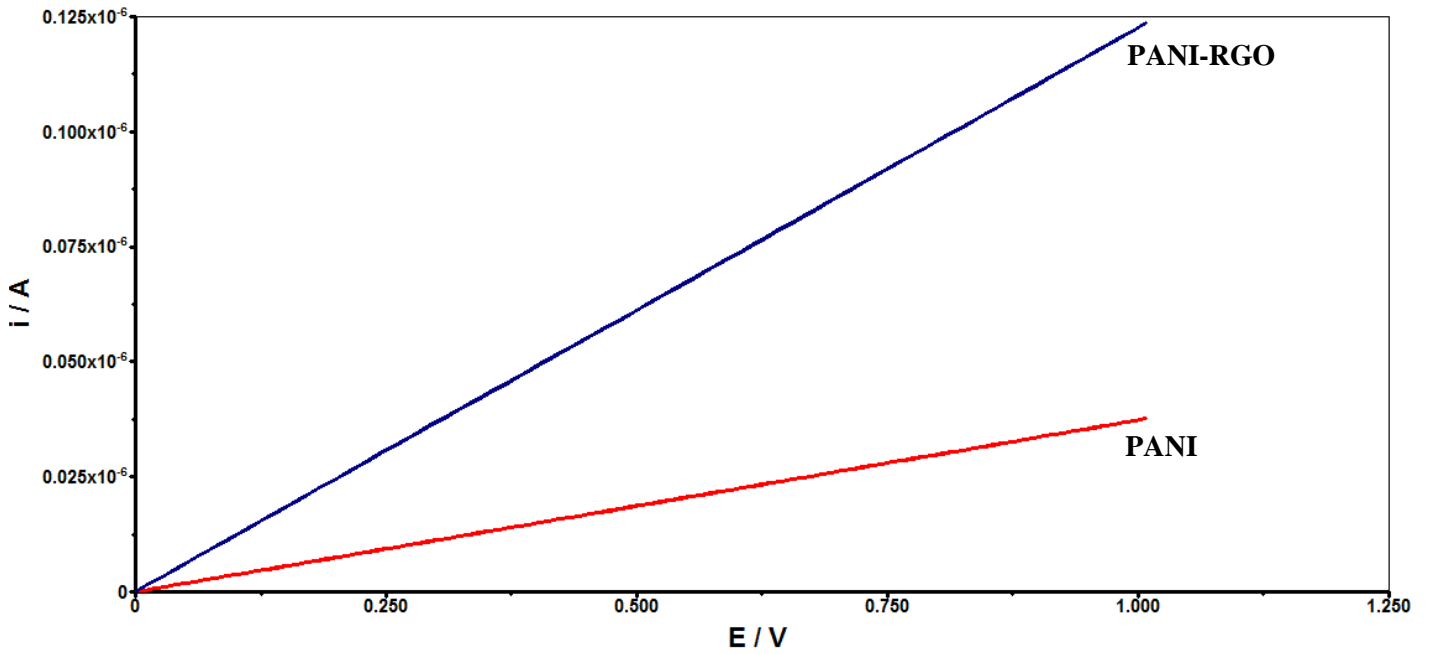
Figure 31. *I-V* characteristics of 0.70 mg /cm^2 of PANI-RGO and PANI nanofibers films in a range of 0 to +1 V.

The previous figures present the *I-V* characteristics of the PANI-RGO and PANI nanofiber films as $E(V) = f(I(A))$. To obtain the corresponding resistivity values only the application of the Ohm law is needed, $R = {V}/{I}$.

10.6. Ammonia gas measurements using PANI- and PANI-RGO nanofibers

The best thickness was found to be the 0.35 mg /cm^2 (section 10.4), however 0.70 mg /cm^2 showed a better response at very low concentrations. This is maybe due to the fact that the used substrate has a millimeter-scale gap between its electrodes, if it had a micrometer scale the results could be different. With a bigger gap the nanofibers have more difficulty to fill the connection in great extent, because the 0.70 mg /cm^2 film was composed of 2 layers of 0.35 mg /cm^2 there is a higher probability of having more connections between the substrate electrodes.

10.6.1. Ammonia gas measurements using PANI nanofibers

The Figure 32 and Figure 33 show the PANI nanofibers' response when exposed to 10, 50, 100 and 500 ppb of ammonia. The resistance of the polymer was found to increase when exposed to ammonia gas. The response times for the 0.35 mg/cm^2 and 0.70 mg/cm^2 were 270-380 s and 285-480 s, respectively. The recovery times were 290-345 s and 295-470 s (calculated

when the resistance was equal to 90% steady-state resistance). The fastest response time was found at higher NH_3 concentrations while the recovery times increased for lower concentrations.

Figure 32. Response waves at several concentrations of ammonia gas using the 0.35 mg /cm^2 PANI nanofiber film.
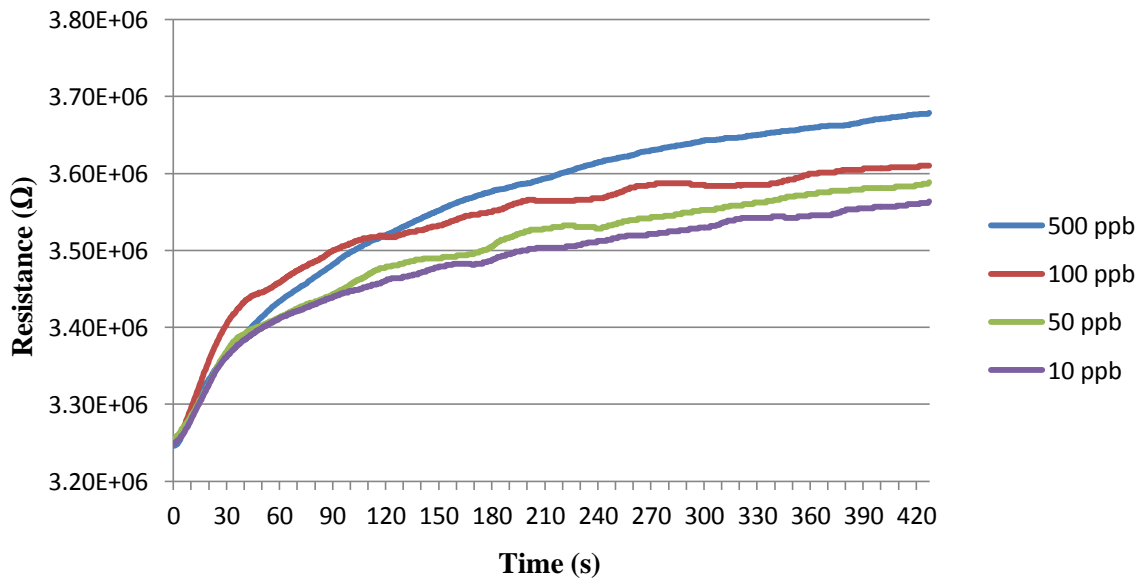
Figure 33. Response waves at several concentrations of ammonia gas using the 0.70 mg /cm^2 PANI nanofiber film.

10.6.2. Ammonia gas measurements using PANI-RGO nanofibers

It is interesting to analyze the ammonia sensing action of PANI-RGO with special reference to the role of RGO. The chemical polymerization increases the interlayer spacing by the intercalation of aniline monomers, producing well-dispersed graphene oxide in the polymer matrix. Reduced graphene oxide was added to the PANI conducting polymer because it has higher mechanical properties (resistance to traction and modulus of elasticity). Besides this, it is referred [141] that the interactions facilitates high molecular level dispersion and enhanced interfacial interaction. Graphene also has a very high electrical conductivity, which gives the possibility of raising the polymer's electrical conductivity. As graphene oxide is electrically insulating, thermal reduction was used to eliminate the functional oxygen groups and restore the electrical conductivity that makes reduced graphene oxide a suitable polymer filler. Despite what has been referred, graphene also has high thermal conductivity and stability and a reduced permeation of gas molecules.

Figure 34 illustrates the response of a PANI-RGO film exposed to ammonia gas, followed by the passing of N_2 for regeneration of the film.
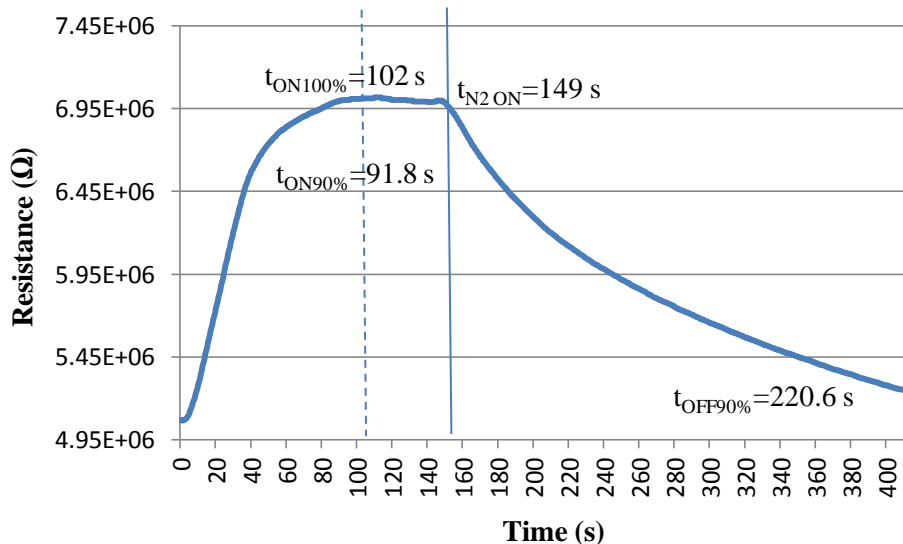
Figure 34. Demonstration of how each measure was performed since ammonia detection response and recovering by nitrogen air blow (PANI-RGO of 0.70 mg /cm^2 at 400 ppb).

Figure 35 and Figure 36 show the response of PANI-RGO nanofibers at different concentrations of ammonia from 1 to 500 ppb. The resistance of the polymer was found to increase when exposed to ammonia gas. The response times for the 0.35 mg /cm^2 and 0.70 mg /cm^2 were 120-365 s and 80-280 s, respectively. The recovery times were 235-370 s and 150-410 s (calculated when the resistance was equal to 90% steady-state resistance). At the higher NH$_3$ concentrations the response time was found to decrease while the recovery time increased. At higher levels of NH$_3$, the NH$_3$ molecules rapidly diffused into the polymer thin film. High concentration of NH$_3$ causes an increased amount of chemisorbed NH$_3$ which enhances the desorption rates and sensing layer renewal. However, at very high concentrations the competition for the sensing sites increases which could lead to irreversible desorption and consequently an increase of the response and recovery times.
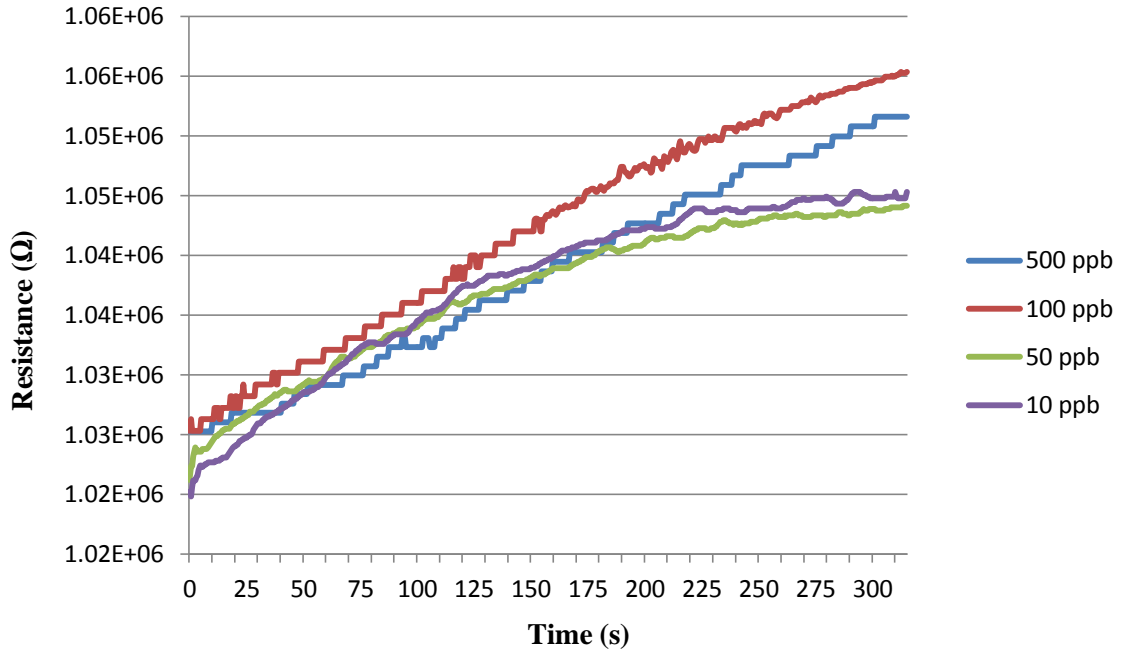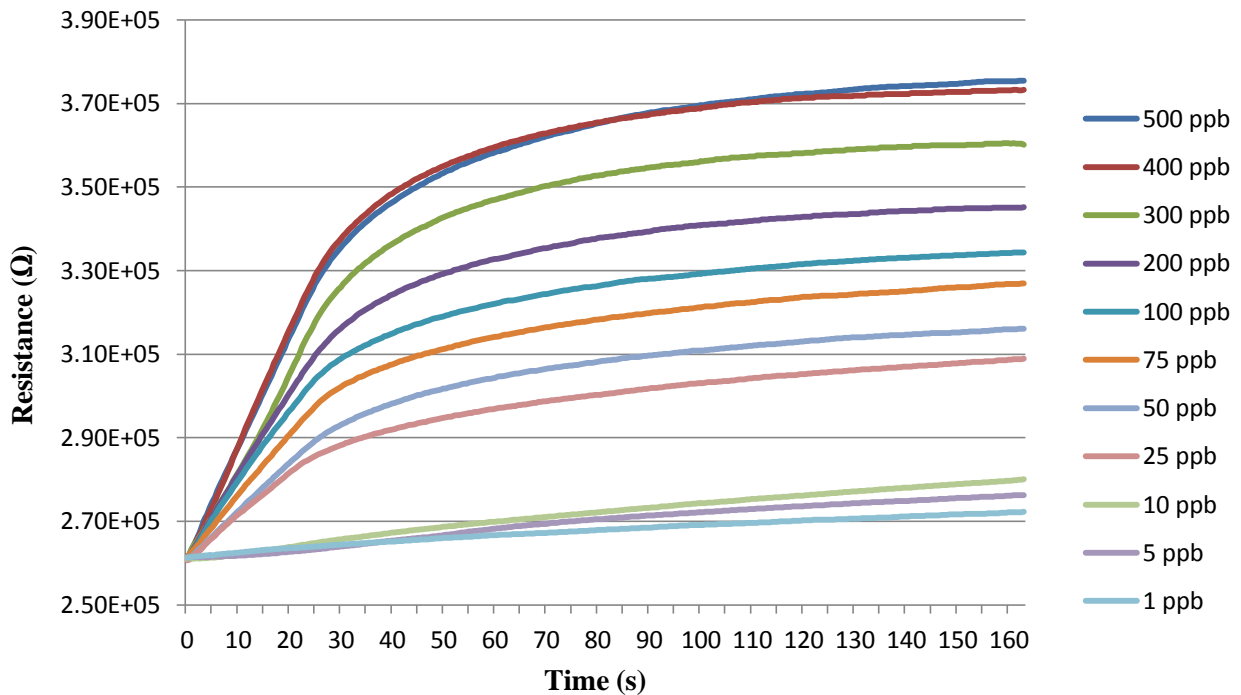

Figure 35. Response waves at several concentrations of ammonia gas using the 0.35 mg/cm^2 PANI-RGO film.
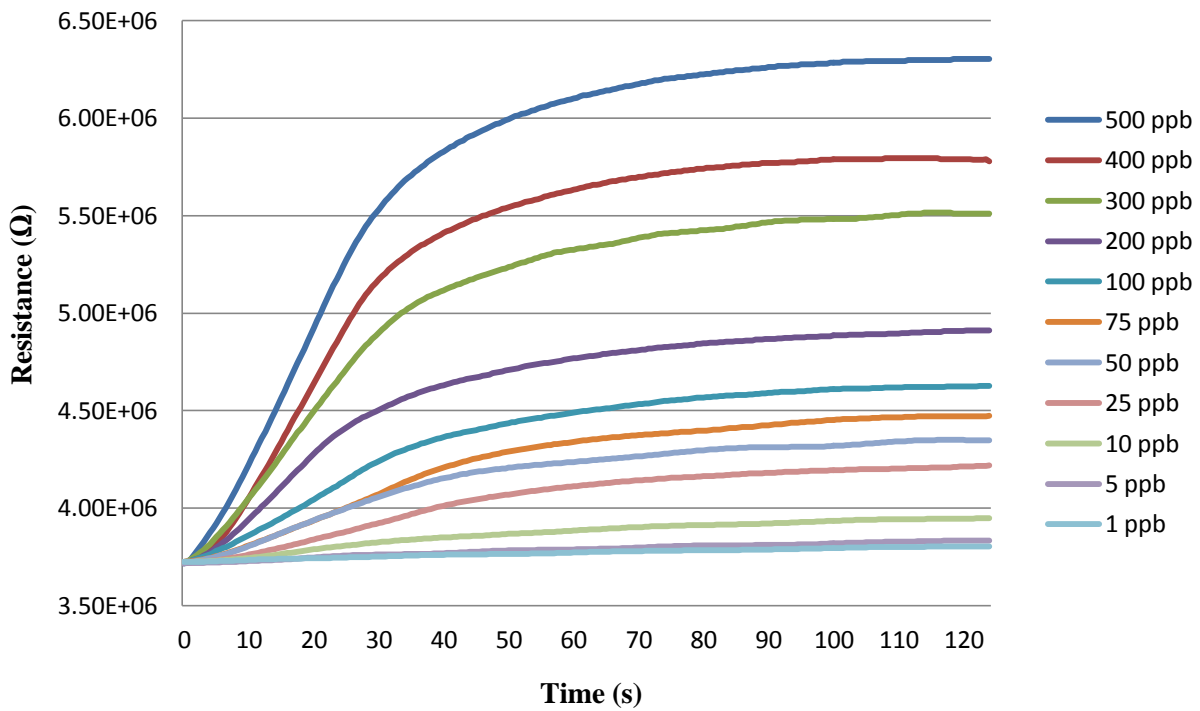
Figure 36. Response waves at several concentrations of ammonia gas using the 0.70 mg/cm^2 PANI-RGO film.

All measurements using the PANI- and PANI-RGO nanofibers were presented in Figure 35 and Figure 36. PANI-RGO showed a better electrical response for ammonia gas. Furthermore, the PANI-RGO composite had fast response times and lower recovery times. In conclusion, the newly developed PANI-RGO composite had been higher sensing behavior than PANI films.

10.7. Calibration plots of PANI nanofibers and PANI-RGO nanofibers

The calibration plots of 0.35 mg /cm^2 and 0.70 mg /cm^2 PANI- and PANI-RGO nanofibers were obtained by the measurements performed as indicated in section 10.6.

10.7.1. Calibration plots of PANI nanofibers

The measurements were carried out by exposing the sensor to several different concentrations (ppb level) of ammonia gas for 4 times. In each measurement the start and finish values were recorded, then the difference between them was calculated, and with the 4 differences the average and standard deviation was calculated. Figure 37 presents the results for the 0.35 mg /cm^2 (20 µL) film and Figure 38 for the 0.70 mg /cm^2 (40 µL) film.
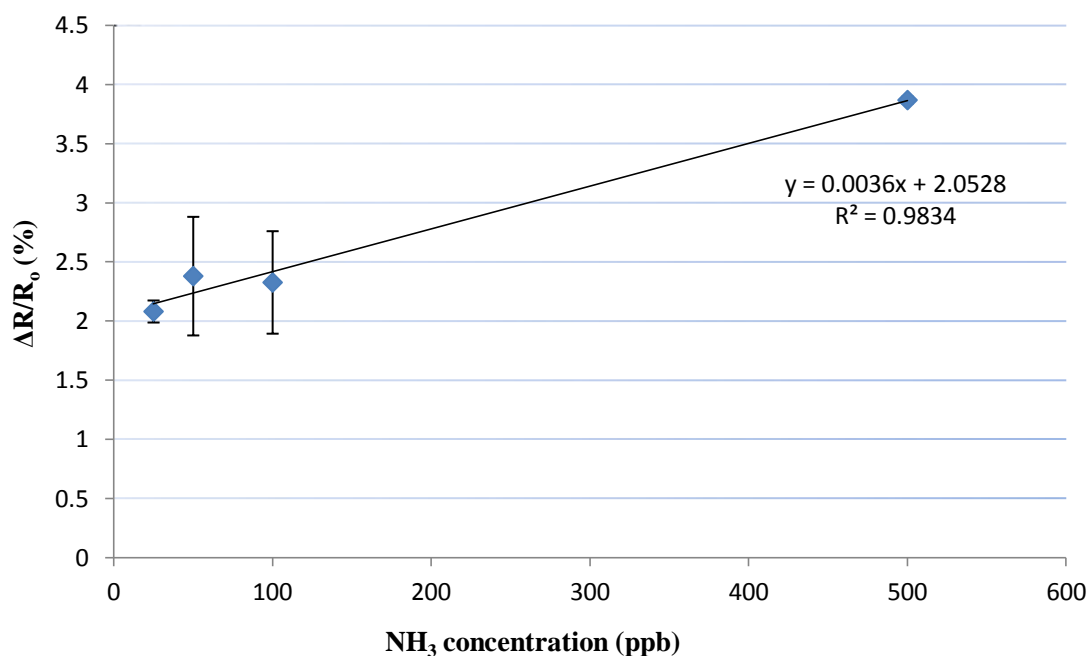
Figure 37. Calibration plot for 25, 50, 100 and 500 ppb of ammonia gas using a SPCE coated with PANI nanofibers with a thickness of 0.35 mg /cm^2, the straight has ~98% of linearity.
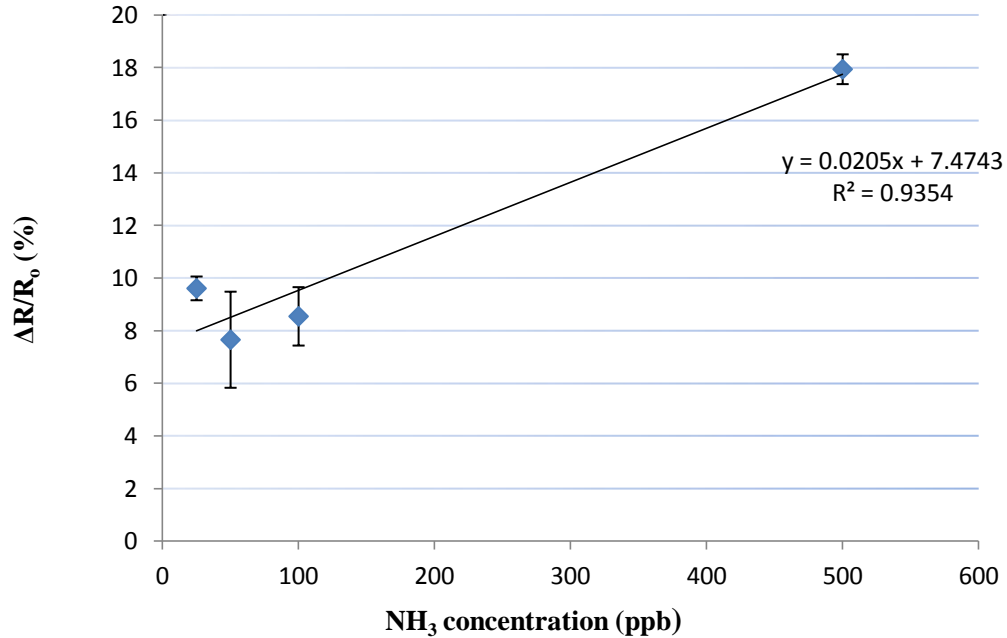
Figure 38. Calibration plot for 25, 50, 100 and 500 ppb of ammonia gas using a SPCE coated with PANI nanofibers with a thickness of 0.70 mg /cm^2, the straight has ~94% of linearity.

As can be seen in Figure 37 and Figure 38 it is noticeable that a better linearity was obtained for the 0.35 mg/cm^2 film, but its response does not exceed 4%. On the other hand, the 0.70 mg /cm^2 film had a 18% response. However, the response level is still low when compared to the PANI-RGO films that are presented in section 10.7.2.

10.7.2. Calibration plots of PANI-RGO nanofibers

The measurement procedure was carried out like in the PANI nanofiber film calibration: exposure of the sensor to several different concentrations (ppb level) of ammonia gas for 4 times. In each measurement the start and finish values were recorded, then the difference between them was calculated, and with the 4 differences the average and standard deviation was calculated. Figure 37 presents the results for the 0.35 mg /cm^2 (20 µL) film and Figure 38 for the 0.70 mg /cm^2 (40 µL) film.
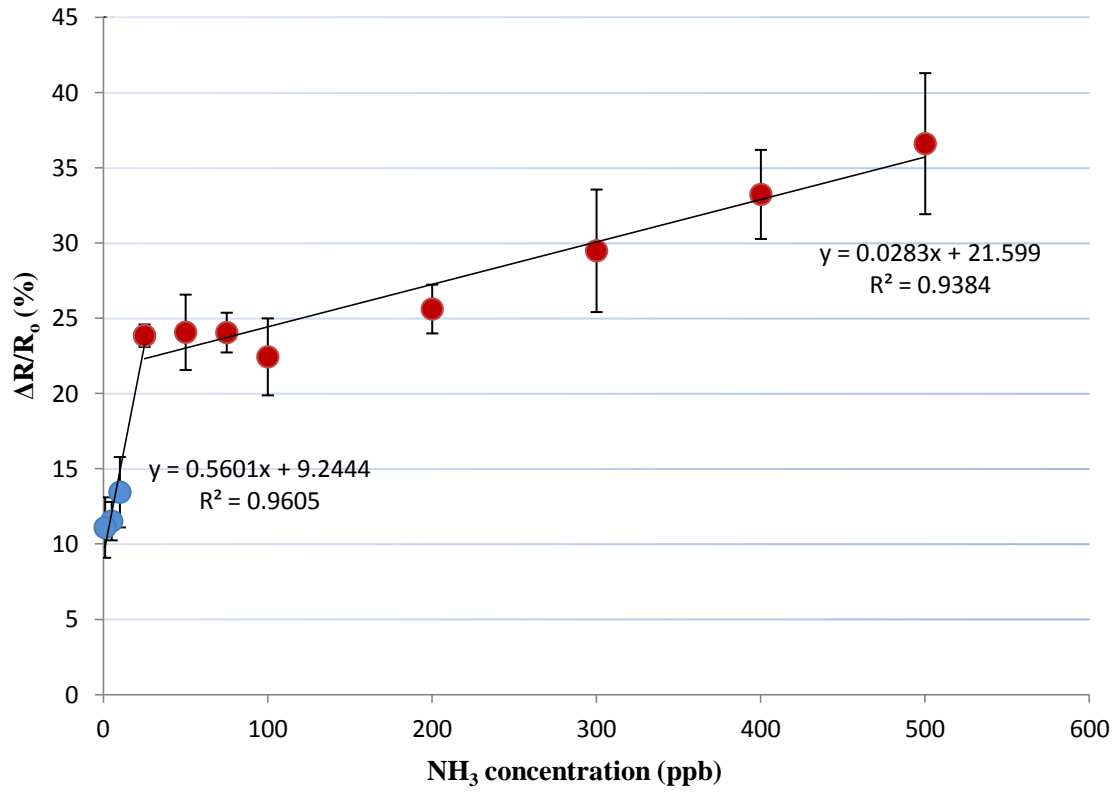
Figure 39. Calibrations plots for 1, 5, 10 and 25 ppb and for 25, 50, 75, 100, 200, 300, 400 and 500 ppb of ammonia gas using an SPCE coated with PANI-RGO nanofibers with a thickness of 0.35 mg /cm^2, the straight lines have ~96% and ~94% of linearity, correspondingly.
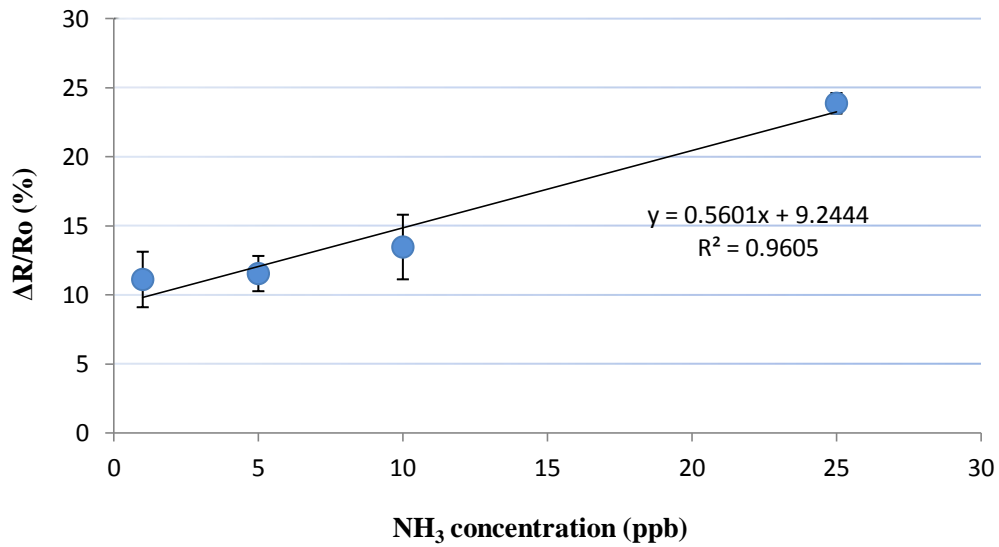
Figure 40. Calibration plot of 1, 5, 10 and 25 ppb, is the same presented in Figure 39 but in a closer look of the first points.
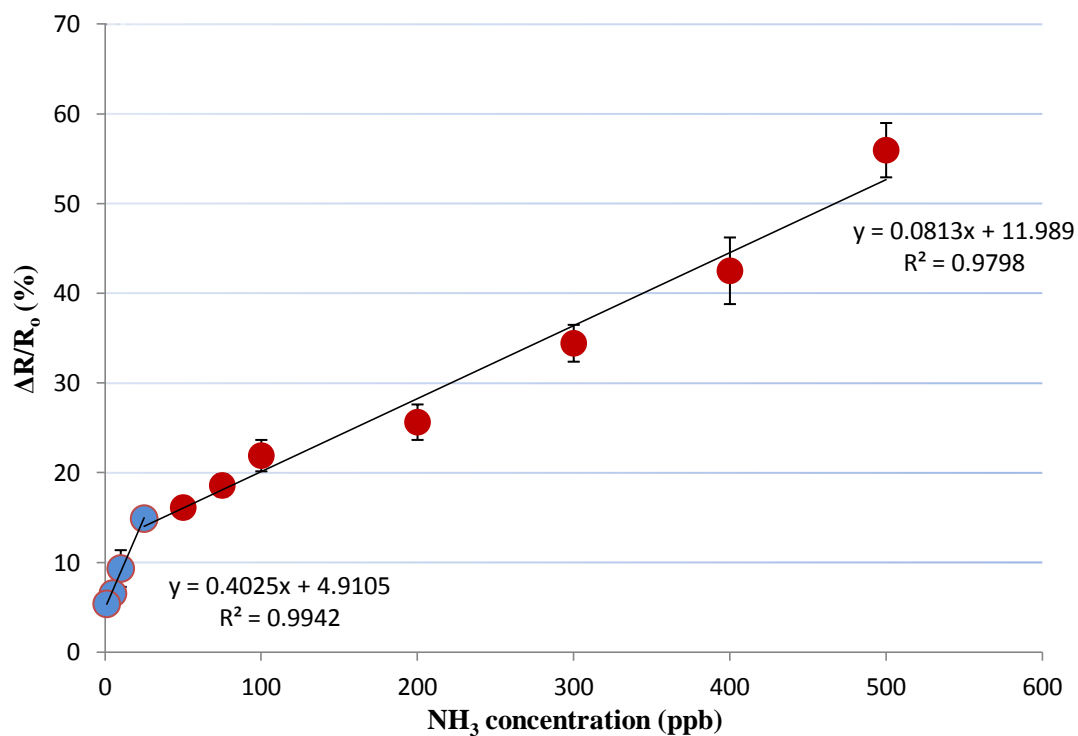
Figure 41. Calibrations plots for 1, 5, 10 and 25 ppb and for 25, 50, 75, 100, 200, 300, 400 and 500 ppb of ammonia gas using an SPCE coated with PANI-RGO nanofibers with a thickness of 0.70 mg/cm^2, the straight lines have ~99% and ~98% of linearity, correspondingly.
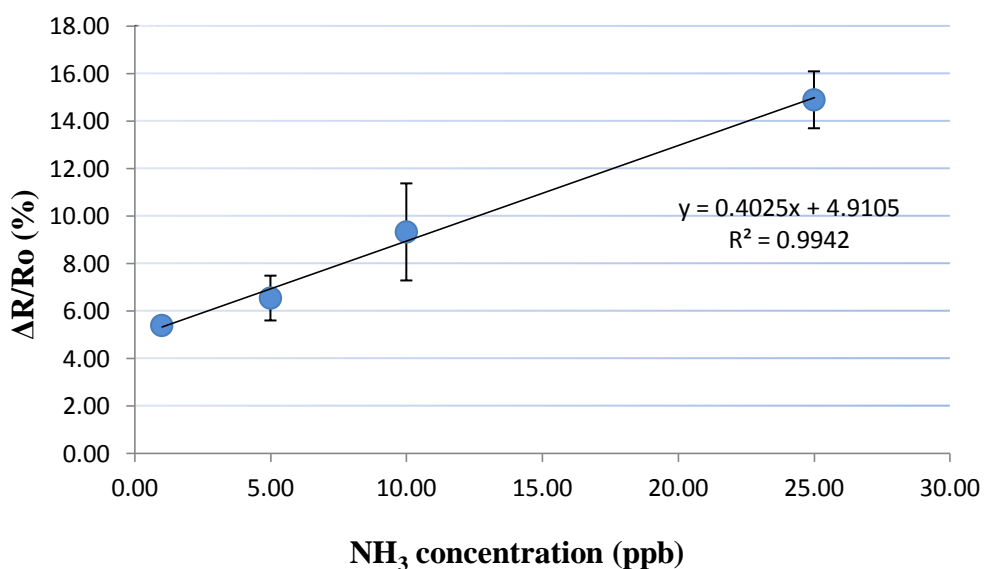
Figure 42. Calibration plot of 1, 5, 10 and 25 ppb, is the same presented in Figure 41 but in a closer look of the first points.

As can be seen in Figure 37 and Figure 38 a better linearity and a higher response (~56%) were obtained for the 0.70 mg/cm^2 film. On the other hand, the 0.35 mg/cm^2 film had a 37%

response. It was also noticed that the PANI-RGO films had a better response than all the PANI film.

In conclusion, the change in response ($\Delta R/R_0$) was found to be linearly proportional to the concentration from 1 to 25 ppb and from 25 to 500 ppb for PANI-RGO films with 0.35 mg/cm^2 and 0.70 mg /cm^2 thicknesses.

10.8. Study of interfering gases in PANI-RGO nanofibers

Studies were performed in order to analyze the effect of selected interfering gases in ammonia sensing measurements. Ammonia, nitrogen dioxide, toluene and acetone are common toxic gases that can be found in many industries. According to the European Agency for Safety and Health at Work (EU-OSHA), the recommended exposure limits are 1 ppm, 50 ppm, 200 ppm and 250 ppm for NO_2, NH_3, toluene and acetone, respectively, for 10 h/day and 40 h/week [150]. So acetone, toluene and NO_2 were selected for these studies.

The interference studies were performed by exposing the PANI-RGO composite (0.70 mg /cm^2 film) sensor to a mixture of ammonia gas (200 ppb) and a selected interferent. The resistance of the sensor was recorded before and after exposure and the response percentage was calculated. The values of 4 replicates were used to obtain the average and standard deviation. Blank experiments were also performed with ammonia gas that was prepared in the setup 3. The study was made in the same way as for the interfering gas testing. The results of this study can be seen in Figure 43.
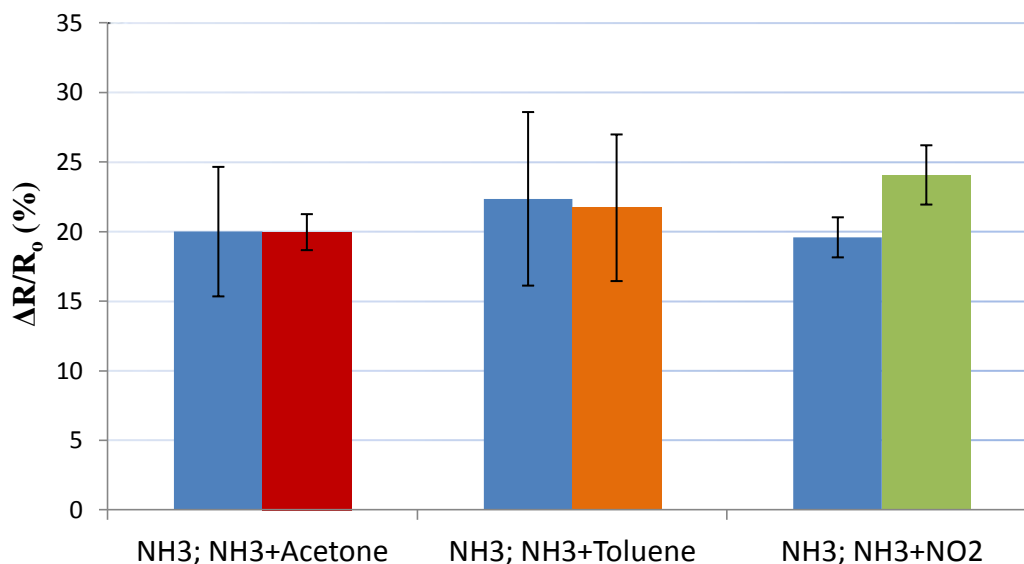
Figure 43. Response ($\Delta R/R_0$) percentage to NH_3 at 200 ppb, and the interfering gases Acetone (~100 ppm), Toluene (~100 ppm) and NO_2 (~1.5 ppm).

As shown in Figure 43, acetone and toluene do not interfere in the ammonia gas sensing. Some interference from NO_2 was observed. This interference was not much significant (response increase in ~4.5%) but can mismatch the real ammonia concentration measured at very low concentrations.

10.9. Conclusion

This research report described the development of an ammonia gas sensor utilizing conducting polymer nanofibers prepared by electrospinning. The response of the conducting PANI nanofibers was enhanced by RGO and tested for ammonia gas sensing. As a result, it was recognized that the resistance of the PANI-RGO significantly changed when exposed to NH_3 gas at concentrations from 1 to 500 ppb. The response after exposure to the gas is totally recoverable as the NH_3 molecules are removed from the PANI-RGO composite by passing N_2 gas, which is a desirable characteristic for sensing application. Moreover, the sensor exhibits stable and reproducible behavior. The new composite showed much better response when compared to PANI nanofibers. It was also verified that the response and recovery times of PANI-RGO were better than PANI films, showing that the newly prepared composite is a progress in polymer-based ammonia gas sensing. The studies of interfering gases (acetone, toluene and nitrogen dioxide) in ammonia determination revealed that the sensor was not affected by these selected gases.

This page has been deliberately left blank.

References

This page has been deliberately left blank.

1. Bharatdwaj, K., *Physical Geography: Atmosphere*. 2006: Discovery Publishing House Pvt. Ltd.

2. Marshall, J. and R.A. Plump, *Atmosphere, Ocean and Climate Dynamics: An Introduction Text*. 2008: Elsevier Academic Press.

3. Prasad, G.K., et al., *Ammonia sensing characteristics of thin film based on polyelectrolyte templated polyaniline.* Sensors and Actuators B: Chemical, 2005. **106**(2): p. 626-631.

4. Nicolas-Debarnot, D. and F. Poncin-Epaillard, *Polyaniline as a new sensitive layer for gas sensors.* Analytica Chimica Acta, 2003. **475**: p. 1-15.

5. Adhikari, B. and S. Majumdar, *Polymers in sensor applications.* Progress in Polymer Science, 2004. **29**(7): p. 699-766.

6. Kukla, A.L., Y.M. Shirshov, and S.A. Piletsky, *Ammonia sensors based on sensitive polyaniline films.* Sensors and Actuators B: Chemical, 1996. **37**(3): p. 135-140.

7. Ullmann, F., *Ammonia in Ullmann's Encyclopedia of Industrial Chemistry*. 2006: Wiley-VCH Verlag GmbH & Co. KGaA.

8. Press, O.U., *The Oxford Essential Guide to Egyptian mythology*. 2003: Berkley.

9. (ECHA), E.C.A. *European Regulation on Classification, Labelling and Packaging (CLP) of chemical substances and mixtures*. Available from: http://echa.europa.eu/clp/labelling_sds_en.asp.

10. Timmer, B., W. Olthuis, and A.v.d. Berg, *Ammonia sensors and their applications—a review.* Sensors and Actuators B: Chemical, 2005. **107**(2): p. 666-677.

11. BASF, *The Haber-Bosch Process and the Era of Fertilizers*, BASF. p. 4.

12. Hager, T., *The Alchemy of Air* 2008: Three Rivers Press.

13. EEA-32, *Ammonia (NH3) emissions (APE 003)*. 2010, European Enviroment Agency.

14. Krupa, S.V., *Effects of atmospheric ammonia (NH3) on terrestrial vegetation: a review.* Environmental Pollution, 2003. **124**(2): p. 179-221.

15. Ohmori, M. and A. Hattori, *Effect of ammonia on nitrogen fixation by the blue-green alga Anabaena cylindrica.* Plant and Cell Physiology, 1974. **15**(1): p. 131-142.

16. Campbell, N.A. and J.B. Reece, *Biology*. 6th ed. 2001: Pearson Education, Inc.

17. Kowalchuk, G.A. and J.R. Stephen, *AMMONIA-OXIDIZING BACTERIA: A Model for Molecular Microbial Ecology.* Annual Review of Microbiology, 2001. **55**(1): p. 485-529.

18. Waneck, P., *Chemistry of the natural atmosphere*. 2nd ed. 2000: Academic Press Inc.

19. Pijolat, C., et al., *Gas detection for automotive pollution control.* Sensors and Actuators B: Chemical, 1999. **59**(2-3): p. 195-202.

20. Durbin, T.D., et al., *Estimates of the emission rates of ammonia from light-duty vehicles using standard chassis dynamometer test cycles.* Atmospheric Environment, 2002. **36**(9): p. 1475-1482.

21. de la Hoz, R.E., D.P. Schlueter, and W.N. Rom, *Chronic lung disease secondary to ammonia inhalation injury: A report on three cases.* American Journal of Industrial Medicine, 1996. **29**(2): p. 209-214.

22. Ament, W., et al., *Respiratory Ammonia Output and Blood Ammonia Concentration During Incremental Exercise.* Int J Sports Med, 1999. **20**(2): p. 71-77.

23. Michaels, R.A., *Emergency planning and acute toxic potency of inhaled ammonia.* Environmental Health Perspectives, 1999. **107**(8): p. 617-627.

24. Narasimhan, L.R., *Correlation of breath ammonia with blood urea nitrogen and creatinine during hemodialysis.* Proceedings of the National Academy of Sciences, 2001. **98**(8): p. 4617-4621.

25. Vakil, N., *Helicobacter pylori: Factors Affecting Eradication and Recurrence.* Am J Gastroenterol, 2005. **100**(11): p. 2393-2394.

26. Suerbaum, S. and P. Michetti, *Helicobacter pylori Infection.* New England Journal of Medicine, 2002. **347**(15): p. 1175-1186.

27. Underwood, J.C.E. and S.S. Cross, *General and Systematic Pathology*. 5th ed. 2009: Churchill Livingstone.

28.   Hibbard, T. and A.J. Killard, *Breath Ammonia Analysis: Clinical Application and Measurement.* Critical Reviews in Analytical Chemistry, 2011. **41**(1): p. 21-35.

29.   Sekhar, P.K., et al., *Application of commercial automotive sensor manufacturing methods for NOx/NH3 mixed potential sensors for on-board emissions control.* Sensors and Actuators B: Chemical, 2010. **144**(1): p. 112-119.

30.   Patil, D.R., L.A. Patil, and P.P. Patil, *Cr2O3-activated ZnO thick film resistors for ammonia gas sensing operable at room temperature.* Sensors and Actuators B: Chemical, 2007. **126**(2): p. 368-374.

31.   Khan, A.A., U. Baig, and M. Khalid, *Ammonia vapor sensing properties of polyaniline–titanium(IV)phosphate cation exchange nanocomposite.* Journal of Hazardous Materials, 2011. **186**(2-3): p. 2037-2042.

32.   Leng, J.-y., et al., *Synthesis and gas-sensing characteristics of WO3 nanofibers via electrospinning.* Journal of Colloid and Interface Science, 2011. **356**(1): p. 54-57.

33.   Bal, A., A. Singh, and R. Bedi, *Characterization and ammonia sensing properties of pure and modified ZnO films.* Applied Physics A: Materials Science & Processing, 2011. **103**(2): p. 497-503.

34.   Tulliani, J.-M., et al., *Room temperature ammonia sensors based on zinc oxide and functionalized graphite and multi-walled carbon nanotubes.* Sensors and Actuators B: Chemical, 2011. **152**(2): p. 144-154.

35.   Raj, V.B., et al., *Cross-sensitivity and selectivity studies on ZnO surface acoustic wave ammonia sensor.* Sensors and Actuators B: Chemical, 2010. **147**(2): p. 517-524.

36.   Zeng, Y., et al., *Enhanced ammonia sensing performances of Pd-sensitized flowerlike ZnO nanostructure.* Sensors and Actuators B: Chemical, 2011. **156**(1): p. 395-400.

37.   Shang, Y., et al., *Optical ammonia gas sensor based on a porous silicon rugate filter coated with polymer-supported dye.* Analytica Chimica Acta, 2011. **685**(1): p. 58-64.

38.   Timmer, B.H., et al., *Miniaturized measurement system for ammonia in air.* Analytica Chimica Acta, 2004. **507**(1): p. 137-143.

39.   Liao, C. and M. Gu, *Electroless deposition of polyaniline film via autocatalytic polymerization of aniline.* Thin Solid Films, 2002. **408**(1-2): p. 37-42.

40.   Rao, P.S., S. Subrahmanya, and D.N. Sathyanarayana, *Inverse emulsion polymerization: a new route for the synthesis of conducting polyaniline.* Synthetic Metals, 2002. **128**(3): p. 311-316.

41.   Palaniappan, S. and A. John, *Polyaniline materials by emulsion polymerization pathway.* Progress in Polymer Science, 2008. **33**(7): p. 732-758.

42.   Cruz, G.J., et al., *Synthesis of polyaniline films by plasma polymerization.* Synthetic Metals, 1997. **88**(3): p. 213-218.

43.   Bai, H. and G. Shi, *Gas Sensors Based on Conducting Polymers.* Sensors, 2007. **7**(3): p. 267-307.

44.   Brady, S., et al., *The Development and Characterisation of Conducting Polymeric-based Sensing Devices.* Synthetic Metals, 2005. **154**(1-3): p. 25-28.

45.   Cho, J.-H., et al., *Sensing behaviors of polypyrrole sensor under humidity condition.* Sensors and Actuators B: Chemical, 2005. **108**(1-2): p. 389-392.

46.   Tongpool, R. and S. Yoriya, *Kinetics of nitrogen dioxide exposure in lead phthalocyanine sensors.* Thin Solid Films, 2005. **477**(1-2): p. 148-152.

47.   Lu, G., L. Qu, and G. Shi, *Electrochemical fabrication of neuron-type networks based on crystalline oligopyrene nanosheets.* Electrochimica Acta, 2005. **51**(2): p. 340-346.

48.   Reemts, J., J. Parisi, and D. Schlettwein, *Electrochemical growth of gas-sensitive polyaniline thin films across an insulating gap.* Thin Solid Films, 2004. **466**(1-2): p. 320-325.

49.   Agbor, N.E., M.C. Petty, and A.P. Monkman, *Polyaniline thin films for gas sensing.* Sensors and Actuators B: Chemical, 1995. **28**(3): p. 173-179.

50.   Xie, D., et al., *Fabrication and characterization of polyaniline-based gas sensor by ultra-thin film technology.* Sensors and Actuators B: Chemical, 2002. **81**(2-3): p. 158-164.

51. Kaur Bal, A., A. Singh, and R.K. Bedi, *Characterization and room temperature sensing of ammonia and ethanol by thermally oxidized indium films.* Physica B: Condensed Matter, 2010. **405**(15): p. 3124-3128.

52. Li, D., et al., *Self-assembly of polyaniline ultrathin films based on doping-induced deposition effect and applications for chemical sensors.* Sensors and Actuators B: Chemical, 2000. **66**(1-3): p. 125-127.

53. Loffredo, F., et al., *Gas Sensor Devices Obtained by Ink-jet Printing of Polyaniline Suspensions.* Macromolecular Symposia, 2007. **247**(1): p. 357-363.

54. Sutar, D.S., et al., *Preparation of nanofibrous polyaniline films and their application as ammonia gas sensor.* Sensors and Actuators B: Chemical, 2007. **128**(1): p. 286-292.

55. Ruckenstein, E. and Z.F. Li, *Surface modification and functionalization through the self-assembled monolayer and graft polymerization.* Advances in Colloid and Interface Science, 2005. **113**(1): p. 43-63.

56. Wu, C.G., et al., *Electroless surface polymerization of ordered conducting polyaniline films on aniline-primed substrates.* Polymer, 2001. **42**(7): p. 2877-2885.

57. Li, Y., et al., *Synthesis of polyaniline nanotubes using Mn2O3 nanofibers as oxidant and their ammonia sensing properties.* Synthetic Metals, 2011. **161**(1-2): p. 56-61.

58. Tai, H., et al., *Preparation, Characterization and Comparative NH3-sensing Characteristic Studies of PANI/inorganic Oxides Nanocomposite Thin Films.* Journal of Materials Science & Technology, 2010. **26**(7): p. 605-613.

59. Gong, J., et al., *Ultrasensitive NH3 Gas Sensor from Polyaniline Nanograin Enchased TiO2 Fibers.* The Journal of Physical Chemistry C, 2010. **114**(21): p. 9970-9974.

60. Srivastava, V. and K. Jain, *Highly sensitive NH3 sensor using Pt catalyzed silica coating over WO3 thick films.* Sensors and Actuators B: Chemical, 2008. **133**(1): p. 46-52.

61. Dikovska, A.O., et al., *Optical sensing of ammonia using ZnO nanostructure grown on a side-polished optical-fiber.* Sensors and Actuators B: Chemical, 2010. **146**(1): p. 331-336.

62. Chougule, M.A.P., S.G. Patil, S.L. Raut, B.T. Godse, P.R. Sen, S. Patil, V.B., *Polypyrrole Thin Film: Room Temperature Ammonia Gas Sensor* Sensors Journal, IEEE 2011. **11**(9): p. 2137-2141.

63. Du, Z., et al., *Ammonia gas detection based on polyaniline nanofibers coated on interdigitated array electrodes.* Journal of Materials Science: Materials in Electronics, 2011. **22**(4): p. 418-421.

64. Sharma, S., et al., *Chloroform vapour sensor based on copper/polyaniline nanocomposite.* Sensors and Actuators B: Chemical, 2002. **85**(1-2): p. 131-136.

65. Chabukswar, V.V., S. Pethkar, and A.A. Athawale, *Acrylic acid doped polyaniline as an ammonia sensor.* Sensors and Actuators B: Chemical, 2001. **77**(3): p. 657-663.

66. Meijerink, M.G.H., et al., *Reproducible fabrication of an array of gas-sensitive chemo-resistors with commercially available polyaniline.* Sensors and Actuators B: Chemical, 2000. **68**(1-3): p. 331-334.

67. Athawale, A.A. and M.V. Kulkarni, *Polyaniline and its substituted derivatives as sensor for aliphatic alcohols.* Sensors and Actuators B: Chemical, 2000. **67**(1-2): p. 173-177.

68. Christie, S., et al., *Remote detection of gaseous ammonia using the near infrared transmission properties of polyaniline.* Sensors and Actuators B: Chemical, 2003. **90**(1-3): p. 163-169.

69. Bansal, L. and M. El-Sherif, *Intrinsic optical-fiber sensor for nerve agent sensing.* Sensors Journal, IEEE 2005. **5**(4): p. 648-655.

70. MacDiarmid, A.G., et al., *Electrostatically-generated nanofibers of electronic polymers.* Synthetic Metals, 2001. **119**(1-3): p. 27-30.

71. Zhou, Y., *Fabrication and electrical characterization of polyaniline-based nanofibers with diameter below 30 nm.* Appl. Phys. Lett., 2003. **83**(18): p. 3800.

72. Pinto, N., *Electrospun polyaniline/polyethylene oxide nanofiber field-effect transistor.* Appl. Phys. Lett., 2003. **83**(20): p. 4244.

73. Kahol, P.K. and N.J. Pinto, *An EPR investigation of electrospun polyaniline-polyethylene oxide blends.* Synthetic Metals, 2004. **140**(2-3): p. 269-272.

74. Aussawasathien, D., J.H. Dong, and L. Dai, *Electrospun polymer nanofiber sensors.* Synthetic Metals, 2005. **154**(1-3): p. 37-40.

75. Zhang, X. and S.K. Manohar, *Polyaniline nanofibers: chemical synthesis using surfactants.* Chemical Communications, 2004(20): p. 2360-2361.

76. Chaudhuri, D., *Self-organization of polyaniline nanorods: Towards achieving a higher conductivity.* Appl. Phys. Lett., 2005. **87**(9): p. 093117.

77. Jackowska, K., A. Bieguński, and M. Tagowska, *Hard template synthesis of conducting polymers: a route to achieve nanostructures.* Journal of Solid State Electrochemistry, 2008. **12**(4): p. 437-443.

78. Chiou, N.-R., L.J. Lee, and A.J. Epstein, *Porous membrane controlled polymerization of nanofibers of polyaniline and its derivatives.* Journal of Materials Chemistry, 2008. **18**(18): p. 2085-2089.

79. Zhang, X., W.J. Goux, and S.K. Manohar, *Synthesis of Polyaniline Nanofibers by "Nanofiber Seeding".* Journal of the American Chemical Society, 2004. **126**(14): p. 4502-4503.

80. Thanpitcha, T., et al., *Synthesis of polyaniline nanofibrils using an in situ seeding technique.* Synthetic Metals, 2008. **158**(17-18): p. 695-703.

81. Xu, P., et al., *Synthesis and Characterization of Novel Coralloid Polyaniline/BaFe12O19 Nanocomposites.* The Journal of Physical Chemistry C, 2007. **111**(34): p. 12603-12608.

82. Ding, H., et al., *Electromagnetic Functionalized Cage-like Polyaniline Composite Nanostructures.* The Journal of Physical Chemistry B, 2008. **112**(31): p. 9289-9294.

83. Tran, H.D., et al., *Toward an Understanding of the Formation of Conducting Polymer Nanofibers.* ACS Nano, 2008. **2**(9): p. 1841-1848.

84. Chao, D., et al., *Preparation of oligoaniline derivative/polyvinylpyrrolidone nanofibers containing silver nanoparticles.* Synthetic Metals, 2009. **159**(5-6): p. 537-540.

85. Chen, J., et al., *The design, synthesis and characterization of polyaniline nanophase materials.* Comptes Rendus Chimie, 2008. **11**(1-2): p. 84-89.

86. Han, Y.-G., T. Kusunose, and T. Sekino, *Facile one-pot synthesis and characterization of novel nanostructured organic dispersible polyaniline.* Journal of Polymer Science Part B: Polymer Physics, 2009. **47**(10): p. 1024-1029.

87. Li, D. and R.B. Kaner, *Shape and Aggregation Control of Nanoparticles: Not Shaken, Not Stirred.* Journal of the American Chemical Society, 2005. **128**(3): p. 968-975.

88. Yakuphanoglu, F., et al., *Nanofiber organic semiconductors: The effects of nanosize on the electrical charge transport and optical properties of bulk polyanilines.* Journal of Applied Polymer Science, 2009. **114**(2): p. 794-799.

89. Dallas, P., et al., *Characterization, magnetic and transport properties of polyaniline synthesized through interfacial polymerization.* Polymer, 2007. **48**(11): p. 3162-3169.

90. Wang, Y. and X. Jing, *Formation of Polyaniline Nanofibers: A Morphological Study.* The Journal of Physical Chemistry B, 2008. **112**(4): p. 1157-1162.

91. Qiang, J., et al., *Polyaniline nanofibers synthesized by rapid mixing polymerization.* Synthetic Metals, 2008. **158**(13): p. 544-547.

92. Sapurina, I. and J. Stejskal, *The mechanism of the oxidative polymerization of aniline and the formation of supramolecular polyaniline structures.* Polymer International, 2008. **57**(12): p. 1295-1325.

93. Subramania, A. and S.L. Devi, *Polyaniline nanofibers by surfactant-assisted dilute polymerization for supercapacitor applications.* Polymers for Advanced Technologies, 2008. **19**(7): p. 725-727.

94. Li, Z.-F., et al., *One-step fabrication of a polyaniline nanofiber vapor sensor.* Sensors and Actuators B: Chemical, 2008. **134**(1): p. 31-35.

95. Wang, J., et al., *Antioxidant activity of polyaniline nanofibers.* Chinese Chemical Letters, 2007. **18**(8): p. 1005-1008.

96. Pillalamarri, S.K., et al., *Radiolytic Synthesis of Polyaniline Nanofibers: A New Templateless Pathway.* Chemistry of Materials, 2004. **17**(2): p. 227-229.

97. Mo, Z., et al., *Synthesis of graphite nanosheets/polyaniline nanorods composites with ultrasonic and conductivity.* Journal of Applied Polymer Science, 2009. **112**(2): p. 573-578.

98. Li, Y., et al., *Effects of ultrasonic irradiation on the morphology of chemically prepared polyaniline nanofibers.* Journal of Applied Polymer Science, 2009. **113**(2): p. 868-875.

99. Du, X.-S., et al., *Novel Solid-State and Template-Free Synthesis of Branched Polyaniline Nanofibers.* Chemistry of Materials, 2008. **20**(12): p. 3806-3808.

100. Zhou, C.F., et al., *Solid phase mechanochemical synthesis of polyaniline branched nanofibers.* Synthetic Metals, 2009. **159**(13): p. 1302-1307.

101. Ding, H., M. Wan, and Y. Wei, *Controlling the Diameter of Polyaniline Nanofibers by Adjusting the Oxidant Redox Potential.* Advanced Materials, 2007. **19**(3): p. 465-469.

102. Chiou, N.-R., L.J. Lee, and A.J. Epstein, *Self-Assembled Polyaniline Nanofibers/Nanotubes.* Chemistry of Materials, 2007. **19**(15): p. 3589-3591.

103. Zhang, X., et al., *Fibrillar Growth in Polyaniline.* Advanced Functional Materials, 2006. **16**(9): p. 1145-1152.

104. Surwade, S.P., N. Manohar, and S.K. Manohar, *Origin of Bulk Nanoscale Morphology in Conducting Polymers.* Macromolecules, 2009. **42**(6): p. 1792-1795.

105. Wang, P.-C., et al., *Simplifying the reaction system for the preparation of polyaniline nanofibers: Re-examination of template-free oxidative chemical polymerization of aniline in conventional low-pH acidic aqueous media.* Reactive and Functional Polymers, 2009. **69**(4): p. 217-223.

106. Amarnath, C.A., et al., *Nanoflakes to nanorods and nanospheres transition of selenious acid doped polyaniline.* Polymer, 2008. **49**(2): p. 432-437.

107. Li, C., H. Bai, and G. Shi, *Conducting polymer nanomaterials: electrosynthesis and applications.* Chemical Society Reviews, 2009. **38**(8): p. 2397-2409.

108. Yu, X., Y. Li, and K. Kalantar-zadeh, *Synthesis and electrochemical properties of template-based polyaniline nanowires and template-free nanofibril arrays: Two potential nanostructures for gas sensors.* Sensors and Actuators B: Chemical, 2009. **136**(1): p. 1-7.

109. Kuila, B.K., et al., *Vertically oriented arrays of polyaniline nanorods and their super electrochemical properties.* Chemical Communications, 2009(38): p. 5749-5751.

110. Peng, X.-Y., et al., *pH-controlled morphological structure of polyaniline during electrochemical deposition.* Electrochimica Acta, 2009. **54**(26): p. 6172-6177.

111. Ghenaatian, H.R., et al., *Electrochemical investigations of self-doped polyaniline nanofibers as a new electroactive material for high performance redox supercapacitor.* Synthetic Metals, 2009. **159**(17-18): p. 1717-1722.

112. Gupta, V. and N. Miura, *Electrochemically Deposited Polyaniline Nanowire's Network.* Electrochemical and Solid-State Letters, 2005. **8**(12): p. A630-A632.

113. Zhou, H., et al., *Electrosynthesis of polyaniline films on titanium by pulse potentiostatic method.* Synthetic Metals, 2007. **157**(2-3): p. 98-103.

114. Liu, F.-J., et al., *Platinum particles dispersed polyaniline-modified electrodes containing sulfonated polyelectrolyte for methanol oxidation.* Synthetic Metals, 2008. **158**(19-20): p. 767-774.

115. Zhou, Z., et al., *Fabrication of polyaniline–silver nanocomposites by chronopotentiometry in different ionic liquid microemulsion systems.* Thin Solid Films, 2009. **517**(24): p. 6767-6771.

116. Huang, J. and R.B. Kaner, *A General Chemical Route to Polyaniline Nanofibers.* Journal American Chemical Society, 2004. **126**: p. 851-855.

117. Chiou, N.R. and A.J. Epstein, *Polyaniline Nanofibers Prepared by Dilute Polymerization.* Advanced Materials, 2005. **17**(13): p. 1679-1683.

118. do Nascimento, G.M., P.Y.G. Kobata, and M.L.A. Temperini, *Structural and Vibrational Characterization of Polyaniline Nanofibers Prepared from Interfacial Polymerization.* The Journal of Physical Chemistry B, 2008. **112**(37): p. 11551-11557.

119.   Hopkins, A.R., R.A. Lipeles, and S.-J. Hwang, *Morphology characterization of polyaniline nano- and microstructures.* Synthetic Metals, 2008. **158**(14): p. 594-601.

120.   Huang, J., et al., *Polyaniline Nanofibers: Facile Synthesis and Chemical Sensors.* Journal of the American Chemical Society, 2002. **125**(2): p. 314-315.

121.   Zhu, Y., et al., *3D-boxlike polyaniline microstructures with super-hydrophobic and high-crystalline properties.* Polymer, 2008. **49**(16): p. 3419-3423.

122.   Zhu, Y., et al., *Conducting and Superhydrophobic Rambutan-like Hollow Spheres of Polyaniline.* Advanced Materials, 2007. **19**(16): p. 2092-2096.

123.   Dersch, R., et al., *Nanoprocessing of polymers: applications in medicine, sensors, catalysis, photonics.* Polymers for Advanced Technologies, 2005. **16**(2-3): p. 276-282.

124.   Ioannis S, C., *Novel nanocomposites and nanoceramics based on polymer nanofibers using electrospinning process—A review.* Journal of Materials Processing Technology, 2005. **167**(2-3): p. 283-293.

125.   Frenot, A. and I.S. Chronakis, *Polymer nanofibers assembled by electrospinning.* Current Opinion in Colloid & Interface Science, 2003. **8**(1): p. 64-75.

126.   Li, D. and Y. Xia, *Electrospinning of Nanofibers: Reinventing the Wheel?* Advanced Materials, 2004. **16**(14): p. 1151-1170.

127.   Norris, I.D., et al., *Electrostatic fabrication of ultrafine conducting fibers: polyaniline/polyethylene oxide blends.* Synthetic Metals, 2000. **114**(2): p. 109-114.

128.   Picciani, P.H.S., et al., *Development of conducting polyaniline/poly(lactic acid) nanofibers by electrospinning.* Journal of Applied Polymer Science, 2009. **112**(2): p. 744-753.

129.   Bhardwaj, N. and S.C. Kundu, *Electrospinning: A fascinating fiber fabrication technique.* Biotechnology Advances, 2010. **28**(3): p. 325-347.

130.   Sun, Z., et al., *Compound Core–Shell Polymer Nanofibers by Co-Electrospinning.* Advanced Materials, 2003. **15**(22): p. 1929-1932.

131.   Czaplewski, D., *Nonlithographic approach to nanostructure fabrication using a scanned electrospinning source.* J. Vac. Sci. Technol. B, 2003. **21**(6): p. 2994.

132.   Welle, A., et al., *Electrospun aliphatic polycarbonates as tailored tissue scaffold materials.* Biomaterials, 2007. **28**(13): p. 2211-2219.

133.   León, M.J.D.-d., *Electrospinning Nanofibers of Polyaniline and Polyaniline / (Polystyrene and Polyethylene Oxide) Blend.* National Conference of Undergraduate Research, University of Kentucky, Lexington, 2001.

134.   Keyur Desai, C.S., *Electrospinning nanofibers of PANI/PMMA blends.* Materials Research Society Symposium Proceedings, 2002. **736**(Electronics on Unconventional Substrates--Electrotextiles and Giant-Area Flexible Circuits): p. 121-126.

135.   Hong, K.H., K.W. Oh, and T.J. Kang, *Preparation of conducting nylon-6 electrospun fiber webs by the in situ polymerization of polyaniline.* Journal of Applied Polymer Science, 2005. **96**(4): p. 983-991.

136.   Teoh, G.L., K.Y. Liew, and W.A.K. Mahmood, *Preparation of polyaniline-Al2O3 composites nanofibers with controllable conductivity.* Materials Letters, 2007. **61**(27): p. 4947-4949.

137.   Dong, H., et al., *Polyaniline/poly(methyl methacrylate) coaxial fibers: The fabrication and effects of the solution properties on the morphology of electrospun core fibers.* Journal of Polymer Science Part B: Polymer Physics, 2004. **42**(21): p. 3934-3942.

138.   Dong, H., et al., *Sub-micrometer Conducting Polyaniline Tubes Prepared from Polymer Fiber Templates.* Chemistry of Materials, 2004. **16**(3): p. 371-373.

139.   Shin, M.K., et al., *Enhanced conductivity of aligned PANi/PEO/MWNT nanofibers by electrospinning.* Sensors and Actuators B: Chemical, 2008. **134**(1): p. 122-126.

140.   Zuo, X., et al., *Graphene Oxide-Facilitated Electron Transfer of Metalloproteins at Electrode Surfaces.* Langmuir, 2009. **26**(3): p. 1936-1939.

141.   Singh, V., et al., *Graphene based materials: Past, present and future.* Progress in Materials Science, 2011. **56**(8): p. 1178-1271.

142.   Zhang, W.L., Y.D. Liu, and H.J. Choi, *Fabrication of semiconducting graphene oxide/polyaniline composite particles and their electrorheological response under an applied electric field.* Carbon, 2012. **50**(1): p. 290-296.

143.   Stankovich, S., et al., *Synthesis of graphene-based nanosheets via chemical reduction of exfoliated graphite oxide.* Carbon, 2007. **45**(7): p. 1558-1565.

144.   Stejskal, J. and R.G. Gilbert, *Polyaniline. Preparation of a Conducting Polymer.* Pure Appl. Chem., 2002. **74**(5): p. 857-867.

145.   Hummers, W.S. and R.E. Offeman, *Preparation of Graphitic Oxide.* Journal of the American Chemical Society, 1958. **80**(6): p. 1339-1339.

146.   Kovtyukhova, N.I., et al., *Layer-by-Layer Assembly of Ultrathin Composite Films from Micron-Sized Graphite Oxide Sheets and Polycations.* Chemistry of Materials, 1999. **11**(3): p. 771-778.

147.   Zhang, K., et al., *Graphene/Polyaniline Nanofiber Composites as Supercapacitor Electrodes.* Chemistry of Materials, 2010. **22**(4): p. 1392-1401.

148.   Dhawan, S.K., et al., *Application of conducting polyaniline as sensor material for ammonia.* Sensors and Actuators B: Chemical, 1997. **40**(2-3): p. 99-103.

149.   Paredes, J.I., et al., *Atomic Force and Scanning Tunneling Microscopy Imaging of Graphene Nanosheets Derived from Graphite Oxide.* Langmuir, 2009. **25**(10): p. 5957-5968.

150.   EU-OSHA. *European Agency for Safety and Health at Work*. 2011; Available from: http://osha.europa.eu/en/front-page.

This page has been deliberately left blank.